

LASER WELDING OF BIODEGRADABLE POLYGLYCOLIC ACID (PGA) BASED  
POLYMER FELT SCAFFOLDS

by

SOUMYA SAMBIT ROUT

B.E., Visvesvariah Technological University, India, 2005

A THESIS

submitted in partial fulfillment of the requirements for the degree

MASTER OF SCIENCE

Department of Industrial and Manufacturing Systems Engineering  
College of Engineering

KANSAS STATE UNIVERSITY  
Manhattan, Kansas

2008

Approved by:

Major Professor  
Dr. Shuting Lei

## **Abstract**

Polyglycolic acid (PGA) is an important polymer in the field of tissue engineering. It has many favorable properties such as biocompatibility, bioabsorbability, high melting point, low solubility in organic solvents, high tensile strength and is used in a variety of medical related applications. Currently there are various methods such as felting, stitching, use of binder/adhesive for joining the non woven meshes of PGA polymer in order to make suitable three dimensional scaffolds. The existing methods for joining the non woven meshes of PGA polymer are usually time consuming and not very flexible. Thus there is a need for a better technique that would overcome the drawbacks of the existing methods. Laser welding offers potential advantages such as high welding rates, easy to automate, improved seam and single sided access such that welds can be performed under various layers of fabric. Therefore, the main objective of this research is to conduct a fundamental study on laser welding of non woven PGA scaffold felts. An experimental setup for spot welding is built that would assist in the formation of tubular structures. A factorial design of experiments is used to study the effects of the operating parameters such as laser power, beam diameter, time duration and pressure on the weld quality. The weld quality is assessed in terms of weld strength and weld diameter. Based on the parametric study, a regression analysis is carried out to form correlations between weld quality and the operating parameters, which could be used to select the optimal operating conditions. The successful welds obtained by the laser welding process have no discoloration and are stronger than the tensile strength of the original non woven sheets of PGA biofelt.

# Table of Contents

List of Figures .....	v
List of Tables .....	viii
Acknowledgements .....	ix
CHAPTER 1 - Introduction .....	1
CHAPTER 2 - Literature review .....	4
2.1 Scaffolds in Tissue Engineering .....	4
2.2 Current Techniques for joining the non woven meshes .....	6
2.3 Laser Welding of Polymers .....	9
2.4 PGA based Biofelts .....	12
2.5 Research Objectives .....	13
CHAPTER 3 – Laser welding of PGA scaffold Biofelt .....	14
3.1 Experimental setup .....	14
3.2 Type of experiments .....	16
3.2.1 Creation of spot welds using BK 7 ball lens .....	16
3.2.1.1 Design of welding experiment .....	17
3.2.1.2 Creation of cylindrical tubes .....	18
3.3 Laser Welding – a parametric study .....	21
3.3.1 Laser Welding parameters .....	21
3.3.1.1 Laser Power .....	21
3.3.1.2 Beam diameter .....	21
3.3.1.3 Time duration .....	23
3.3.1.4 Weld Pressure .....	23
3.3.2 Weld Quality Parameters .....	25
3.3.2.1 Weld Diameter .....	25
3.3.2.2 Weld Strength .....	28
3.3.3 Effects of operating parameters on Weld Diameter .....	30
3.3.3.1 Influence of Laser Power on Weld Diameter .....	30
3.3.3.2 Influence of Pressure on Weld Diameter .....	36
3.3.3.3 Influence of Beam diameter on Weld Diameter .....	39

3.3.3.4 Influence of Time duration on Weld Diameter.....	43
3.3.4 Effects of operating parameters on Weld Strength.....	48
3.3.4.1 Influence of Laser Power on Weld Strength.....	48
3.3.4.2 Influence of Contact Pressure on Weld Strength.....	50
3.3.4.3 Influence of Time duration on Weld strength.....	53
3.3.4.4 Influence of Beam diameter on Weld strength .....	55
3.3.4.5 Influence of Laser Intensity on Weld Diameter and Weld Strength.....	58
3.4 Comparison of weld strength.....	61
3.4.1 Experimental setup for Tensile strength test of PGA non woven mesh.....	61
3.4.2 Experimental Run.....	62
3.4.3 Summary and Observations.....	64
3.4.3.1 Regression Analysis.....	67
CHAPTER 4 - Conclusion and future research .....	73
4.1 Conclusions.....	73
4.2 Future reserach.....	74
References.....	75
Appendix ‘A’: Tensile test specimen.....	78
Appendix ‘B’: Factorial Analysis .....	80

## List of Figures

Figure 1.1 Non-woven PGA scaffold structure .....	2
Figure 2.1 Tissue engineering approach involving scaffold biomaterial.....	4
Figure 2.2 Tissue engineered blood vessel implanted into a pig model .....	5
Figure 2.3 Formation of a tubular scaffold by P4HB solvent.....	8
Figure 2.4 Different joining techniques for polymers .....	9
Figure 2.5 Laser Transmission welding approach .....	10
Figure 2.6 Globo Welding concept.....	11
Figure 2.7 PGA based Biofelt scaffold.....	12
Figure 2.8 Tubular PGA scaffolds .....	12
Figure 3.1: Experimental setup for laser welding of PGA polymer scaffolds.....	14
Figure 3.2: Use of BK 7 Ball lens in the experimental setup.....	15
Figure 3.3: Experimental setup for creating tubular PGA scaffold.....	19
Figure 3.4: Tubular PGA scaffold.....	19
Figure 3.5: Laser Power Dial.....	21
Figure 3.6: Measuring beam diameters with burn paper.....	22
Figure 3.7: Measuring beam diameter with burn paper.....	22
Figure 3.8: Measuring Time with a Stopwatch.....	23
Figure 3.9: Measuring weld diameter for strong weld with hole formed .....	26
Figure 3.10: Measuring weld diameter for nice weld with melted region.....	26
Figure 3.11: Measuring weld diameter for No hole condition .....	27
Figure 3.12: Setup for measurement of weld strength .....	28
Figure 3.13: Optical images of welded holes with different laser power (a) Laser Power=70 W (b) Laser Power=75 W (c) Laser Power=80 W.....	32
Figure 3.14 Optical images of weld diameters with different laser power (a) Beam diameter=1mm (b) Beam diameter= 1.5 mm .....	34
Figure 3.15: Gaussian beam profile.....	35
Figure 3.16: Variation of weld diameter with laser power for beam diameter of 1 mm...35	
Figure 3.17: Variation of weld diameter with laser power for beam diameter of 1.5 mm.....	36

Figure 3.18: Variation of weld diameter with laser power .....	36
Figure 3.19: Optical images of weld diameters with different contact pressures	
(a) Beam diameter=1 mm (b) Beam diameter=1.5 mm.....	38
Figure 3.20: Variation of weld diameter with pressure for beam diameter of 1 mm.....	39
Figure 3.21: Variation of weld diameter with pressure for beam diameter of 1.5 mm....	39
Figure 3.22: Variation of weld diameter with pressure .....	40
Figure 3.23: Optical Images of weld diameters with different beam diameters	
(a) Laser Power=70 W (b) Laser Power=75 W.....	42
Figure 3.24: Variation of weld diameter with beam diameter for laser power of 70 W...	43
Figure 3.25: Variation of weld diameter with beam diameter for laser power of 75 W...	43
Figure 3.26: Variation of weld diameter with beam diameter .....	44
Figure 3.27: Optical images of weld diameters with different time duration	
(a) Beam diameter=1 mm (b) Beam diameter=1.5 mm.....	47
Figure 3.28: Variation of weld diameter with time duration for beam diameter of	
1 mm .....	47
Figure 3.29: Variation of weld diameter with time duration for beam diameter of	
1.5 mm .....	48
Figure 3.30: Variation of weld diameter with time duration.....	48
Figure 3.31: Optical images of weld diameter with different laser powers at beam diameter of 1.5 mm .....	50
Figure 3.32: Variation of weld strength with laser power.....	51
Figure 3.33: Optical images of weld diameter with different contact pressures at beam diameter of 1 mm.....	53
Figure 3.34: Variation of weld strength with pressure.....	53
Figure 3.35: Optical images of weld diameter with different time duration at beam diameter of 1.5 mm .....	55
Figure 3.36: Variation of weld strength with time duration .....	55
Figure 3.37: Optical images of weld diameter for different beam diameter .....	57
Figure 3.38: Variation of weld strength with beam diameter .....	58
Figure 3.39: Variation of weld strength with laser intensity.....	59
Figure 3.40: Variation of weld strength with laser intensity.....	59

Figure 3.41: Variation of weld diameter with laser intensity.....	60
Figure 3.42: Variation of weld diameter with laser intensity.....	60
Figure 3.43: Experimental setup for tensile test of PGA .....	61
Figure 3.44: PGA Biofelt sample placed between the pneumatic fiber grips .....	62
Figure 3.45: PGA Biofelt fibers breaking at maximum load during tensile test .....	63
Figure 3.46: Verification plot for weld diameter .....	69
Figure 3.47: Verification plot for weld strength .....	71
Figure 3.48: Residual Plots for weld diameter and weld strength .....	72
Figure 3.49: Tensile test specimen before loading .....	79
Figure 3.50: Tensile test specimen after loading .....	79
Figure 3.51: Main Effects plot for Weld diameter.....	85
Figure 3.52: Main Effects plot for Weld Strength.....	85
Figure 3.53: Interaction plot for Weld diameter .....	86
Figure 3.54: Interaction plot for Weld Strength .....	86

## List of Tables

Table 3.1 Operating conditions for welding experiments.....	16
Table 3.2 Operating parameters at different levels.....	17
Table 3.3 Test conditions for creating welds on PGA felt.....	18
Table 3.4 Operating conditions for the creation of various cylindrical tubes.....	20
Table 3.5 Mechanical properties of BK 7 and silicon nitride.....	25
Table 3.6 Contact properties under different loading conditions .....	25
Table 3.7 Weld conditions for beam diameter of 1 mm .....	31
Table 3.8 Weld conditions for beam diameter of 1.5 mm .....	33
Table 3.9 Weld conditions for beam diameter of 1 mm .....	37
Table 3.10 Weld conditions for beam diameter of 1.5 mm .....	37
Table 3.11 Weld conditions for laser power of 70 W.....	41
Table 3.12 Weld conditions for laser power of 75 W.....	41
Table 3.13 Weld conditions for beam diameter of 1 mm .....	45
Table 3.14 Weld conditions for beam diameter of 1.5 mm .....	45
Table 3.15 Weld conditions and results for laser power.....	49
Table 3.16 Weld conditions and results for contact pressure .....	52
Table 3.17 Weld conditions and results for time duration.....	54
Table 3.18 Weld conditions and results for beam diameter.....	56
Table 3.19 Tensile stress values.....	63
Table 3.20 Types of Welds Obtained .....	64
Table 3.21 Verification of weld diameter values.....	68
Table 3.22 Verification of weld strength values.....	70

## **ACKNOWLEDGEMENTS**

I would like to express my sincere thanks to my advisor Dr. Shuting Lei, for all his encouragement and support throughout the duration of this research. He has been a wonderful advisor and great person to work with always motivating, supporting and guiding me in all facets of life. It has been a sincere privilege to work under his guidance and learn important things that molded me as a better person and be successful in my present job. I would also like to thank Dr. Mark Weiss, Dr Shing I. Chang and Dr. Zenghu Chang for all their suggestions and valuable inputs. In all without their active support, guidance and encouragement, this thesis would not have been possible.

I would also like to acknowledge Dr. Bradley Kramer, Head of the Department, and the entire Industrial and Manufacturing Systems Engineering Department at KSU for giving me an opportunity to pursue my Masters and making my stay a wonderful learning experience.

I also extend my sincere gratitude and appreciation to my research colleague Brant, who devoted countless hours and assisted me for conducting experiments.

Finally, I would like to thank my parents, family and friends who have been a source of confidence, guidance, providing me with all their love and support throughout my life in all my endeavors.

## **CHAPTER 1 – Introduction**

Atherosclerosis is one of the most severe forms of heart disease which results in narrowing of the arteries. Replacement of diseased arteries by cardiac bypass or peripheral bypass surgery is the most common method for coronary circulation [1]. There has been an increasing interest to develop artificial and biological replacements for such arteries and small diameter vascular grafts are one of the emerging discoveries in the treatment of this particular kind of heart disease.

A vascular graft should ideally have sufficient mechanical strength, blood compatibility, a structure that does not permit hemorrhage through the wall, and good suture retention [2]. Poly (ethylene terephthalate) (polyester or Dacron) or expanded polytetrafluoroethylene (ePTFE Teflon) are the most common synthetic polymer materials used in the preparation of vascular grafts. These materials have been effective for large diameter grafts but are not conducive for vessels having an inner diameter less than 6 mm.

Tissue Engineering has received considerable attention since the last few years and has been labeled as one of the more promising domains within the broader field of 'biotechnology' [3]. The use of tissue engineered small diameter blood vessels is gaining wide acceptance as they overcome the limitations such as risk of infection and mechanical property mismatches. The tissue engineered materials such as collagen gel based grafts, decellularized grafts, cell-polymer constructs and completely biological grafts are used for replacement of diseased arteries and all these materials share a common goal of providing sufficient mechanical integrity in order to sustain the systemic arterial pressures. However, the most common tissue engineered materials for cardiovascular treatment are the biodegradable cell-polymer constructs.

Polyglycolic acid (PGA) scaffold is a popular synthetic biodegradable polymer that is used in these constructs and possesses many favorable properties such as biocompatibility, bioabsorbability, and high tensile strength. The biodegradable scaffold plays a vital role acting as a matrix that provides the cells with specific tissue environment and architecture [4]. Polyglycolic acid (PGA) scaffolds have large void volumes that support cellular infiltration, cellular attachment, and extracellular matrix deposition. This material degrades over time and loses its mechanical integrity during the first 3 weeks in tissue culture or other aqueous conditions [5]. Figure 1.1 shows a non-woven PGA scaffold structure that is used in the field of tissue engineering. Vacanti and coworkers [5, 6, 7] investigated the use of PGA tubular scaffolds for culturing small diameter vascular conduits. The polymer scaffold degrades after 8 weeks and is replaced by a dense smooth muscle cell medial layer and an inner endothelial lining. The engineered vessels possess burst pressures of more than 2000 mmHg and also most of the physiological and mechanical characteristics of the native arteries. The PGA scaffolds can be manufactured in many forms with their required characteristics for specific applications. Fiber scaffolds are more commonly used in the field of vascular tissue engineering as the fiber meshes have large surface area, volume ratio and high porosity [8]. Polymer extrusion and textile processing are the traditional fabrication methods for creating the PGA scaffolds which are non woven in nature.

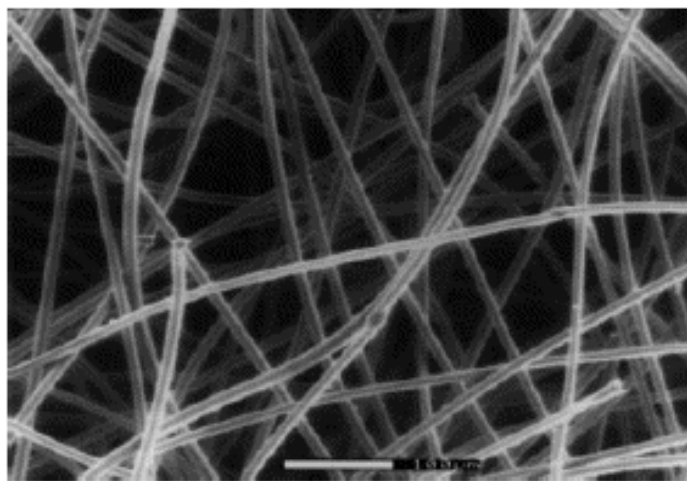


**Figure 1.1: Non-woven PGA scaffold structure [9]**

Joining these fabricated non woven meshes of polymer scaffolds is an area of interest. Currently there are various methods being used, such as needling, thermal bonding, use of external binders, sewing, etc. Each method has its own advantages and disadvantages. Some of the disadvantages include limited melt viscosity at the bonding interface, weak inter-fiber attachments, reduced web loft, limitation of amount of available space for tissue in growth, properties conforming to the binder material, difficulty in obtaining a regular pore size and creation of complex 3-D scaffolds. Therefore, there is an increasing need towards developing a better joining technique that will overcome the limitations of the existing methods and provide a novel joining process that is flexible, easy, fast, and does not affect the structural and mechanical properties of the scaffold.

The applications of laser welding technology have been numerous and extend from manufacturing to biomedical engineering because of the many advantages that this method provides such as short process times, non contact and binderless process, absence of process induced vibrations and minimal contamination [10]. Since laser welding offers many advantages over other conventional techniques, we attempt to develop a laser welding technique for joining non woven polymer fiber sheets and create 3-D scaffolds like tubular structures. Therefore, the objective in this research is to conduct a fundamental study of laser welding of PGA scaffold biofelt sheets and to create tubular scaffold structures that would be useful in the area of vascular tissue engineering for the repair of damaged arteries or blood vessels.

## Chapter 2 - Literature review

### 2.1 Scaffolds in Tissue Engineering

Tissue engineering is a promising field and aims to purposefully induce the growth of new functional tissues, rather than just replacing diseased or injured tissues with nonviable implantable parts [11]. A matrix or scaffolding guides the tissue development and regeneration by assisting in the formation of new and functional living tissues using living cells that are associated with each other [12]. According to Ma [13], there are three approaches in tissue engineering: (1) the use of isolated cells or cell substitutes to replace those cells that supply the needed function; (2) the delivery of tissue inducing substances, such as growth and differentiation factors, to targeted locations; and (3) growing cells in three dimensional scaffolds. The three dimensional scaffold that contains these cells is then delivered in the patient's body to assist in new tissue formation, after which the scaffold degrades over time. Figure 2.1 shows the approach in which cells are seeded onto the scaffold biomaterial which is then implanted with growth factors and specific nutrients in a bioreactor. The engineered tissue is then transplanted in the patient's body to facilitate the formation of functional tissues and organs.

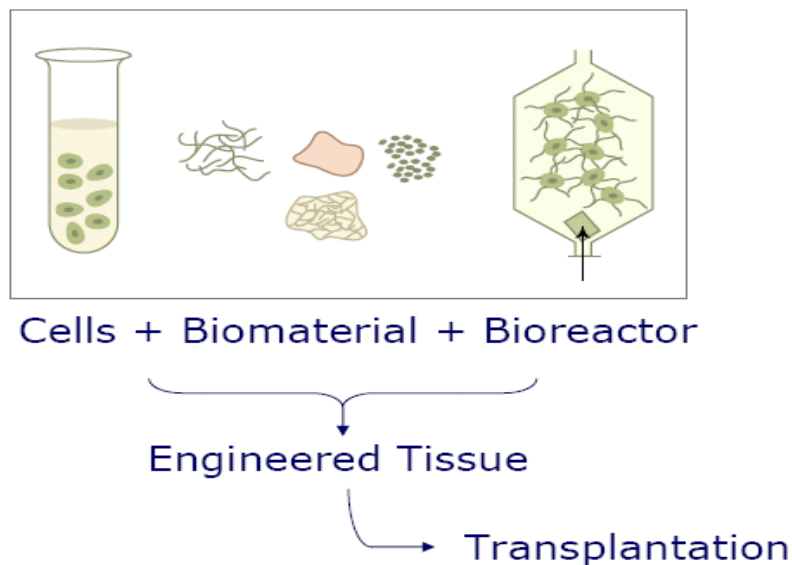
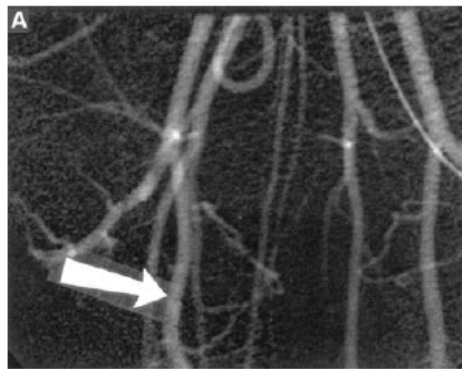


Figure 2.1: Tissue engineering approach involving scaffold biomaterial [14]

The desirable characteristics for any type of scaffold material in the field of tissue engineering are biocompatibility (i.e., not to provoke any unwanted tissue response to the implant), high porosity and proper pore size, high surface area, structural strength and mechanical integrity to maintain the predesigned tissue structure, manufacturing feasibility and biodegradability (i.e., degradable into nontoxic products, leaving the desired living tissue) [12, 15, 16, 17]. The scaffold materials can be made up of natural polymers, synthetic polymers, ceramics, metals, or combinations of these materials [12, 18, 19]. Naturally occurring scaffold material examples include collagen, glycosaminoglycans (GAGs), chitosan and alginates. Synthetic scaffold material examples include polymers, ceramics, glasses and bioactive glasses. The scaffolds used in the field of tissue engineering possess different properties such as porosity and pore size, biodegradability and biocompatibility, surface properties, and mechanical properties.

The tissue engineered scaffolds are used in a variety of clinical applications like bone repair, cartilage repair, nerve repair, skin repair, gene therapy cells and vascular repair [20]. In this research we concentrate only on the PGA fiber felts that are used as vascular grafts in the area of vascular tissue engineering for the repair of blood vessels. Figure 2.2 shows vascular graft used in the tissue engineering of blood vessels in an autologous pig model where smooth muscle cells are seeded into porous PGA tubes and cultured under different pulsing conditions. As a result the tissue engineered arteries last for more than 3 weeks without occluding.



**Figure 2.2: Tissue engineered blood vessel implanted into a pig model [12].**

## 2.2 Current techniques for joining the non woven meshes

### *Needling:*

Non woven PGA meshes are produced from the multifilament yarn by polymer extrusion, stretching and relaxation at high temperatures. The yarn is then crimped, cut, carded and needled to entangle the fibers and lock them in order to create a non woven fiber mesh. The sheets of non woven PGA fiber meshes are then needled together to form different shapes such as tubular structures with the application of heat by the heated plates and thereby increasing the dimensional stability of the overall structure [21]. But the main drawback of this method is that it is difficult to obtain a regular pore size.

### *Spray casting:*

In this technique, non woven meshes of PGA fibers are attached to a rotating Teflon cylinder. The scaffolds are joined and reinforced by spray casting with a solution of polylactic acid (PLA) or co-polymer of PGA and PLA called (PLGA) and results in a thin coat that bonds the cross points of the PGA fibers [22]. The behavior of the transplanted cells is then determined by the PLA or PLGA coating instead of the PGA mesh. Mechanical strength is provided by both the coating and the fibers and is designed in such a way to withstand mechanical stresses or composite degradation of PLA or PLGA. This method is useful only for the fabrication of thin scaffolds and a major drawback is that this method does not allow the creation of complex three dimensional scaffolds as the coating is very thin.

### *Fusion:*

The fusion technique helps in the fabrication of tubular scaffolds made of PLGA polymers. The porous PLGA membranes obtained from solvent casting and particulate leaching method are used and wrapped around a Teflon cylinder. The overlapping ends of the fibers are fused together with chloroform that acts as a binder. The Teflon core is then removed to leave a hollow tube [23]. This technique is used to shape the scaffolds into three dimensional 3-D structures but the drawback is that it is limited only to tubular

scaffolds with a low ratio of wall thickness to inner diameter because of the relatively brittle nature of the porous membrane used.

#### *Fiber Bonding:*

The PGA non woven mesh obtained from textile processing is casted with a solution of PLLA dissolved in methylene chloride [24]. The solvent is allowed to evaporate and the construct is then heated above the melting point of PGA. When the PGA-PLLA constructs cool, PLLA is removed by dissolving in methylene chloride. This process results in the mesh of PGA fibers being joined at their cross points. The disadvantage is that this technique cannot be used to create 3-D scaffold structures.

#### *Use of external binder:*

External binders are used for the joining of fibers along with some application of pressure [25]. This technique results in production of complex three dimensional scaffold structures but the main drawback includes uniformity of binder distribution throughout the non woven web causing the properties of the entire web to become limited by the properties of the binder.

#### *Thermal Bonding:*

In one of the thermal bonding techniques, a non woven web is formed from 50% PGA: 50% TMC copolymer. The web is then compressed under 0.14 MPa (20 psi) pressure to reduce porosity and cut into rectangles of 2.25 cm by 1.75 cm. These sheets are then wrapped around a 4 mm stainless steel mandrel creating a tube with an overlapping seam. This seam is then pressed together using moderate finger pressure allowing the membrane to bond at this point. The membranes and mandrels were then placed in an oven, preheated to 70 °C for one hour and then removed. When the resulting seam bond of a selected sample was checked with tweezers, it appeared to have strength similar to that of the starting web. The application of heat and pressure causes a localized melting of the fibers and allows for fusion of the non woven web filaments at the fiber crossover points [26].

This technique has several limitations such as limited melt viscosity at the bonding interface, relatively weak inter-fiber attachments, compression under heat reduces web loft therefore increasing the apparent or overall density and limiting the relative amount of overall space available for tissue in growth.

*Sewing:*

The scaffold is sewn into a cylindrical construct with the help of 6-0 PGA suture (US Surgical, Norwalk, CT) around a cylindrical tube that acts as a support [27]. This technique creates an axially aligned suture line on each vessel. The major drawback is that the PGA tube primarily fails by tearing along the suture line, at the region of highest polymer concentration and highest stress.

*Use of P4HB solvent:*

In this technique, sheets of PGA having dimensions of approximately 80 x 5 x 1 mm are wrapped around a rod having a diameter of 3 mm. The ends of the sheet are secured with suture and the whole setup is dip coated in a 1w/v% P4HB solution as shown in Figure 2.3.

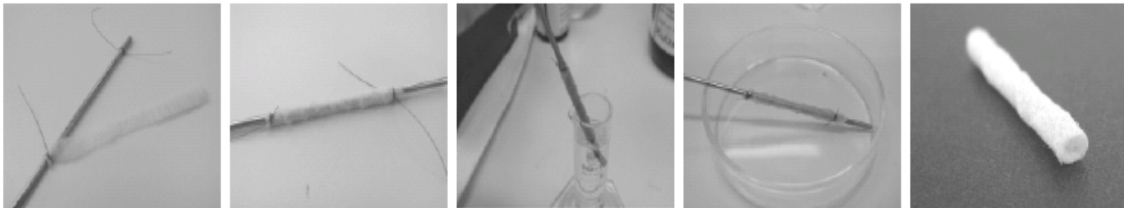


**Figure 2.3: Formation of a tubular scaffold by P4HB solvent [28]**

After evaporation of the solvent, the tubular construct can be removed from the rod. The solvent remnants which may sometime be present can be removed by drying the scaffolds under vacuum [28]. The PGA sheet has to be carefully wrapped around the rod so that the turns are close to each other and results in a well connected uniform tube. This technique results in a thick layer that helps in improving the mechanical properties of the scaffold. The drawback is that dense outer layer causes complications in cell seeding.

## 2.3 Laser Welding of Polymers

There are various methods available for welding polymers as shown in Figure 2.4. An ideal welding technique should be applicable to different joint configurations, taking into consideration of small and large bonding areas, flexible for automation and on-line inspection, and providing reproducible, strong, and reliable welds at optimal cost [29].

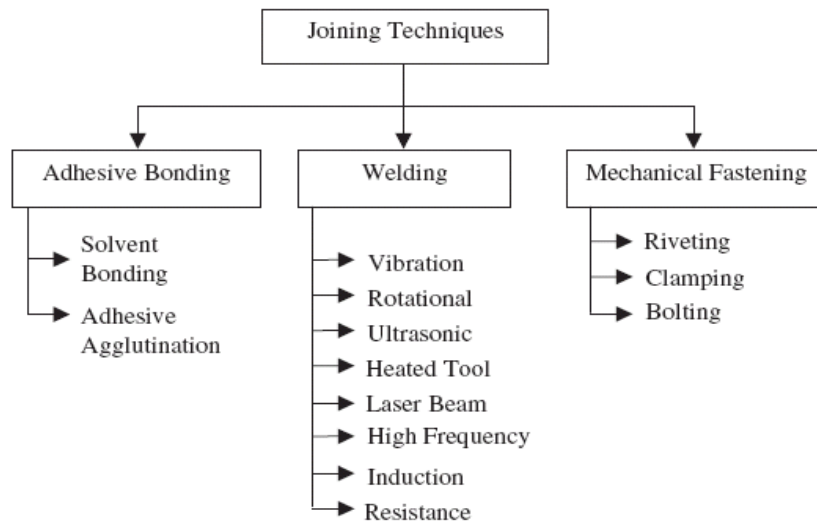


**Figure 2.4: Different joining techniques for polymers [29]**

Laser welding seems to be a promising technique in this sense. In laser welding of polymers, the energy must be harnessed and converted into heat. Laser light must be absorbed at the joint interface to generate enough heat to produce a weld. The use of lasers in welding of thermoplastic textiles can be an alternative to the traditional method like sewing. The main benefits of laser welding of polymers are as follows:

- Ability to weld all thermoplastic textiles including nylon, PP and polyester
- Weld strength capable of reaching the strength of the parent material
- Clean, aesthetically pleasing seam appearance
- Enabling the sewing and seam sealing process to be combined into one
- High Energy – allows for high processing speeds

- Clean – non-contact allows total process to remain clean from debris and overheated material
- Flexible – various methods of beam delivery allow for easy changeover from one part to the next
- Controllable – the laser light is very easy to control and allows for precise delivery of the correct amount of energy
- Easy to automate – laser can be integrated with a robot for automatic control

Yousefpour [30] and coworkers investigated the laser welding of thermoplastic polymers and their composite parts. The laser beam passes along the bondline of the two pressed parts. During this process some of the polymer burns along its path and leaves a thin layer of molten polymer at the bond line. The whole melt is brought together under pressure and allowed to solidify resulting in a weld. Laser transmission welding [31, 32] is another technique for welding polymers like thermoplastic materials. There are two parts namely top (transmissive) and bottom (absorbent) part. The laser beam penetrates the top laser-transmissive thermoplastic and is converted into heat by either a bottom laser absorbent thermoplastic or by a laser absorbent dye at the weld interface. The pressure is applied by an external force which clamps the two parts and allows for the conduction of heat to form a bond. Thermal expansion in the welding zone creates an internal pressure and leads to a strong weld between the parts. Figure 2.5 shows the laser transmission welding approach as discussed above.

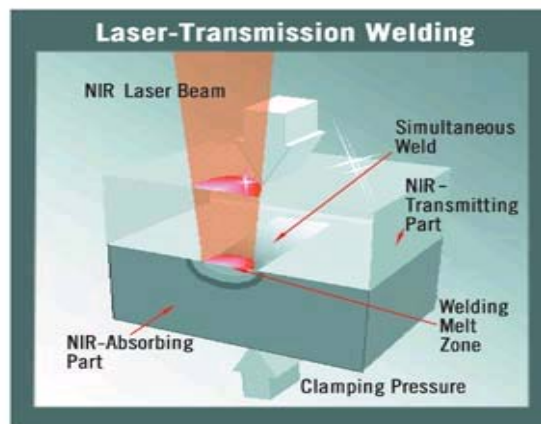


**Figure 2.5: Laser transmission welding approach [32]**

In laser welding of plastics, among the various methods like contour, quasi-simultaneous, mask and simultaneous welding, the most flexible method is the spot or contour welding. In this method, the laser is focused onto a single point that is then traced along the length of the weld. This spot can be anywhere from 0.6 to 5 mm in diameter and moved along the weld line. The workpiece can be fixed to an X-Y table or the laser can be attached to a robotic arm, or a combination of the two. The current trend is towards using diode or fiber lasers transmitting light in the 810 to 980 nanometer wavelength range [33].

An example of laser contour welding is Globo welding as illustrated in Figure 2.6. A laser beam is focused at a point on the plane via an air bearing, frictionless, freely rotating glass sphere [34]. The glass sphere is used to focus the laser beam on the joining surface and also act as a clamping tool. The sphere applies continuous pressure at a point on the joining surface while rolling on it and the laser beam is also focused only at the point where the contact pressure is applied. The glass sphere replaces the mechanical clamping device and expands the scope of laser welding for both continuous and three-dimensional applications.

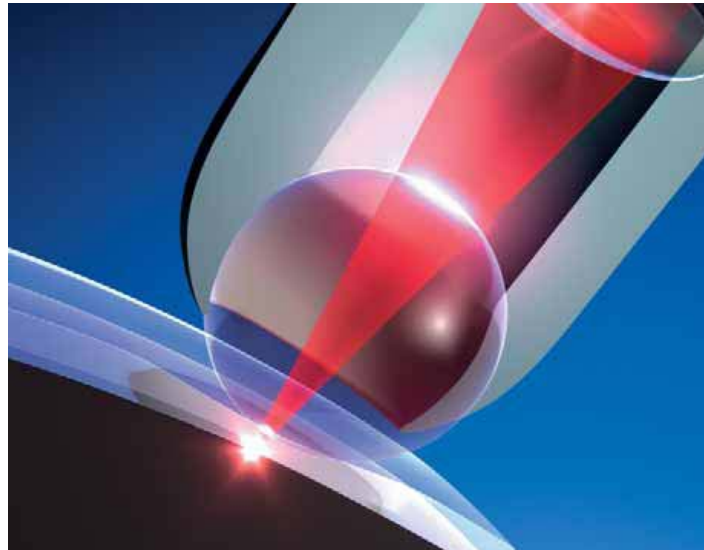


**Figure 2.6: Globo welding concept [34]**

## 2.4 PGA based Biofelts

BIOFELT(TM) as shown in Figure 2.7 is a branded absorbable 3D non-woven PGA felt scaffold manufactured at Concordia Manufacturing, LLC. This PGA felt scaffold can rapidly grow cells and form an organized 3D tissue structure. It has a porosity factor of >97% and excellent flexibility and softness. The standard size is 20 cm x 30 cm felts with thickness in the range from 1 to 5 mm and bulk density in the range from 25 to 100 mg/cc [35]. There are numerous uses of these felts and they can be used for ligament replacement, vessel replacement, localized radiation and common tissue repair. These felts are designed to support the growth of stem cells teased out of fat cells. The company makes tubular scaffolds as shown in Figure 2.8 from these PGA felts by a seaming process with punched needles [35]. The tubular scaffold is denser at the seams and the lead time to make these tubes is about 2 weeks with an additional cost of \$ 200 per tube. This structure can be put in a bioreactor where the blood cells can be taken from a patient's body and grown. The cells get differentiated and are grown into a suitable vascular structure.



**Figure 2.7: PGA based Biofelt scaffold [35]**



### **Figure 2.8: Tubular PGA scaffolds [36]**

In this research, we are going to use these PGA Biofelt scaffolds with the following specifications: dimension of 20 cm x 30 cm felt, thickness of 1mm and mass density of 50 mg/cc. A continuous wave (CW type) diode laser with a central wavelength of 937 nm will be used to create a series of spot welds in order to make a tubular scaffold.

## **2.5 Research Objectives**

The goal of this research is to develop a laser spot welding process for PGA (polyglycolic acid) based scaffold felts which are non-woven. The specific objectives of this study can be summarized in the following way:

- 1) To carry out a fundamental study of laser welding of PGA scaffolds.
- 2) To design an experimental setup and conduct experiments for the laser welding of non-woven PGA fiber felts.
- 3) To determine the operating process parameters and measure their effects on the weld quality wherein the weld quality is characterized in terms of weld diameter, discoloration and weld strength.

This thesis is organized in the following manner. Chapter 2 gives a brief literature review on the background of scaffolds in tissue engineering, the existing joining techniques for attaching the non woven fibers, and laser welding processes of polymers. Chapter 3 deals with the experimental setup and laser welding experiments. The results obtained from the experiments will be analyzed to determine the influences of the process parameters on the weld quality. The weld strength will be compared with the original tensile strength of the PGA material. A regression analysis will be done based on the results obtained and a regression model thus derived will be used to help optimize the laser welding process. Finally, the conclusions and future work will be summarized in Chapter 4.

## CHAPTER 3 - Laser welding of PGA scaffold Bio Felt

### 3.1 Experimental setup

Laser welding of the biodegradable PGA Biofelt is carried out with the experimental setup as shown in Figure 3.1. In this setup the high power diode laser system (central wavelength of 937 nm, continuous wave output and power range 0-500 W) is used.

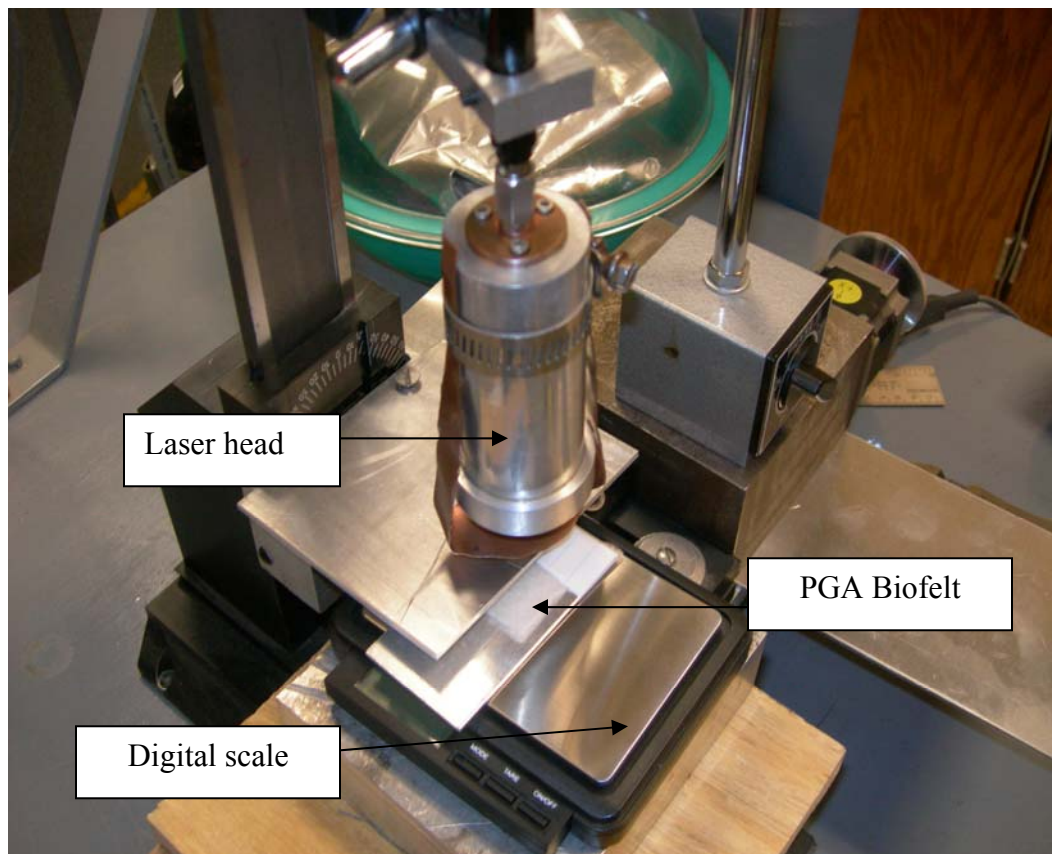


**Figure 3.1: Experimental setup for laser welding of PGA polymer scaffolds**

In our experiments, the sample sheets of PGA fiber felt are mounted on top of a silicon nitride ceramic plate that is placed on the digital scale. The scale is in turn mounted on the translation stage of a CNC controlled worktable and a computer controls its movement. The laser power is varied from 0-100 W. A ball lens made of BK 7 glass having a diameter of 5 mm is used to control the spot size at the focal plane as shown in

Figure 3.2. The laser spot size varies from 1 to 2 mm from our measurements in Section 3.3.1.2. The fixture is designed in such a way that the laser beam is focused vertically down from the ball lens onto the sample. A flat plate having a beveled hole with the diameter of 4 mm is attached to the setup in order to apply load on the ball lens and permit the laser beam to pass through the cavity. The applied load is measured using the digital scale. The laser beam diameter is determined with the help of a burn paper at a constant power of 80 W and fixed time duration of 1 sec below the ball lens at a distance of 0.5 mm. A stopwatch is used to record the time duration for which the laser is on at different levels of power.

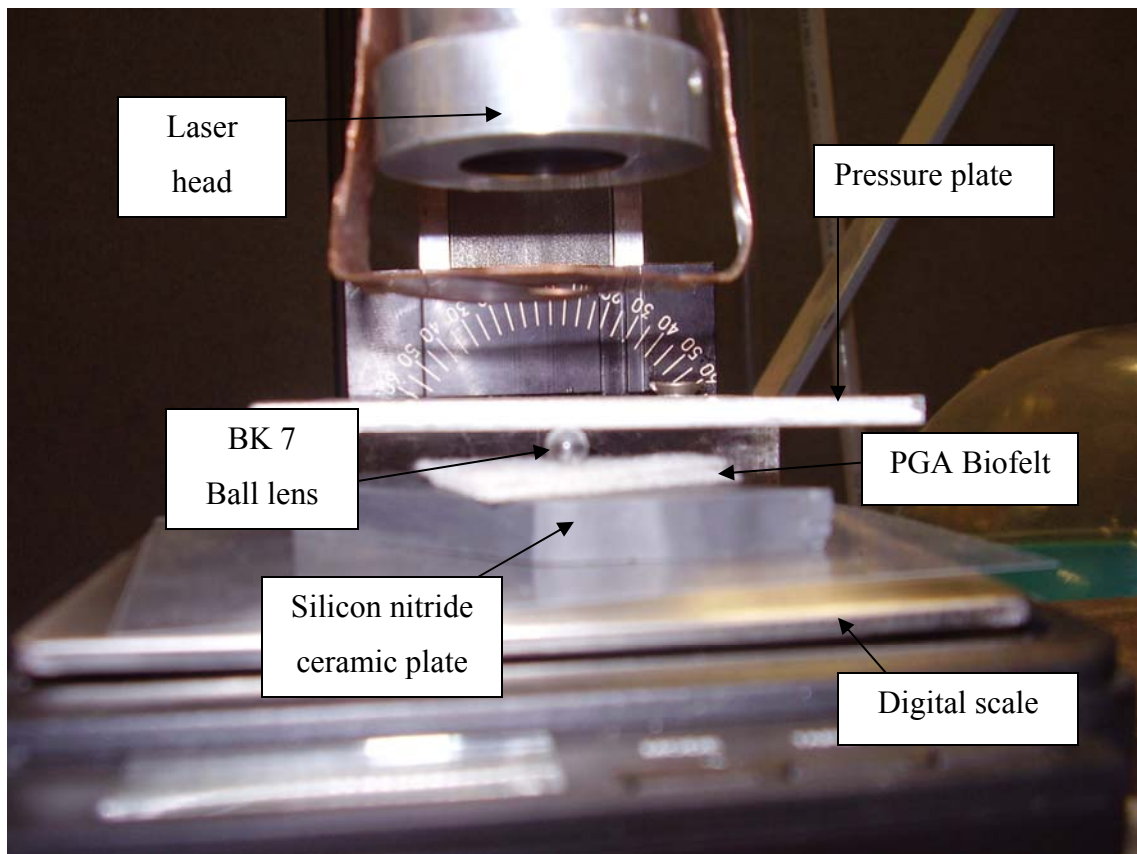


**Figure 3.2: Use of BK 7 ball lens in the experimental setup**

## 3.2 Types of Experiments

### 3.2.1 Creation of spot welds using BK 7 ball lens

In our experiments different spot welds are created on the PGA fiber felts using various operating parameters. Since it is difficult to come up with proper conditions while welding these sensitive fibers, in order to determine the suitable conditions several parameters need to be considered like laser power, beam diameter, time duration and weld pressure. The optimal conditions for creating a successful weld with good weld qualities such as high strength, no discoloration and medium weld diameters are obtained by carrying out a design of experiment. Table 3.1 shows the operating conditions for laser welding experiments.

**Table 3.1 Operating conditions for welding experiments**

Laser welding parameters	Laser power (W)	70, 75, 80
	Beam diameter (mm)	1, 1.5, 2
	Time duration (sec)	5, 10, 15, 20
	Pressure (MPa)	26, 29, 31
Work Specimen	Two sheets of PGA polymer felts placed on top of each other having dimensions of 3.1 x 2.8 mm	
Support Base	The two sheets of PGA fibers are placed on top of a silicon nitride ceramic plate.	

### 3.2.1.1 Design of welding experiment

The welding conditions are selected after some initial testing such that proper welds without any discoloration and holes are generated. Different patterns can be obtained with the help of these conditions such as cylindrical tubes with a series of spot welds in a sequential manner. For the design of welding experiments the operating conditions are selected as shown in Table 3.1 and a full factorial design is carried out to determine the number of runs. In our experiments there are four factors out of which three factors namely laser power, beam diameter and pressure are at three levels and the last factor time duration is at four levels as shown in Table 3.2.

**Table 3.2 Operating parameters at different levels**

Level	Level [1]	Level [2]	Level [3]	Level [4]
Laser power (W)	70	75	80	
Beam diameter (mm)	1	1.5	2	
Pressure applied (MPa)	26	29	31	
Time duration (sec)	5	10	15	20

Based on the factorial design, a total of 108 experimental runs are obtained to carry out the experiments. However, under certain conditions, excessive discoloration, large holes and lens damage are noticed. These conditions are thus considered unacceptable and removed from the factorial design. The final experimental conditions chosen are outlined in Table 3.3. The values 1, 2, and 3 indicate the different levels of the various operating factors such as level [1], level [2], and level [3]. The runs are randomized and based on the ANOVA analysis and p-value statistics it is observed that the main factors are laser power, beam diameter, pressure and time duration. The interaction effects of the operating parameters are negligible and considered insignificant based on the p-values obtained.

**Table 3.3 Test conditions for creating welds on PGA felt**

Std Order	Run Order	Pt Type	Blocks	Power (W)	Beam Diameter (mm)	Time Duration (sec)	Pressure (MPa)
12	1	1	1	1	2	3	2
6	2	1	1	1	1	3	2
17	3	1	1	2	1	3	1
7	4	1	1	1	2	1	1
9	5	1	1	1	2	2	1
26	6	1	1	3	1	1	2
22	7	1	1	2	2	2	2
16	8	1	1	2	1	2	2
23	9	1	1	2	2	3	1
14	10	1	1	2	1	1	2
19	11	1	1	2	2	1	1
2	12	1	1	1	1	1	2
34	13	1	1	3	2	2	2
25	14	1	1	3	1	1	1
1	15	1	1	1	1	1	1
30	16	1	1	3	1	3	2
36	17	1	1	3	2	3	2
20	18	1	1	2	2	1	2
24	19	1	1	2	2	3	2
11	20	1	1	1	2	3	1
8	21	1	1	1	2	1	2
3	22	1	1	1	1	2	1
27	23	1	1	3	1	2	1
15	24	1	1	2	1	2	1
33	25	1	1	3	2	2	1
31	26	1	1	3	2	1	1
4	27	1	1	1	1	2	2
32	28	1	1	3	2	1	2
28	29	1	1	3	1	2	2
18	30	1	1	2	1	3	2
5	31	1	1	1	1	3	1
21	32	1	1	2	2	2	1
10	33	1	1	1	2	2	2
35	34	1	1	3	2	3	1
29	35	1	1	3	1	3	1
13	36	1	1	2	1	1	1

**3.2.1.2 Creation of cylindrical tubes**

Cylindrical tubes can be created out of these PGA felt sheets with the help of laser spot welding. The experimental setup as shown in Figure 3.3 is used to carry out the welding process. A cylindrical rod made of silicon nitride having diameters of 5 mm and 10 mm is used as the base material, on which the PGA fiber sheet is rolled. The laser

beam is focused using the BK 7 ball lens onto the ends of the fiber sheet in order to create a series of spot welds.

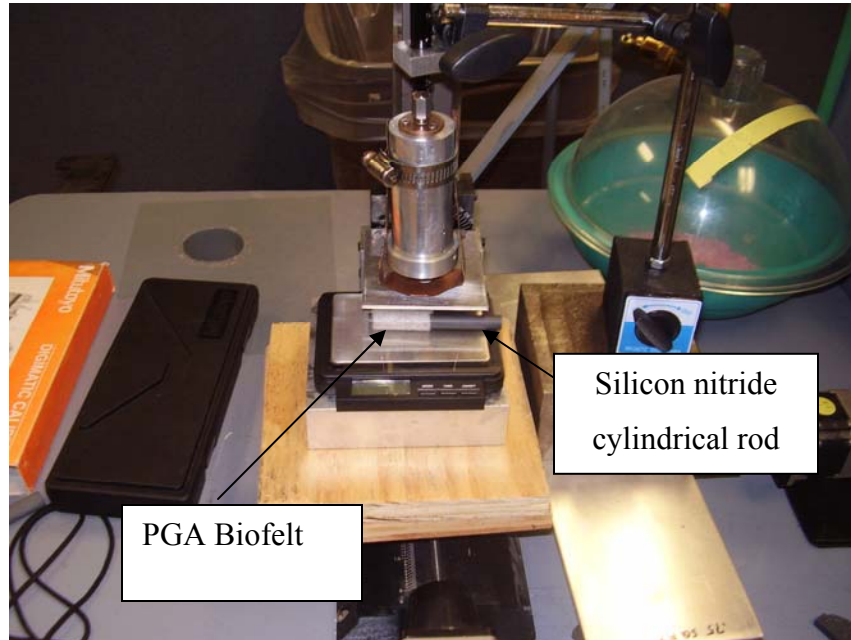


**Figure 3.3: Experimental setup for creating tubular PGA scaffold**

Based on the results obtained from the experiments, the conditions that are favorable in creating successful welds without discoloration, having adequate weld strength and optimal weld diameter are used in this case for creating spot welds such that a cylindrical tubular scaffold is obtained as shown in Figure 3.4.



**Figure 3.4: Tubular PGA scaffold**

Different samples (e.g. varied lengths and diameters) of these tubular PGA scaffolds are obtained by carrying out the laser spot welding.

**Table 3.4 Operating conditions for the creation of various cylindrical tubes**

Tubular scaffold dimensions	Laser Power (W)	Beam Diameter (mm)	Time Duration (sec)	Pressure (MPa)
Diameter 6 mm	70	1	5	26
Diameter 7 mm	75	1.5	5	26
Diameter 10 mm	75	1.5	5	29

Table 3.4 gives a list of operating conditions that yield welds to form tubular scaffolds. The diameters of the tubular scaffolds obtained are 6, 7 and 10 mm and corresponds to the diameter of the cylindrical silicon nitride mandrels that we used in the experiment. It is possible to get dimensions of different diameters of the tubular scaffold based on the diameter of the cylindrical mandrel around which the PGA biofelt is wrapped. The laser power when used in the lower range such as 70 and 75 W along with other parameters gives a good weld. Higher power of 80 W with a combination of other factors lead to holes being burnt or discoloration and the reason is explained in the next section while performing the design of experiments. The beam diameter is operated at Level [1] and Level [2] along with other parameters and yields favorable weld conditions. At Level [3] the highest beam diameter corresponds to a weak weld or no weld condition as the distance between the laser source and the PGA specimen is too large. As the distance between the laser source and the target material increases the concentration of the laser radiation on the PGA material decreases and hence leads to weaker or no weld conditions. The time duration is operated at Level [1] and Level [2] in order to achieve good welds within a short time duration. It is desired that we operate the laser welding process with faster processing times. The pressure is also operated at a low level that is at Level [1] since at higher levels in combination with other factors, the welds obtained are not favorable as they lead to holes being formed or discoloration and is explained in the next section.

### 3.3 Laser Welding – a parametric study

#### 3.3.1 Laser Welding Parameters

##### 3.3.1.1 Laser Power

Laser Power is an important parameter in welding applications. The laser power output from the laser system ranges from 0 to 500 W. By turning the laser power dial button in a clockwise direction and operating it in a manual mode, we obtain the laser power in an increasing manner. The Beam On button as shown in Figure 3.5 on the front panel is pressed to activate the laser beam at a specified power level to carry out the welding operations. In our experiments the maximum laser power is 80 W.



**Figure 3.5: Laser Power Dial**

##### 3.3.1.2 Beam Diameter

The beam diameter is measured with the help of a burn paper. The laser beam is focused with a ball lens on the burn paper as shown in Figure 3.6 and the distance of the laser source from the ball lens denoted by  $h$  mm is varied in order to obtain different beam diameters. The burn paper is kept below the ball lens at a distance of 0.5 mm. The laser power is operated at 80 W for a period of 1 sec and the holes formed on the burn paper as shown in Figure 3.7 are then measured with a digital microscope to get the beam diameter readings. In our experiments the beam diameter is varied from 1 to 2 mm.

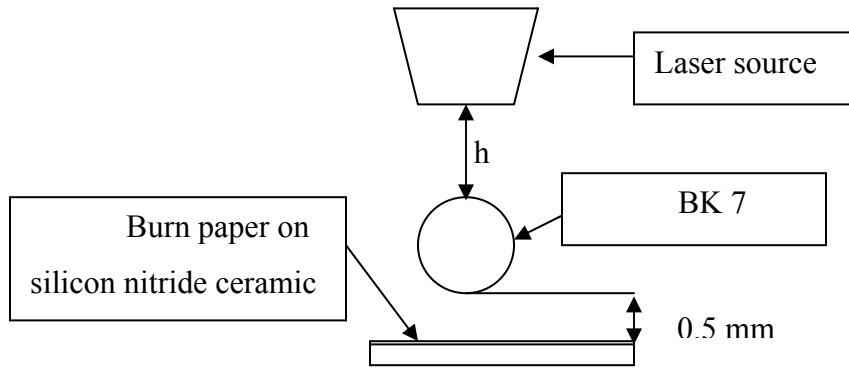


**Figure 3.6: Measuring beam diameter with burn paper**

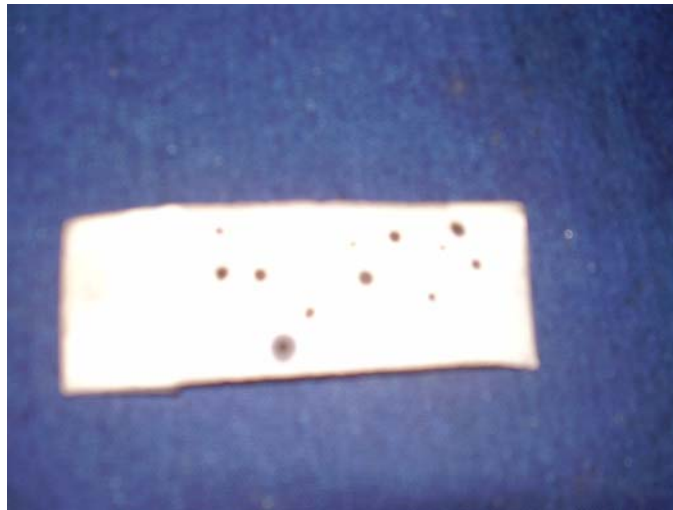


**Figure 3.7: Measuring beam diameters with burn paper**

### 3.3.1.3 Time Duration

The time duration for which the laser beam is turned on at a specified laser power is measured using a stopwatch as shown in Figure 3.8. As soon as the Beam On button is pressed, the stopwatch is started simultaneously to determine the amount of time for which the material or the specimen is exposed to the laser beam. The time duration in our experiments is varied from 5 to 20 sec.



**Figure 3.8: Measuring time with a stopwatch**

### 3.3.1.4 Weld Pressure

The pressure required for carrying out the spot welding process is determined by dividing the load applied on the ball lens by the area of contact on the base material. To determine the contact area, we follow some assumptions of the Hertz theory and perform calculations based on the load applied. When two smooth nonconforming surfaces initially come in contact, they touch at a single point [Johnson, 1985]. As the load increases, deformation occurs in the area of that point, the area of contact grows, and so does the distribution and magnitude of surface tractions.

During this process, Hertz theory predicts the shape and area of contact, as well as the distribution and magnitude of surface tractions over the surface. The relative radius of curvature of the two contacting bodies is given by

$$\frac{1}{R} = \frac{1}{R_1} + \frac{1}{R_2} \quad (3.1)$$

where  $R_1$  is the radius of the BK 7 ball lens and  $R_2$  is the radius of the contacting object.

When the ball lens and the silicon nitride base material containing the PGA non woven biofelt come into contact, with a known load  $P$ , the resulting contact area has a radius of  $a$ ,

$$a = \left( \frac{3PR}{4E^*} \right)^{1/3} \quad (3.2)$$

$$\frac{1}{E^*} = \frac{1-\nu_1^2}{E_1} + \frac{1-\nu_2^2}{E_2} \quad (3.3)$$

where  $E_1$  is the modulus of elasticity of the silicon nitride plate and  $E_2$  is the modulus of elasticity of the BK 7 ball lens.  $\nu_1$  is the Poisson's Ratio for the silicon nitride material, and  $\nu_2$  is the Poisson's Ratio of the BK 7 ball lens. The values are given in Table 3.5.

**Table 3.5 Mechanical properties of BK 7 and silicon nitride [37, 38]**

Material/Property	$E_1$ (GPa)	$E_2$ (GPa)	$\nu_1$	$\nu_2$	$R_1$ (mm)	$R_2$
BK 7	8.2	-	0.206	-	2.5	-
Silicon Nitride	-	310	-	0.27	-	-

**Table 3.6 Contact properties under different loading conditions**

Load	4.17 N	5.65 N	6.95 N
Contact radius a (mm)	0.225	0.249	0.267
Contact area A (mm <sup>2</sup> )	0.159	0.194	0.223
Pressure applied $P_z$ (MPa)	26	29	31

Therefore from the above Table 3.6 we can see that the weld pressures needed to carry out the spot welding of PGA biofelts can be obtained by dividing the load applied on the ball lens P by the contact area A.

### 3.3.2 Weld Quality Parameters

#### 3.3.2.1 Weld Diameter

Weld Diameter can be measured with the help of a digital microscope and it usually is circular in shape because of the nature of the laser beam. The weld diameter can be assessed by the nature of the weld assessed in terms of (hole formed) strong weld, nice weld without any holes (melted region) and no holes. The weld diameter can be easily measured for the case when a hole is formed on the PGA biofelt as shown in Figure 3.9, as the boundaries of the hole are clearly visible.

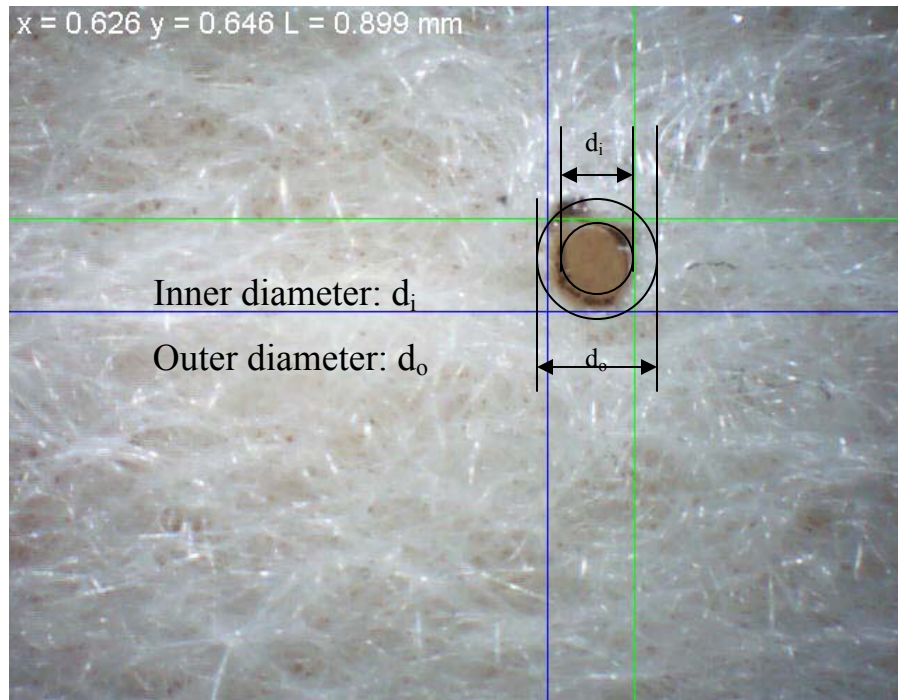


**Figure 3.9: Measuring weld diameter for strong weld with hole formed**

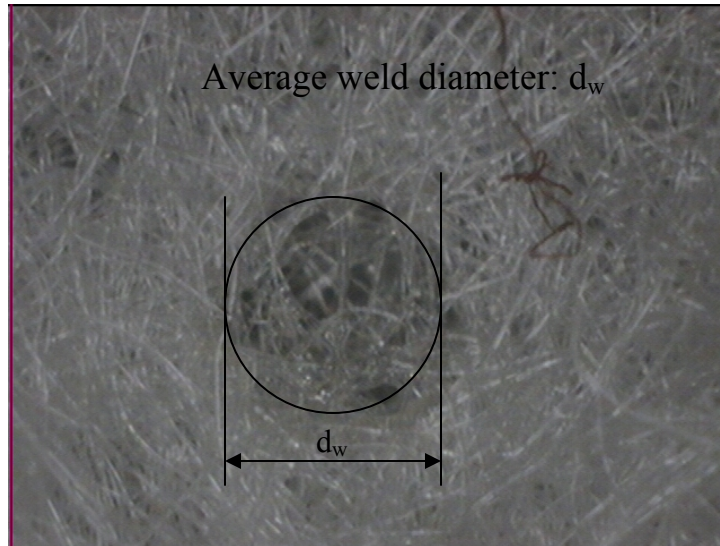


**Figure 3.10: Measuring weld diameter for nice weld with melted region**

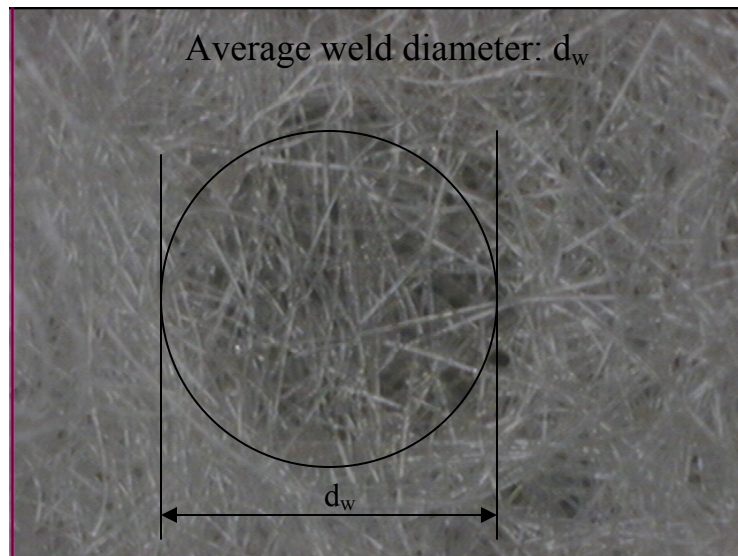


**Figure 3.11: Measuring weld diameter for No hole condition**

It becomes a little complicated in determining the exact boundaries for the conditions with melted as shown in Figure 3.10 and no hole region as shown in Figure 3.11. In such cases, multiple measurements are made for the weld diameters and average values are used for each case to minimize the measurement error and increase the repeatability. The weld diameters are measured with the help of a digital microscope that is calibrated to give the actual readings with a maximum percentage error of 5.75 % for 1 mm beam diameter conditions and 6.7 % error for the 1.5 mm beam diameter conditions. The formula to calculate the percentage error is shown below:

$$\text{Maximum \% Error} = \left( \frac{x_{\max} - x_{\text{mean}}}{x_{\text{mean}}} \right) * 100 \quad (3.4)$$

where  $x_{\max}$  is the experimental measurement of the maximum weld diameter,  $x_{\text{mean}}$  is the average of the measured weld diameters.

$$x_{\text{mean}} = \left( \frac{x_{\text{exp } 1} + x_{\text{exp } 2} + \dots + x_{\text{exp } n}}{n} \right) \quad (3.5)$$

### 3.3.2.2 Weld Strength

Weld strength is a useful output parameter for determining the strength of the weld formed on the PGA specimen. The pull-off load measurement is made with the help of a scale balance that can measure the load needed to pull apart the welded fibers. The setup for measuring the pull-off load of the welded fibers is shown in Figure 3.12, where the PGA welded fiber sheet is held on an aluminum plate by fixing the bottom sheet on the plate using a tape. The aluminum plate is then clamped on a bench vise and one of the ends of the top sheet is grabbed using a scale balance. The welded fiber sheets are pulled apart giving the reading in gram-force on the scale balance.



**Figure 3.12: Setup for measurement of weld strength**

The weld strength can then be determined by dividing the pull-off load by the area of the weld obtained and this value is compared with the tensile strength of the original PGA biofelt sample to determine how strong the weld is. The tensile strength of the PGA biofelt is measured using an Instron testing machine and is discussed in Section 3.4.1.

For a given weld area of  $A_w$ , the pull-off load  $P$  is related to the weld strength  $\sigma_w$  by the following equation:

$$P = A_w * \sigma_w \quad (3.6)$$

Since the welds formed are circular in cross section, the weld area  $A_w$  for the welds formed can be obtained by:

$$A_w = \pi * r^2 \quad (3.7)$$

where  $r$  is the radius of the circular weld formed on the PGA specimen felts.

In some cases where proper boundary conditions do not exist, we take multiple readings and calculate the average value of the circular diameter in order to calculate the weld area  $A_w$ . For cases when there is a hole, the outer and inner weld diameters are measured and the weld area  $A_w$  is given by the following formula:

$$A_w = \pi * (r_1^2 - r_2^2) \quad (3.8)$$

where  $r_1$  and  $r_2$  are the radius of the outer and inner circular welds respectively.

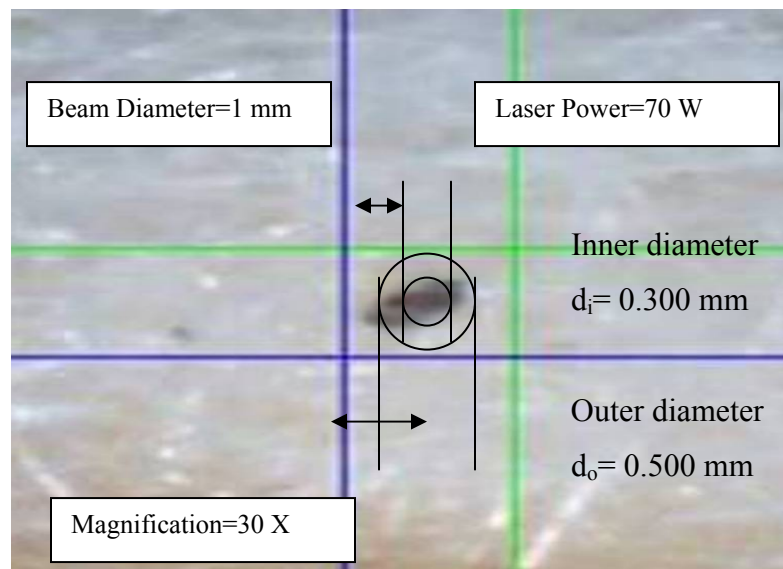
### 3.3.3 Effects of Operating Parameters on Weld Diameter

#### 3.3.3.1 Influence of Laser Power on Weld Diameter

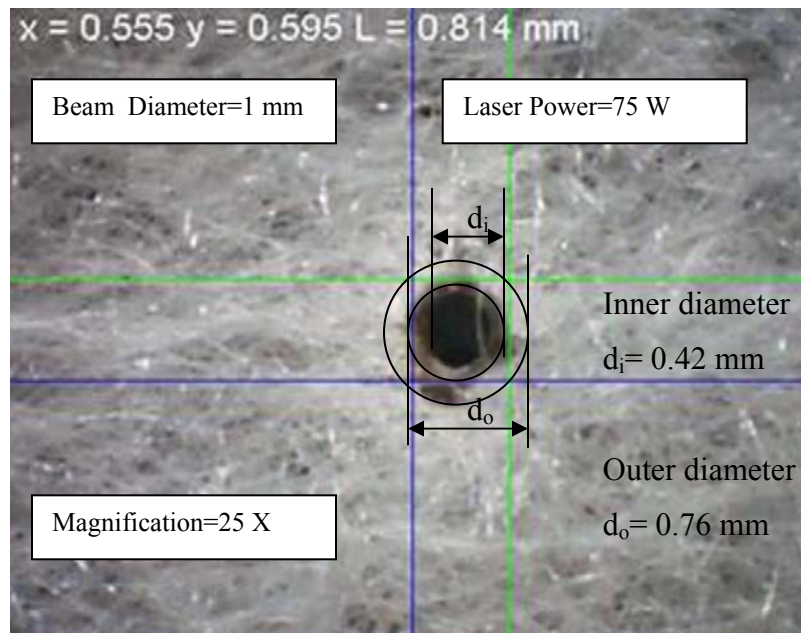
Laser power directly affects the weld diameter and its quality. For the low power, weld diameter with less HAZ is obtained. As the power of the laser beam increases from 70 W to 80 W (other laser parameters are the same), the weld diameter increases with more HAZ. Tables 3.7 and 3.8 give the weld conditions and results for each case.

**Table 3.7 Weld conditions for beam diameter of 1 mm**

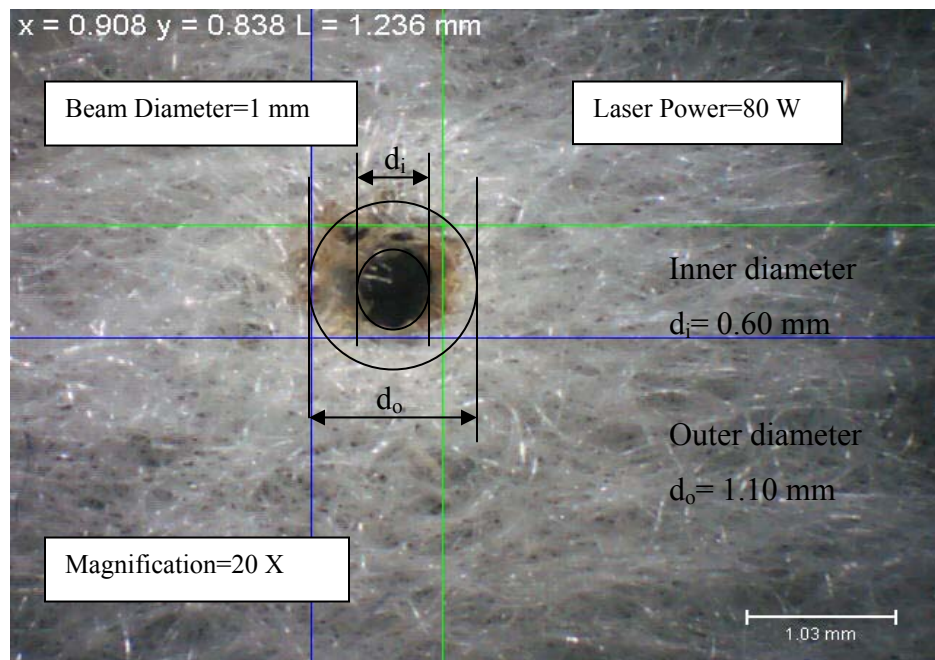
Power (W)	Beam diameter (mm)	Time duration (sec)	Pressure (MPa)	Weld diameter (mm)	Observations
70	1	5	26	0.400	Hole formed
75	1	5	26	0.600	Hole formed
80	1	5	26	0.850	Hole formed



(a)



(b)



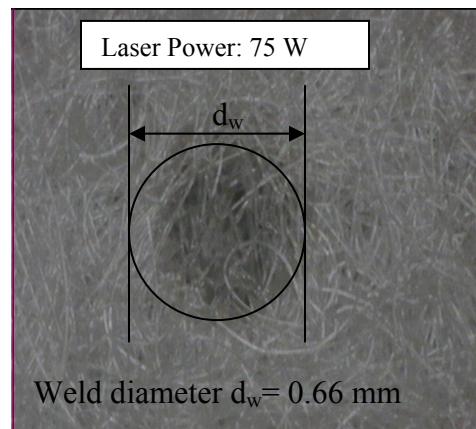
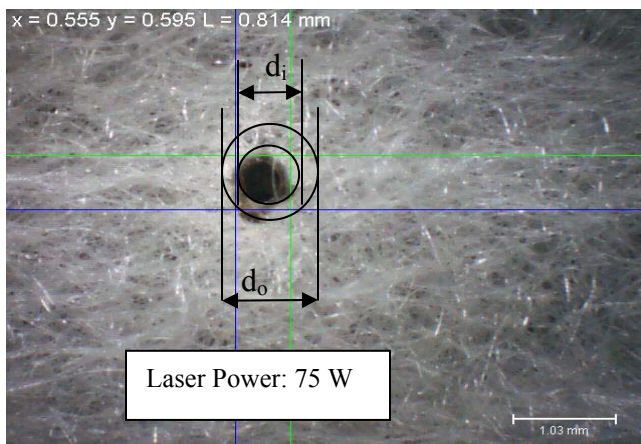
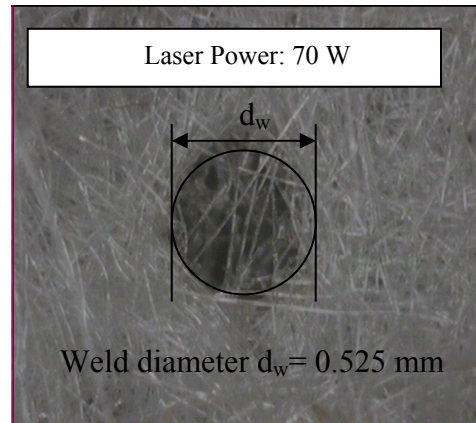
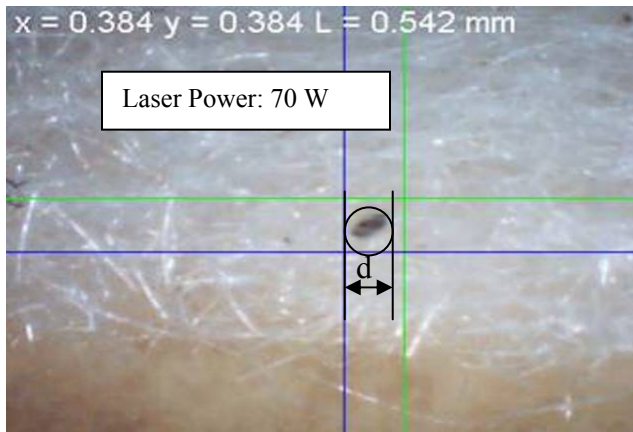
(c)

Figure 3.13 Optical images of welded holes with different laser power

(a) Laser Power=70 W (b) Laser Power=75 W (c) Laser Power=80 W

Table 3.8 Weld conditions for beam diameter of 1.5 mm

Power (W)	Beam diameter (mm)	Time duration (sec)	Pressure (MPa)	Weld diameter (mm)	Observations
70	1.5	5	26	0.525	Melted region
75	1.5	5	26	0.660	Melted region
80	1.5	5	26	0.900	Melted region



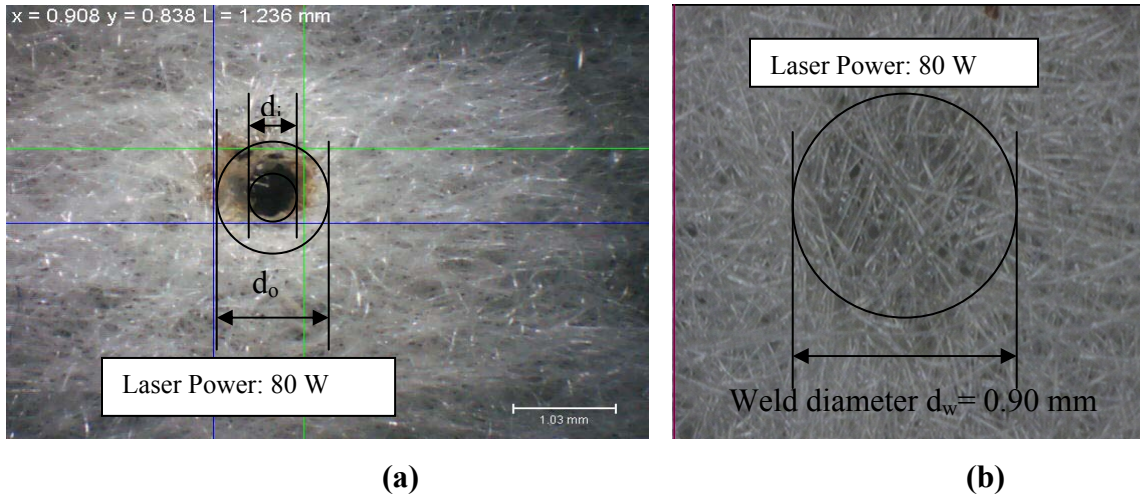


**Figure 3.14 Optical images of weld diameters with different laser power**  
**(a) Beam diameter=1mm (b) Beam diameter= 1.5 mm**

To understand the effect of laser power, weld diameter and HAZ of the welded holes are directly measured from the optical images as shown in Figures 3.13 and 3.14. Figures 3.13 (a), (b) and (c) show the weld images for increasing laser power at a beam diameter of 1 mm. The inner and outer diameters are measured and the average weld diameter value is determined for the holes formed. The weld hole as shown in Figure 3.13 (a) is not circular in shape. The optical images in Figure 3.14 (a) are used for comparison with optical images in Figure 3.14 (b). Figure 3.14 (b) shows the weld images for increasing laser power at a beam diameter of 1.5 mm and magnification of 40 X. The weld regions are circular in shape and the weld diameters are measured for each case. In the case of melted regions, the average weld diameter value is determined for each case and used for comparison with other conditions. Since the laser beam follows Gaussian intensity profile as shown in Figure 3.15, increase in power leads to ablation of more surrounding materials. This makes the weld diameter on the PGA fiber felts increase almost linearly with laser power. The graphs are plotted in Figures 3.16, 3.17 and 3.18. It is evident from the graph in Figures 3.16 and 3.17 that as the laser power increases, the weld diameter increases at different beam diameter conditions. The results obey the generally observed relationship between weld diameter and laser power.

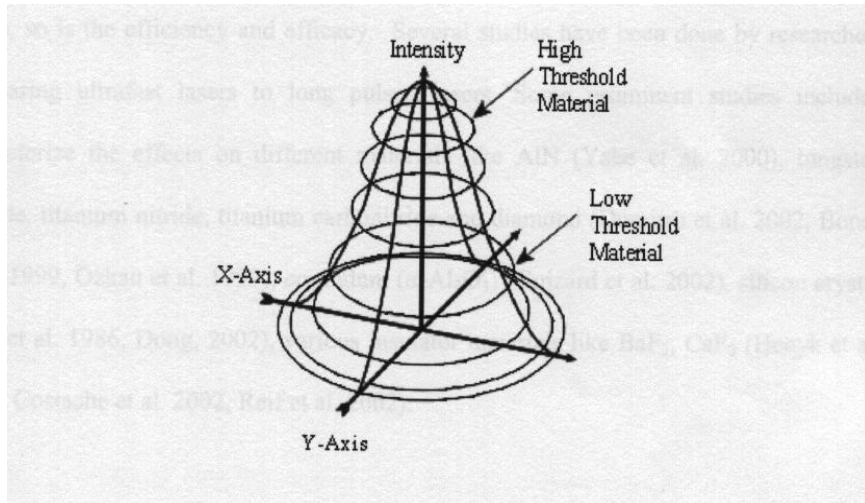


**Figure 3.15: Gaussian beam profile**

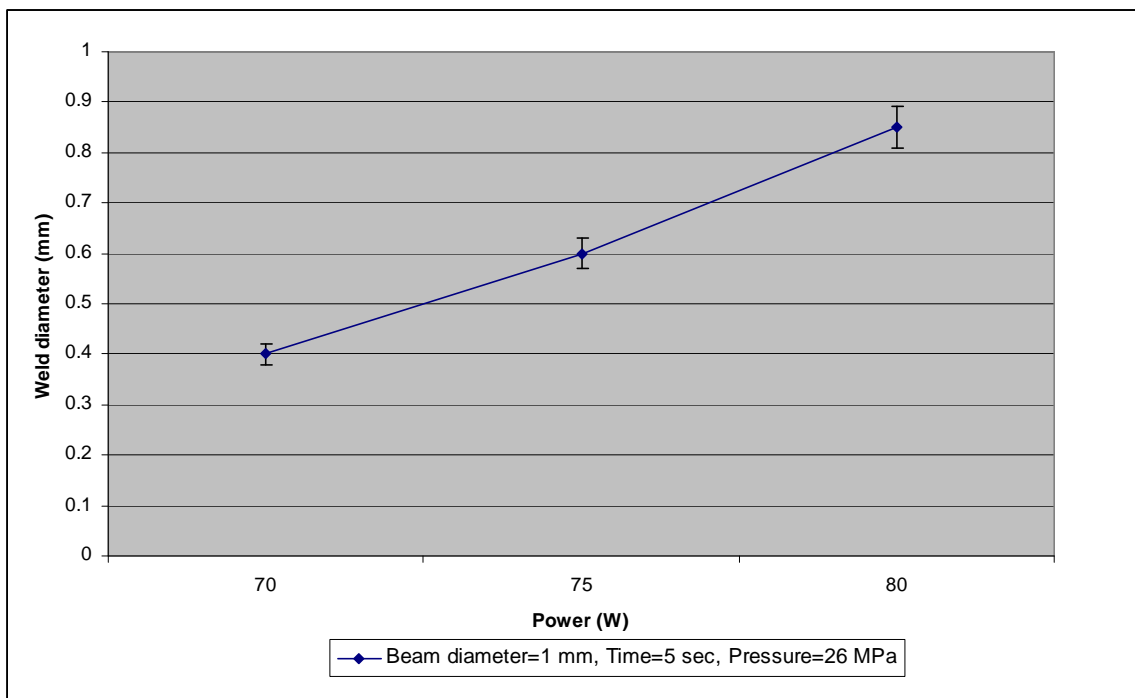


**Figure 3.16: Variation of weld diameter with laser power for beam diameter of 1 mm**

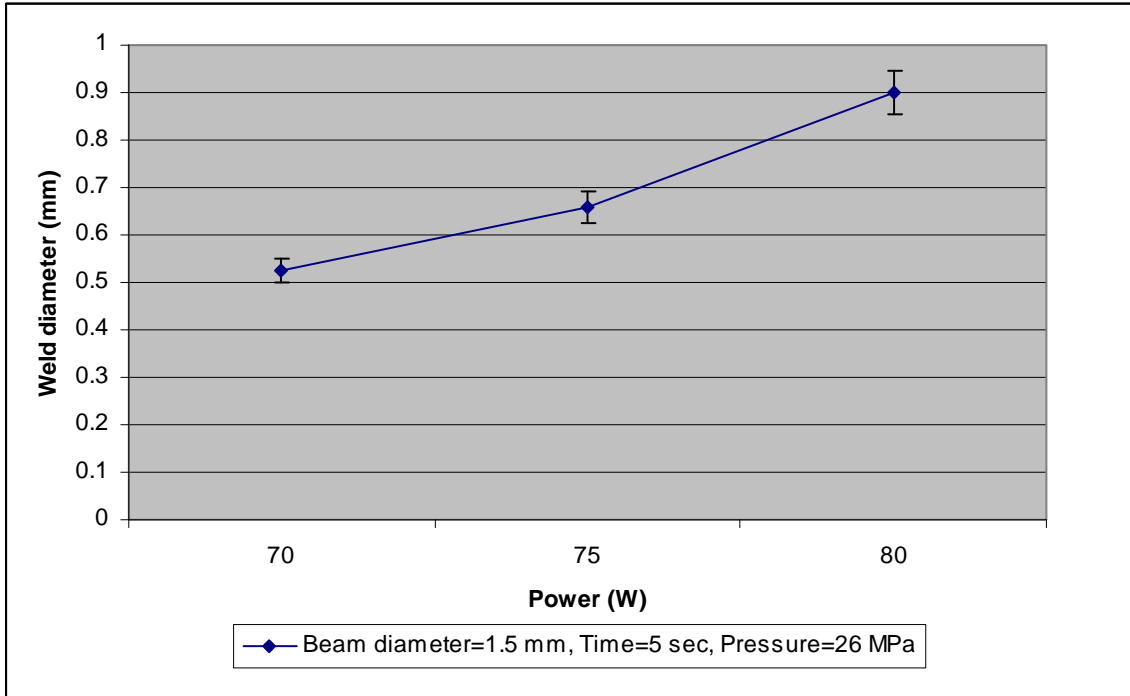


**Figure 3.17: Variation of weld diameter with laser power for beam diameter of 1.5 mm**

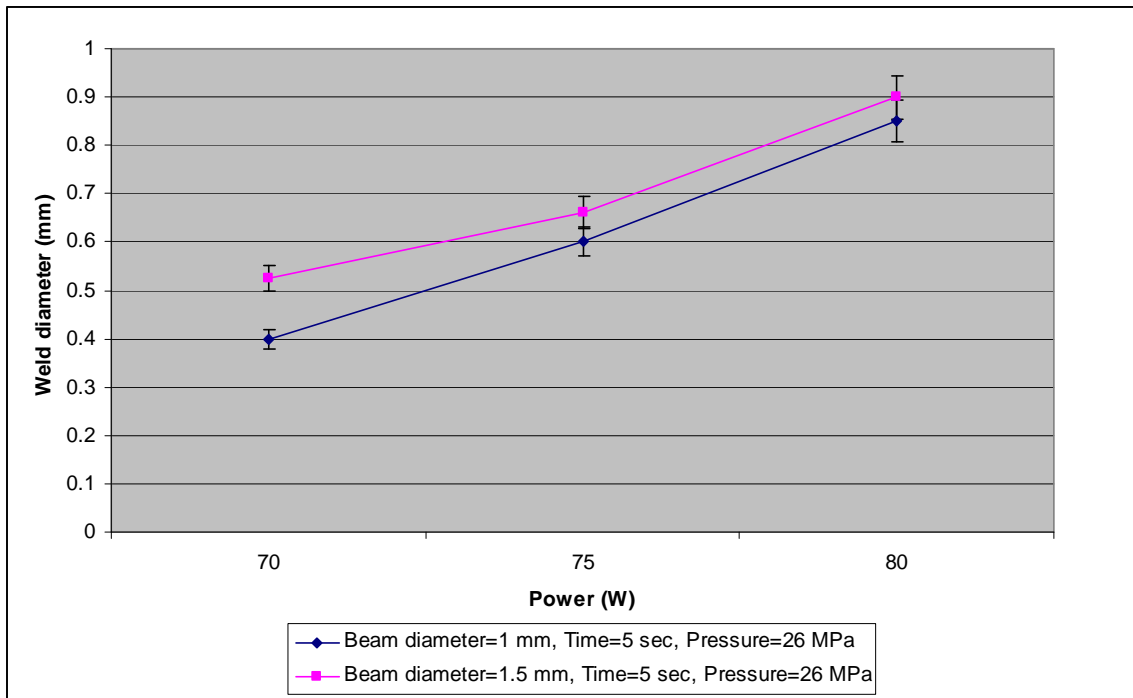


**Figure 3.18: Variation of weld diameter with laser power**

**3.3.3.2 Influence of Pressure on Weld Diameter**

The pressure applied on the spherical ball lens also affects the weld diameter and weld strength. The weld conditions and results are listed in Tables 3.9 and 3.10. Figure 3.19 (a) and (b) shows the weld diameters with different weld pressures at beam diameters of 1 and 1.5 mm respectively. The weld images for beam diameters of 1 mm and 1.5 mm are at a magnification of 17 X and 40 X respectively. The results are shown in Figures 3.20, 3.21 and 3.22. It is clear from the graphs that the weld diameter increases with contact pressure. The increase in weld diameter corresponds to an increase in the weld area for the condition when there is a hole. This is due to the fact that the molten polymer is squeezed as pressure is increased and this causes the weld diameter to increase. For the case when there is only melted region, the increase in pressure also corresponds to increase in weld diameter and weld area.

**Table 3.9 Weld conditions for beam diameter of 1 mm**

Power (W)	Beam diameter (mm)	Time duration (sec)	Pressure (MPa)	Weld diameter (mm)	Weld area (mm <sup>2</sup> )	Observations
75	1	5	26	0.600	0.324	Hole formed
75	1	5	29	0.794	0.594	Hole formed
75	1	5	31	0.965	0.861	Hole formed

**Table 3.10 Weld conditions for beam diameter of 1.5 mm**

Power (W)	Beam diameter (mm)	Time duration (sec)	Pressure (MPa)	Weld diameter (mm)	Weld area (mm <sup>2</sup> )	Observations
75	1.5	5	26	0.660	0.342	Melted region
75	1.5	5	29	0.820	0.528	Melted region
75	1.5	5	31	1.01	0.801	Melted region

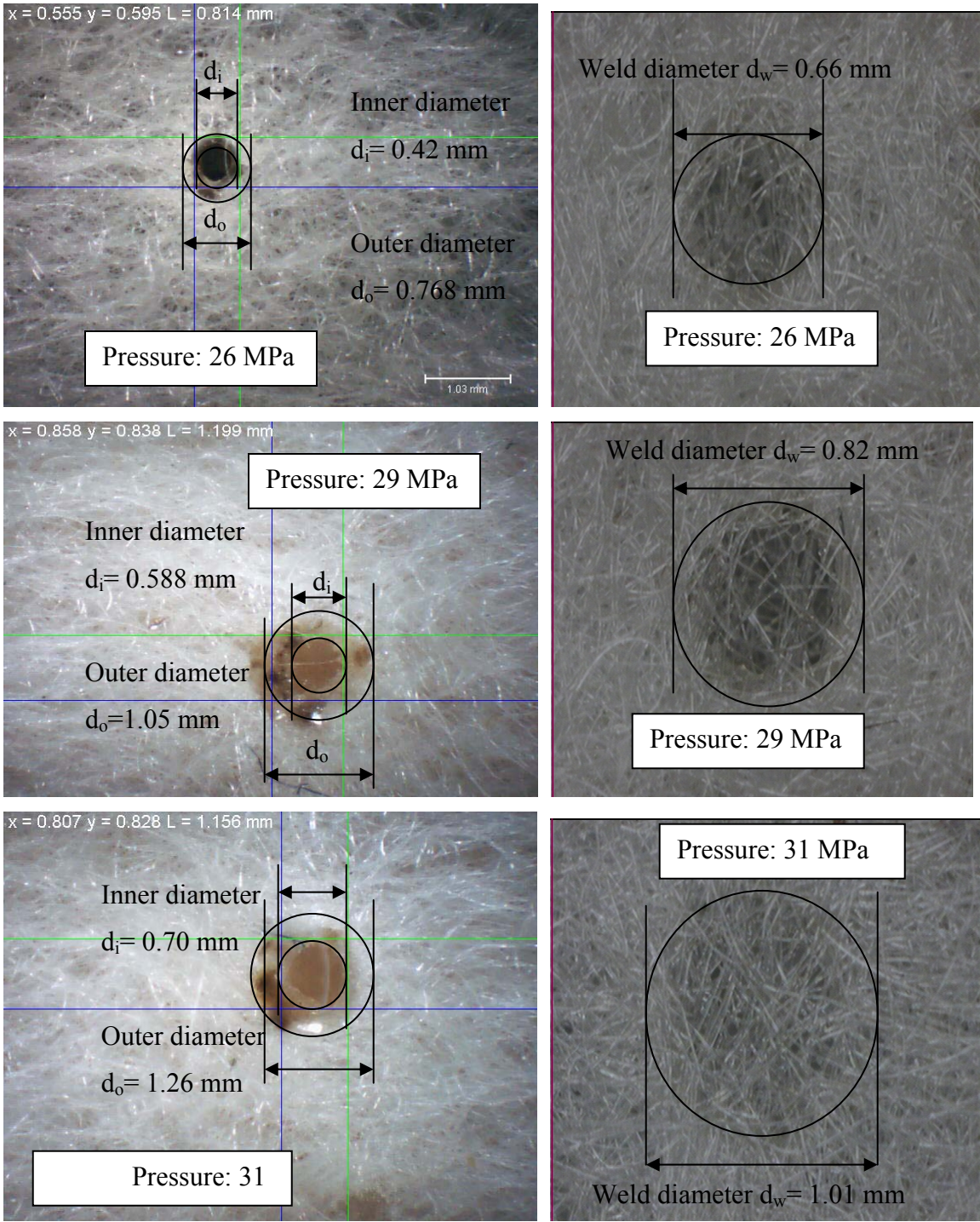


**Figure 3.19: Optical images of weld diameters with different contact pressures**

**(a) Beam diameter=1 mm (b) Beam diameter=1.5 mm**

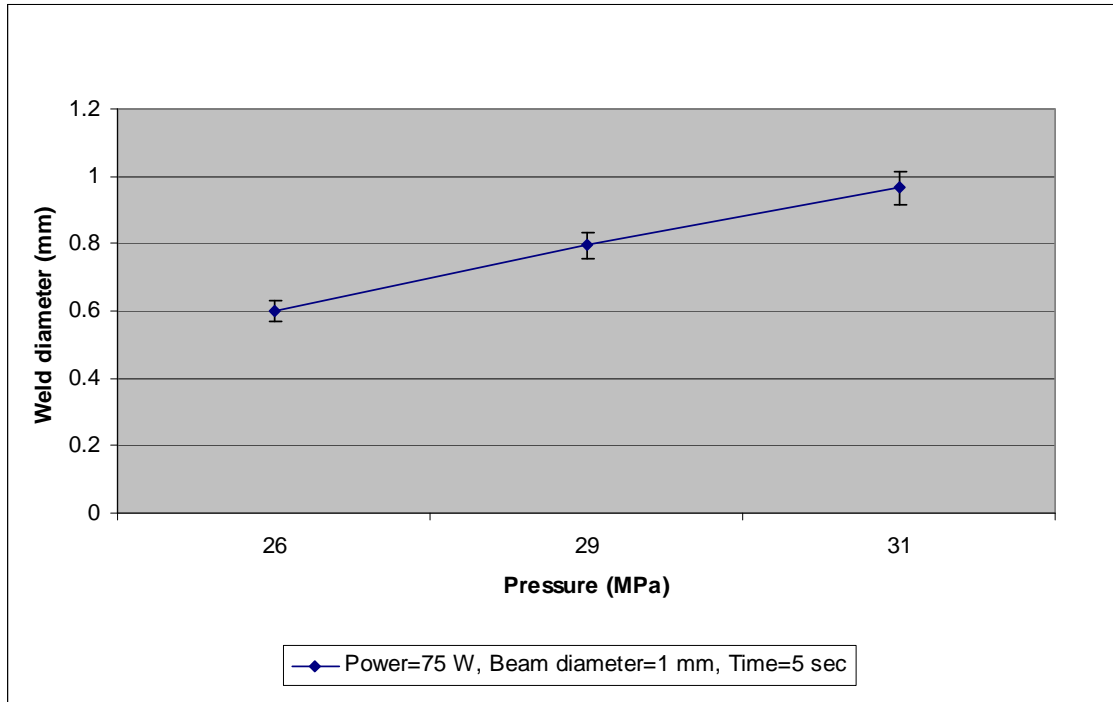


**Figure 3.20: Variation of weld diameter with pressure for beam diameter of 1 mm**

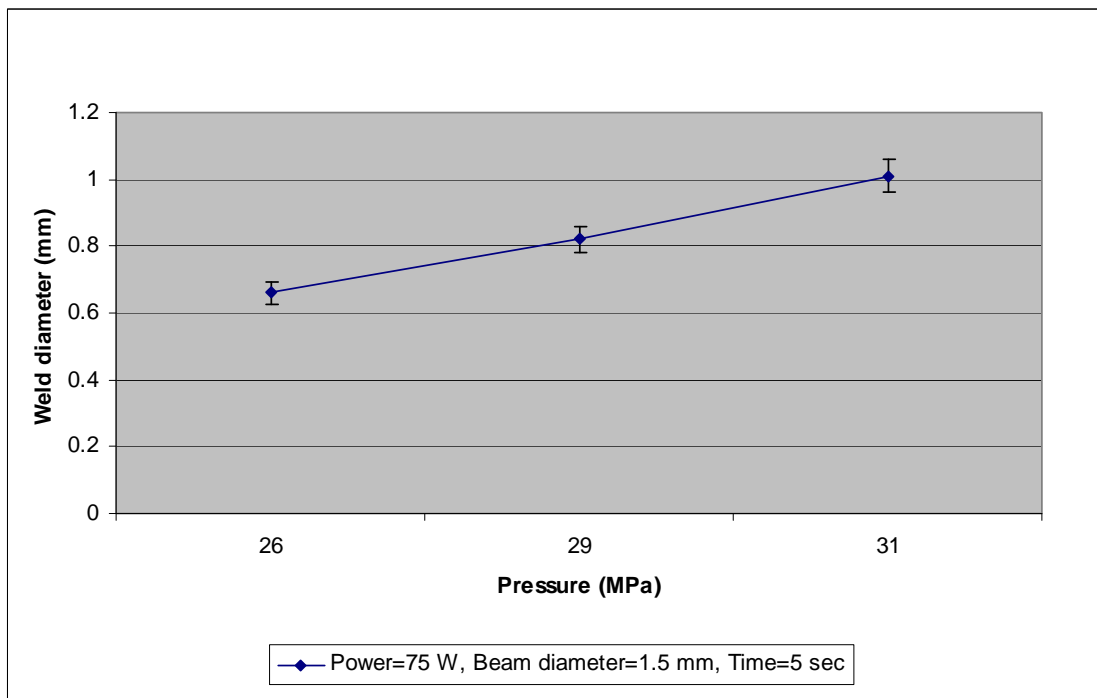


**Figure 3.21: Variation of weld diameter with pressure for beam diameter of 1.5 mm**

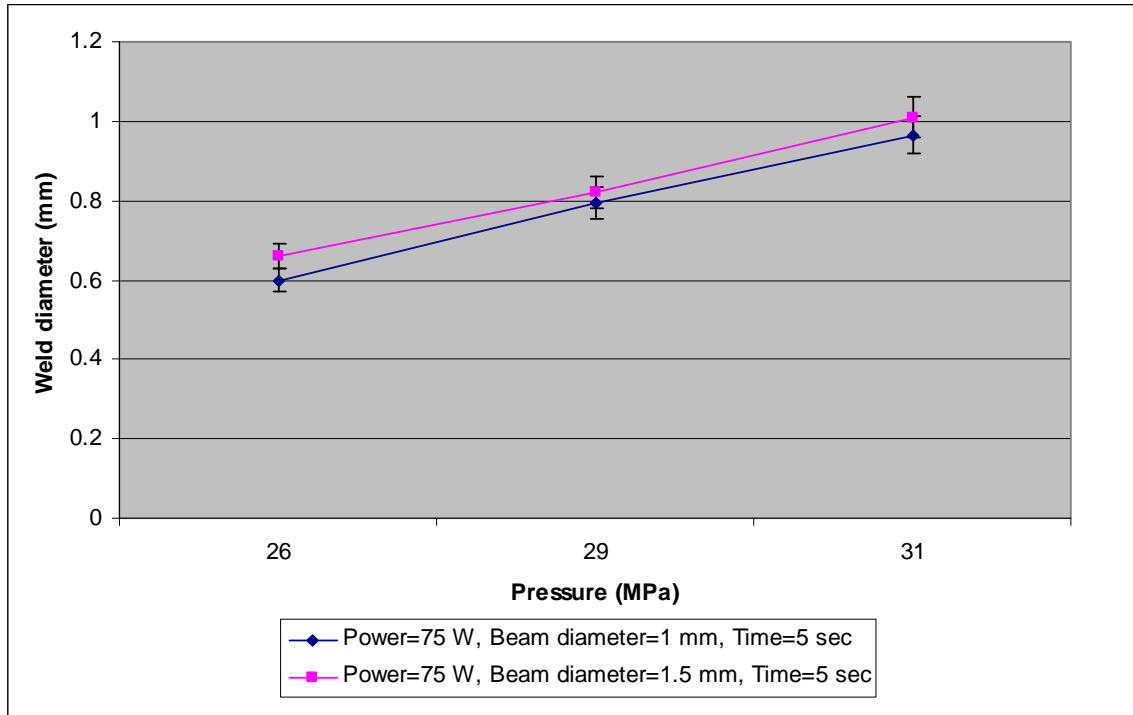


**Figure 3.22: Variation of weld diameter with pressure**

Figure 3.22 compares the cases in which beam diameter is constant at 1 mm and at 1.5 mm. The weld diameters are slightly greater for the beam diameter of 1.5 mm than 1 mm while other parameters being constant.

### 3.3.3.3 Influence of Beam Diameter on Weld Diameter

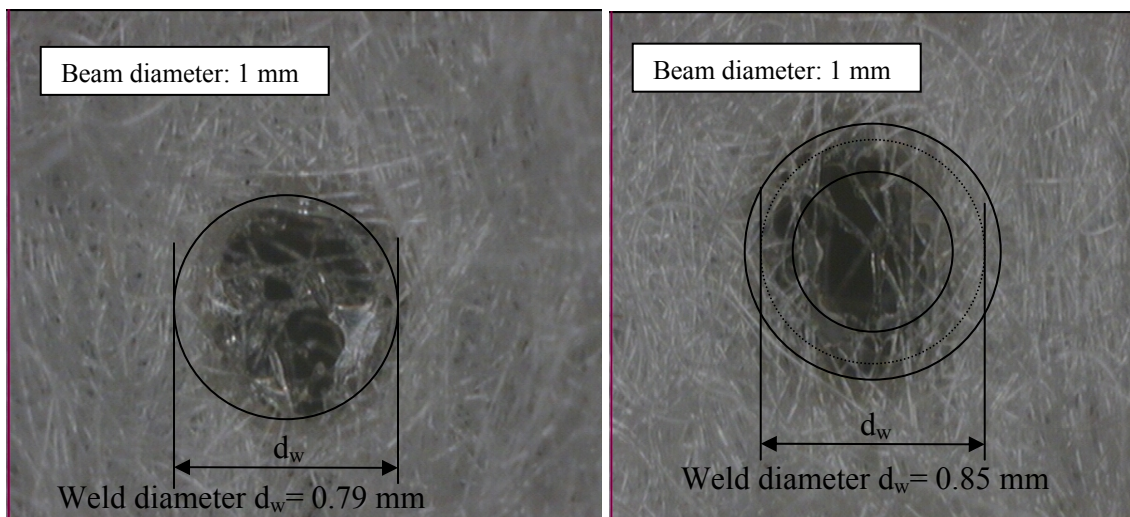
The weld conditions and results for increasing beam diameter are listed in Tables 3.11 and 3.12. Figures 3.23 (a) and (b) show the weld diameter images with increasing beam diameters at power levels of 70 and 75 W respectively at a magnification of 40 X. Partial holes are formed at the 1 mm beam diameter conditions for 70 and 75 W laser power levels (other parameters being constant). The average diameter  $d_w$  (mm) is measured since there is no proper hole. The results are plotted in Figures 3.24, 3.25 and 3.26. It is clear from the graphs that weld diameter increases with beam diameter as the area of laser exposure increases.

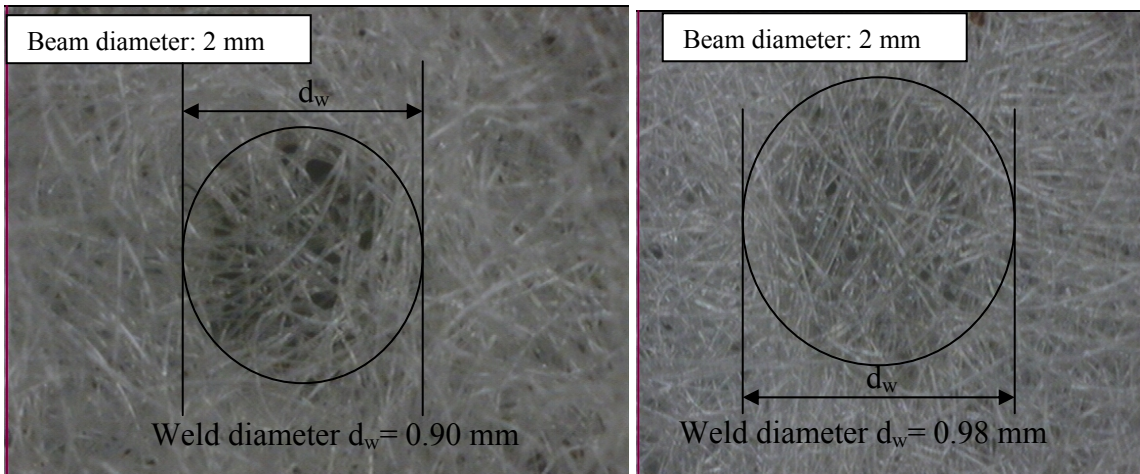
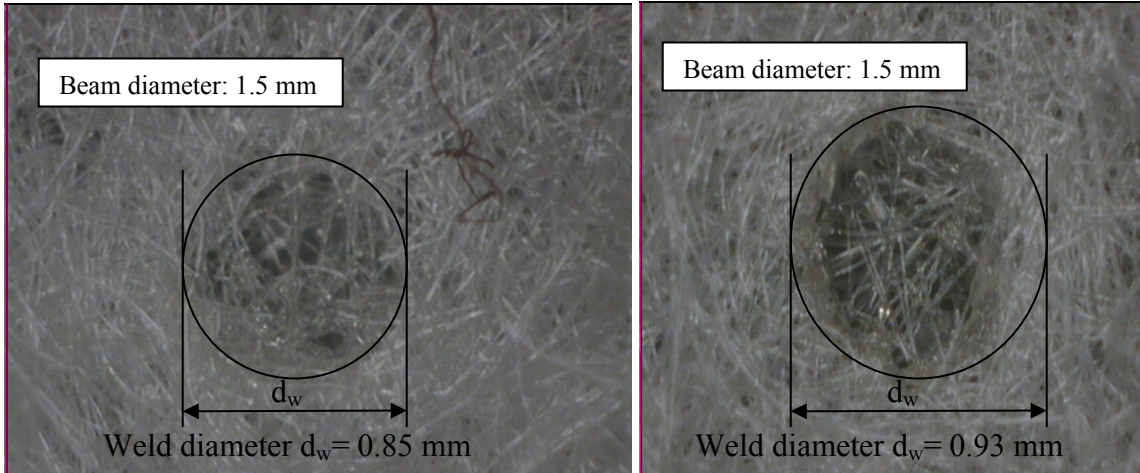
**Table 3.11 Weld conditions for laser power of 70 W**

Power (W)	Beam diameter (mm)	Time duration (sec)	Pressure (MPa)	Weld diameter (mm)	Observations
70	1	15	26	0.79	Partial hole
70	1.5	15	26	0.85	Melted region
70	2	15	26	0.90	No hole

**Table 3.12 Weld conditions for laser power of 75 W**

Power (W)	Beam diameter (mm)	Time duration (sec)	Pressure (MPa)	Weld diameter (mm)	Observations
75	1	15	26	0.85	Partial hole
75	1.5	15	26	0.93	Melted region
75	2	15	26	0.98	No hole





(a)

(b)

**Figure 3.23: Optical Images of weld diameters with different beam diameters**

**(a) Laser Power=70 W (b) Laser Power=75 W**

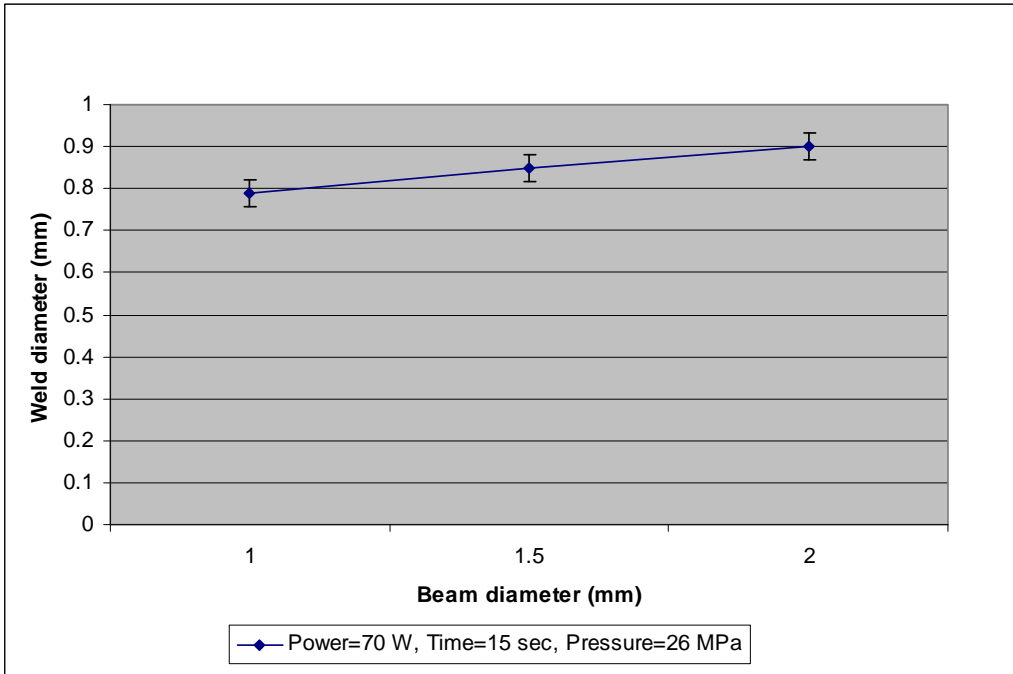


**Figure 3.24: Variation of weld diameter with beam diameter for laser power of 70 W**

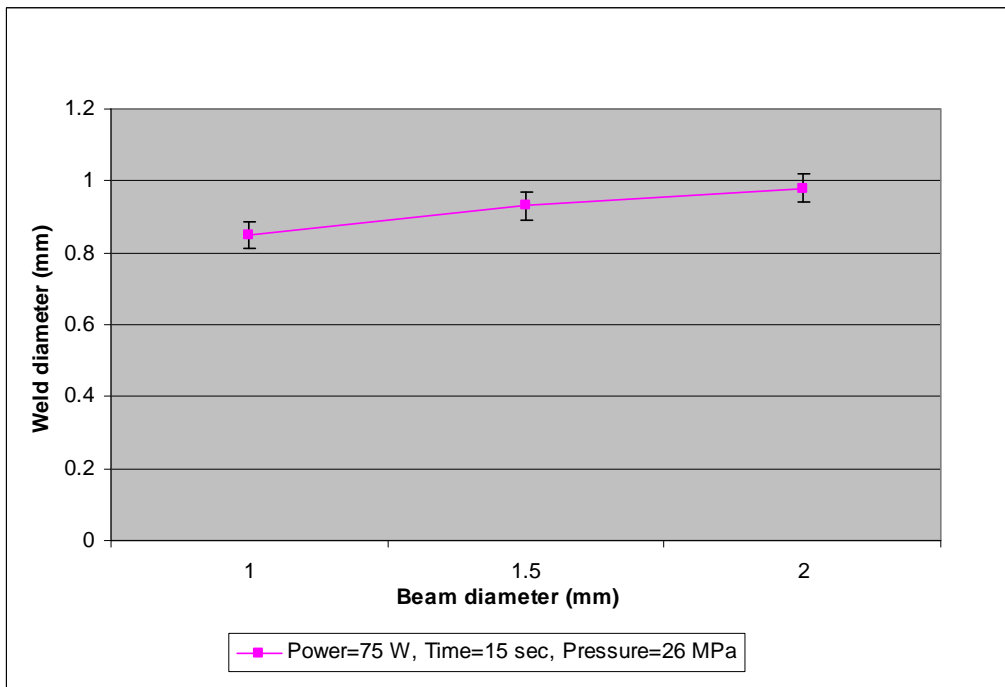


**Figure 3.25: Variation of weld diameter with beam diameter for laser power of 75 W**

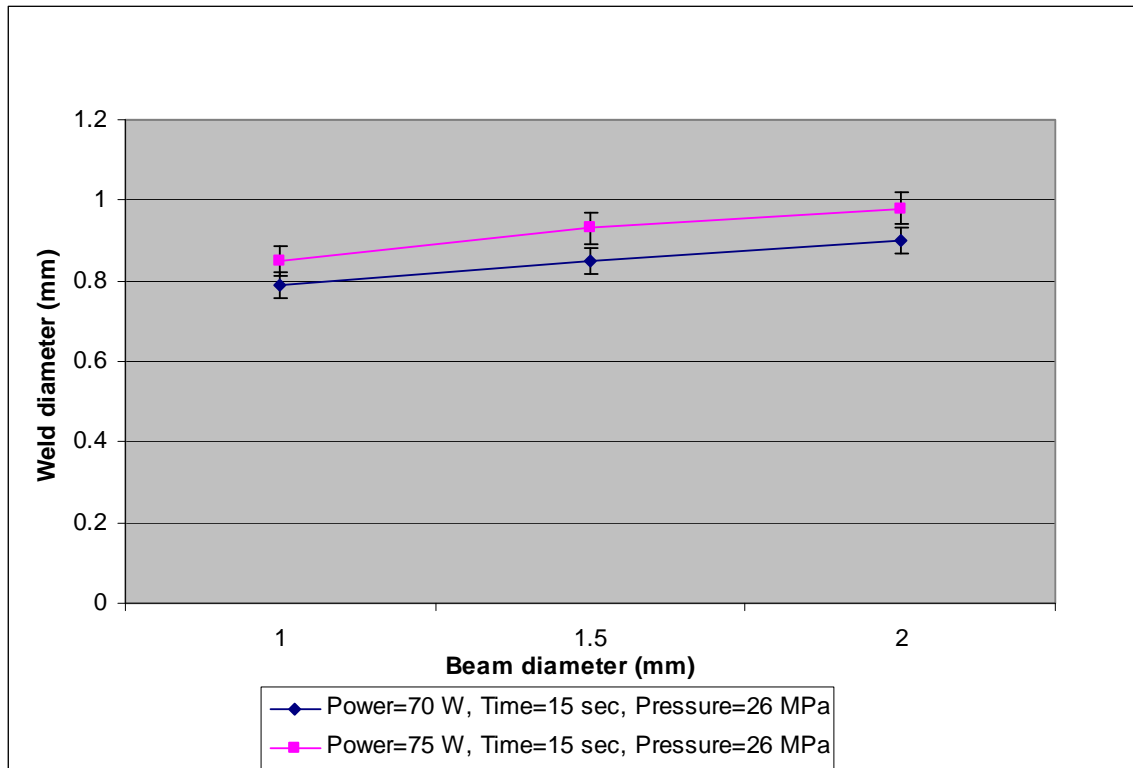


**Figure: 3.26 Variation of weld diameter with beam diameter**

Figure 3.26 compares the cases in which laser power level is operated at 70 and 75 W. For the 70 W conditions, the weld diameters increase with beam diameter and there is a partial hole formed with slight discoloration at the boundary for 1 mm beam diameter. The weld diameters are greater for 75 W conditions and increase with increasing beam diameter as shown in Figure 3.26.

### 3.3.3.4 Influence of Time Duration on Weld Diameter

Time duration affects the weld diameter and its quality. As the time duration increases from 5 sec to 15 sec (other laser parameters are the same), the weld diameter increases. Tables 3.13 and 3.14 give the weld conditions and results for each case. To understand the effect of time duration, weld diameter and HAZ of the welded holes are directly measured from the optical images as shown in Figures 3.27 (a) and (b).

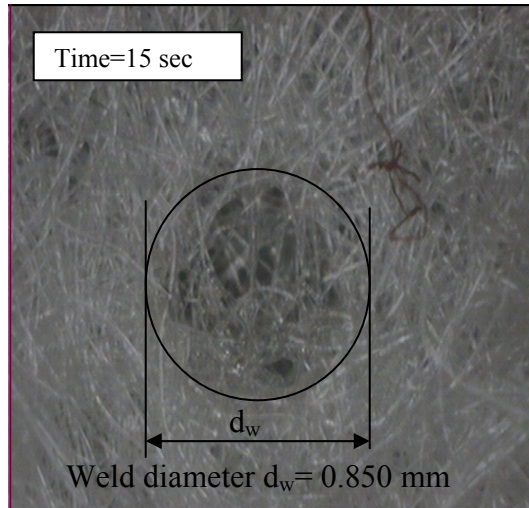
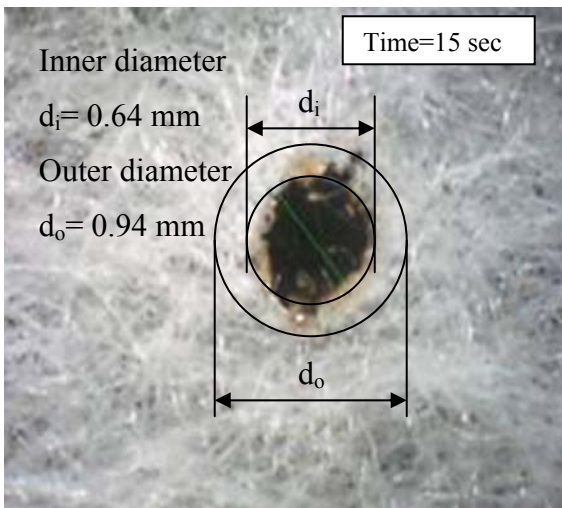
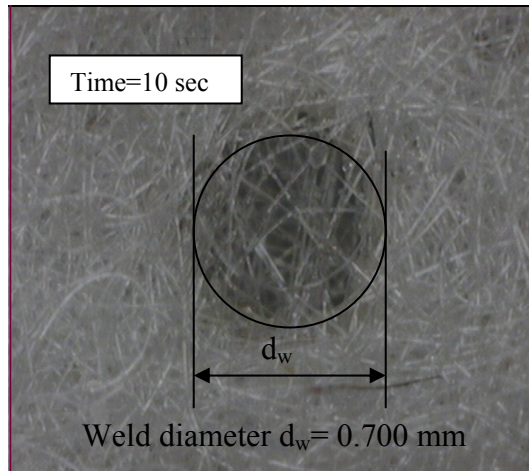
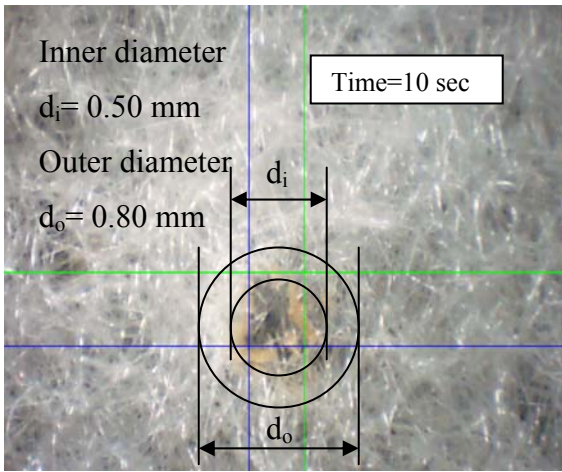
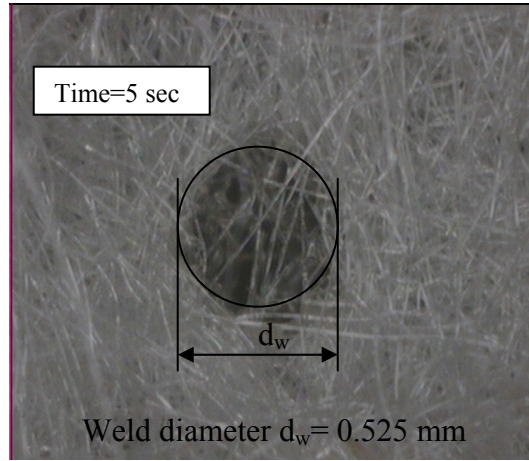
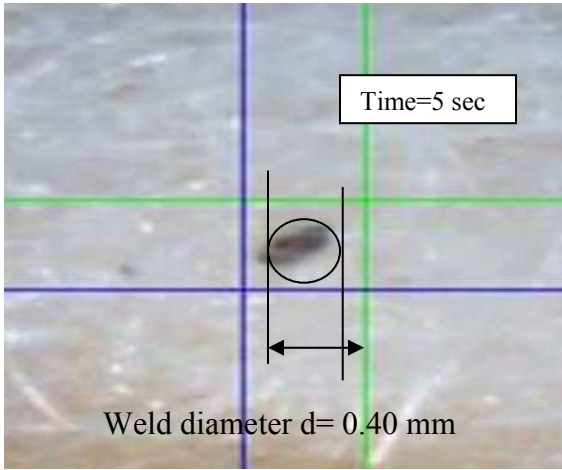
**Table 3.13 Weld conditions for beam diameter of 1 mm**

<b>Power (W)</b>	<b>Beam diameter (mm)</b>	<b>Time duration (sec)</b>	<b>Pressure (MPa)</b>	<b>Weld diameter (mm)</b>	<b>Observations</b>
70	1	5	26	0.400	Hole formed
70	1	10	26	0.650	Hole formed
70	1	15	26	0.790	Hole formed
70	1	20	26	0.820	Hole formed

**Table 3.14 Weld conditions for beam diameter of 1.5 mm**

<b>Power (W)</b>	<b>Beam diameter (mm)</b>	<b>Time duration (sec)</b>	<b>Pressure (MPa)</b>	<b>Weld diameter (mm)</b>	<b>Observations</b>
70	1.5	5	26	0.525	Melted region
70	1.5	10	26	0.700	Melted region
70	1.5	15	26	0.850	Melted region
70	1.5	20	26	0.880	Melted region

Figures 3.27 (a) and (b) show the weld diameters with different time duration at a magnification of 26 and 36 X respectively. The inner and outer diameters are measured for the holes formed. The welded holes as shown in Figure 3.27 (a) have slight discoloration at the boundaries. Figure 3.27 (b) shows the weld images for increasing time duration at a beam diameter of 1.5 mm. The weld regions are circular in shape for conditions with beam diameter of 1 mm. The inner and outer weld diameters are measured whenever there is a hole formed. In the case of melted regions, average weld diameter value  $d_w$  is measured for each case and used for comparison with other conditions. The results are plotted with weld diameter vs. time duration in Figures 3.28, 3.29 and 3.30. It is clear from the graphs that the weld diameter increases with time duration. Figure 3.30 compares the cases in which beam diameter is constant at 1 mm and at 1.5 mm. There is no significant increase in weld diameter at different beam diameters with increasing time duration.



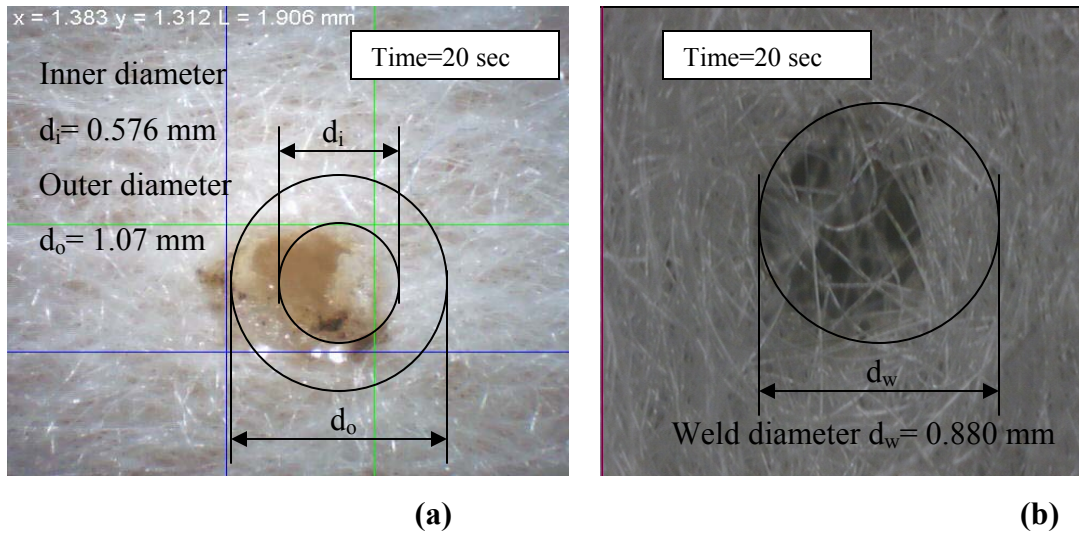


**Figure 3.27: Optical images of weld diameters with different time duration**  
**(a) Beam diameter=1 mm (b) Beam diameter=1.5 mm**

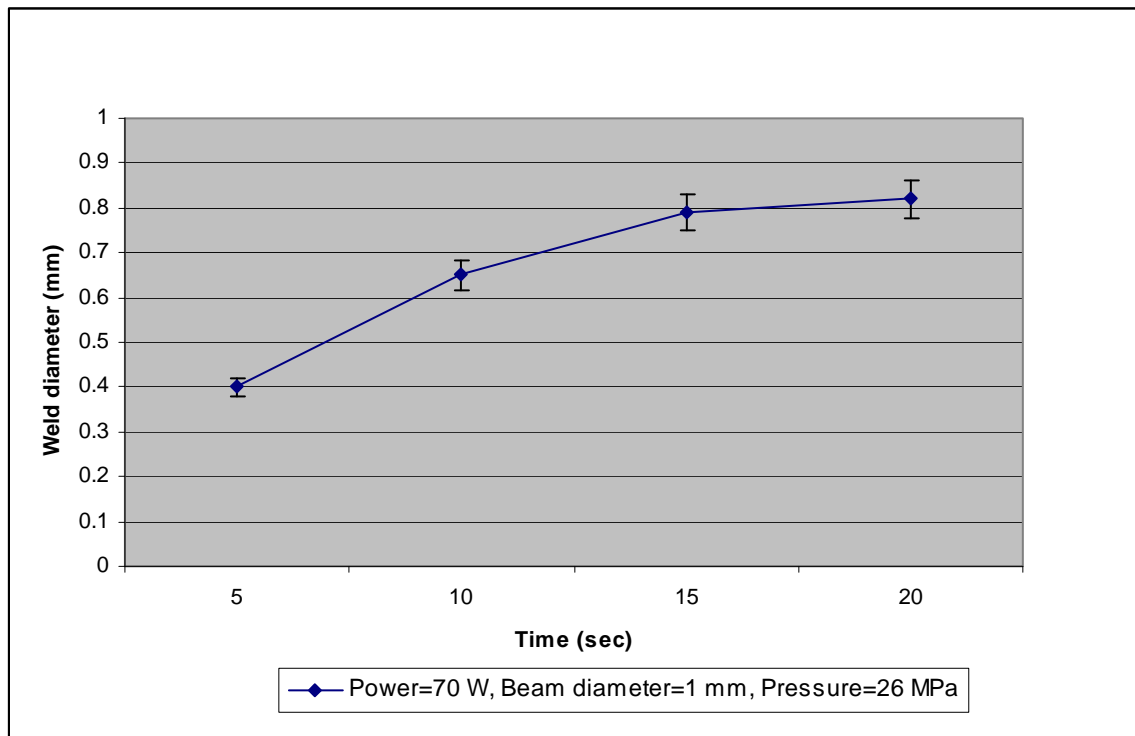


**Figure 3.28: Variation of weld diameter with time duration for beam diameter of 1 mm**

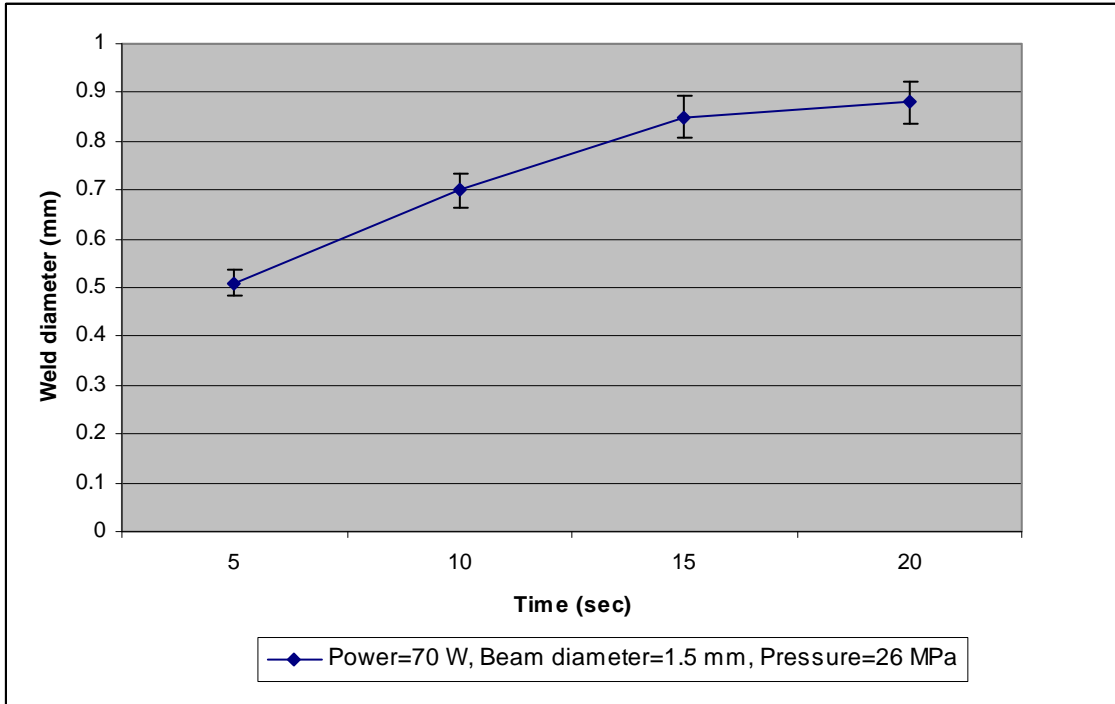


**Figure 3.29: Variation of weld diameter with time duration for beam diameter of 1.5 mm**

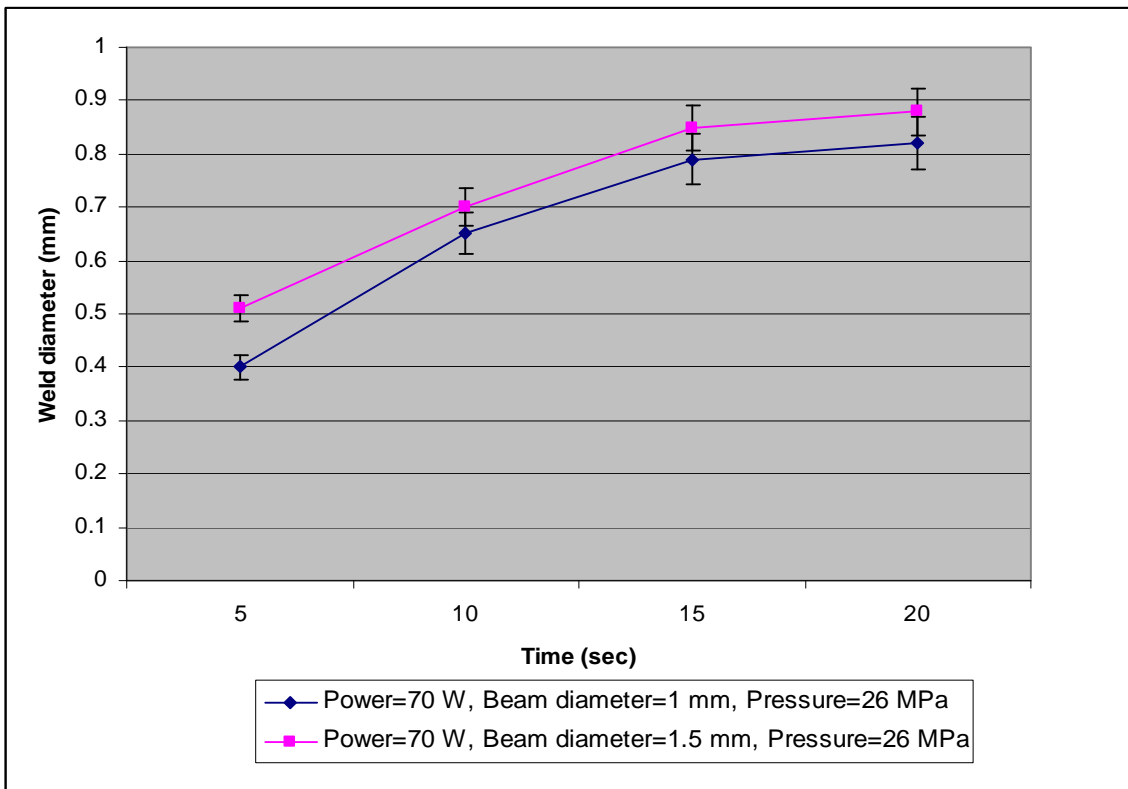


**Figure 3.30: Variation of weld diameter with time duration**

### 3.3.4 Effects of Operating Parameters on Weld Strength

#### 3.3.4.1 Influence of Laser Power on Weld Strength

Laser power directly affects the weld strength. As the power of the laser beam increases from 70 W to 80 W (other laser parameters are the same), the weld strength increases. The weld conditions and results are listed in Table 3.15. The optical images of weld strength vs. laser power are shown in Figure 3.31 for beam diameter of 1 mm at a magnification of 40 X. From Figure 3.31 it can be clearly seen that as the laser power increases the size of the weld diameter increases. The increase in weld diameter corresponds to an increase in the weld area. To understand the effect of laser power, a graph is plotted with increase in weld strength vs. laser power in Figure 3.32. It is evident from the graph that as the laser power increases, the weld strength of the welded PGA felt increases. The increase in laser power results in increased melting of the fibers and thus a strong weld is formed. The increase in the welded area is simply due to a more energetic heating process that spreads and covers the complete area irradiated by the laser beam.

**Table 3.15 Weld conditions and results for laser power**

<b>Power (W)</b>	<b>Beam diameter (mm)</b>	<b>Time (sec)</b>	<b>Pressure (MPa)</b>	<b>Pull-Off Load (gf)</b>	<b>Weld diameter (mm)</b>	<b>Weld area (mm<sup>2</sup>)</b>	<b>Weld Strength (MPa)</b>
70	1.5	5	26	3	0.525	0.216	0.136
75	1.5	5	26	6	0.660	0.342	0.169
80	1.5	5	26	13	0.900	0.636	0.199

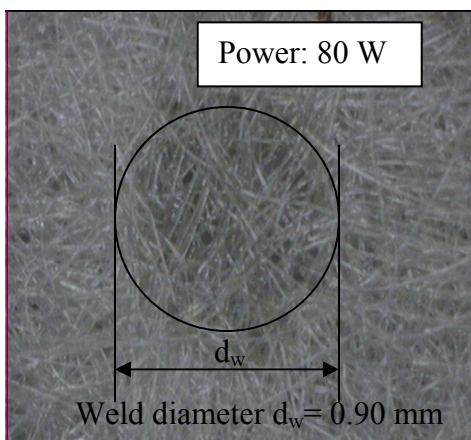
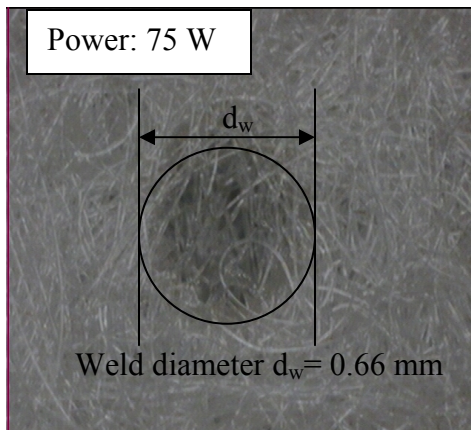
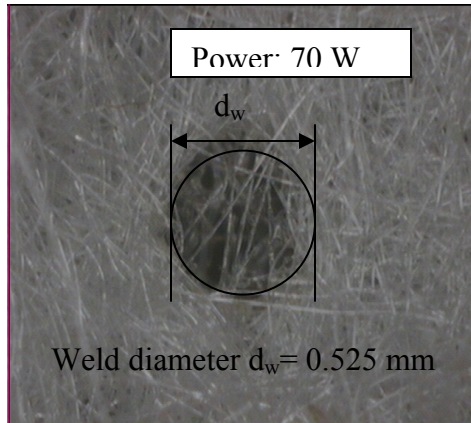


**Figure 3.31: Optical images of weld diameter with different laser powers at beam diameter of 1.5 mm**

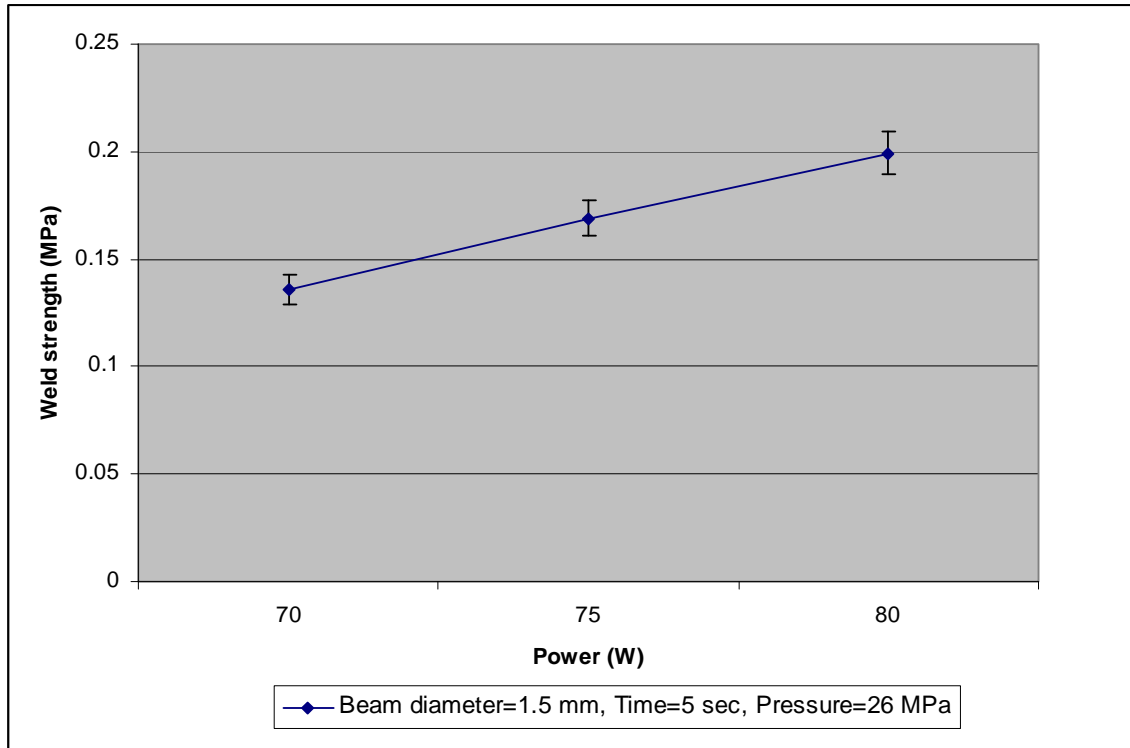


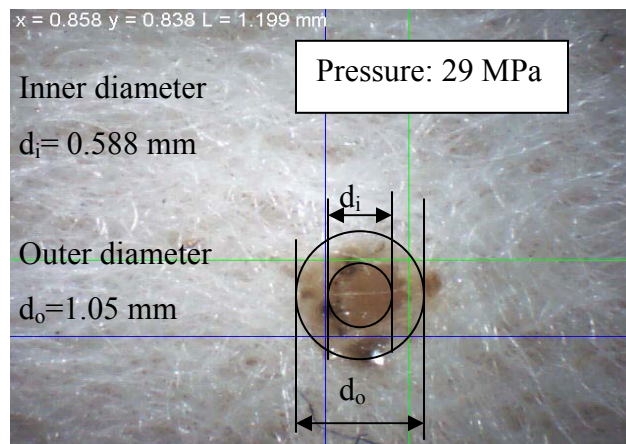
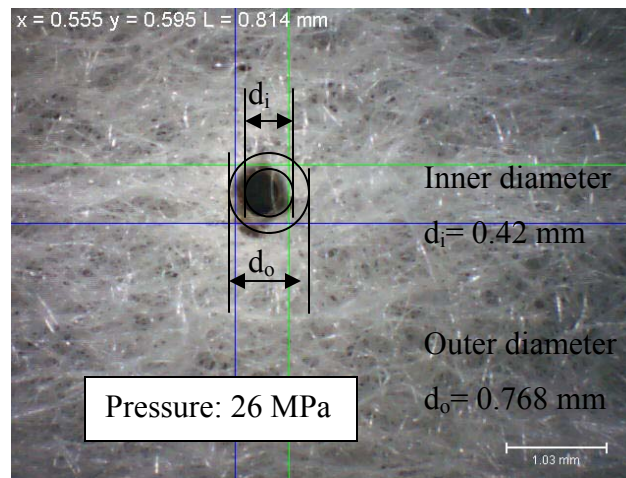
**Figure 3.32: Variation of weld strength with laser power**

### 3.3.4.2 Influence of Contact Pressure on Weld Strength

The contact pressure on the spherical ball lens affects the weld strength. The weld conditions and results are listed in Table 3.16. The optical images of weld strength vs. pressure are shown in Figure 3.33 at a magnification of 17 X. It can be clearly seen that holes are burnt in each case with discoloration at the boundaries. The inner and outer weld diameters are measured and the weld area is calculated. As the pressure increases the weld area also increases. A graph is plotted with weld strength vs. pressure in Figure 3.34. It is clear from Figure 3.34 that the weld strength decreases almost linearly with pressure. When the pressure increases from 26 MPa to 31 MPa, the flow rate of the melt also increases from the interface of the PGA felts. The higher weld pressures squeeze out the molten polymer resulting in an increase in the weld area. The heat is conducted away from the interface resulting in cold surfaces being brought together causing a decrease in weld strength. As a result it can be seen from Figure 3.34 that as the weld pressure increases from 26 MPa to 31 MPa, the weld strength decreases from 0.361 MPa to 0.330 MPa.

**Table 3.16 Weld conditions and results for contact pressure**

Power (W)	Beam diameter (mm)	Time (sec)	Pressure (MPa)	Pull-Off Load (gf)	Inner diameter $d_i$ (mm)	Outer diameter $d_o$ (mm)	Weld area (mm <sup>2</sup> )	Weld Strength (MPa)
75	1	5	26	12	0.420	0.768	0.324	0.361
75	1	5	29	22	0.588	1.050	0.594	0.346
75	1	5	31	29	0.700	1.260	0.861	0.330



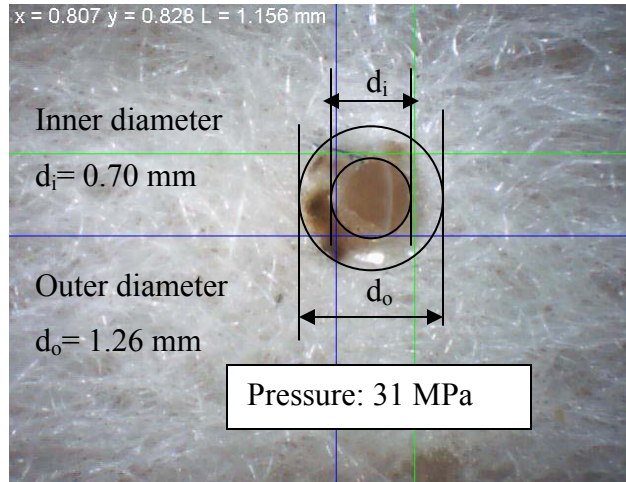


**Figure 3.33: Optical images of weld diameter with different contact pressures at beam diameter of 1 mm**

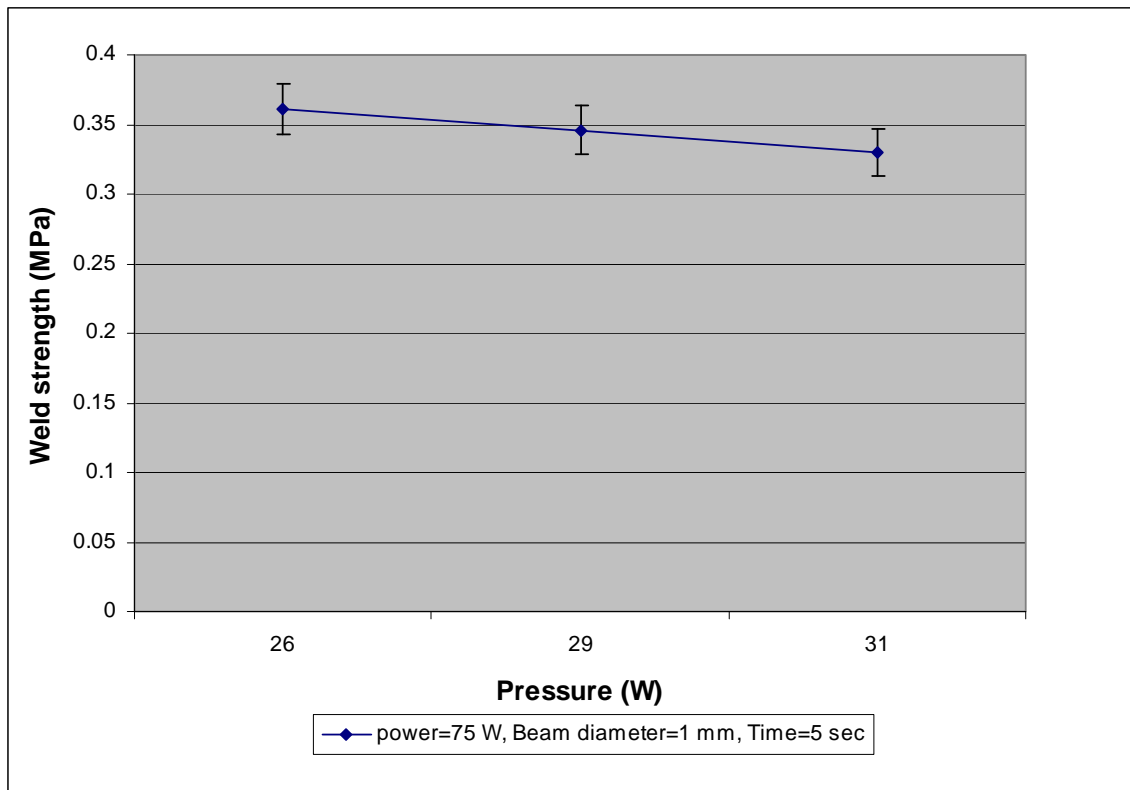


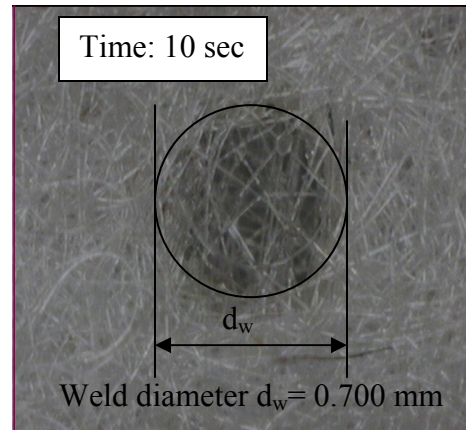
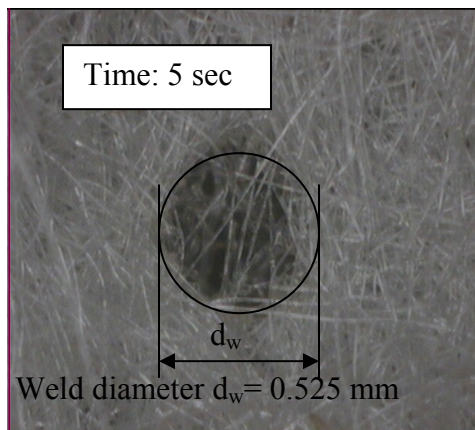
**Figure 3.34: Variation of weld strength with pressure**

### 3.3.4.3 Influence of Time Duration on Weld Strength

Time duration affects the weld strength. As the time duration increases from 5 sec to 15 sec (other laser parameters are the same), the weld strength decreases. Table 3.17 gives the weld conditions and results. The optical images of weld strength vs. time duration are shown in Figure 3.35 at a magnification of 36 X and the weld area is calculated for each case by measuring the average weld diameter. The variation of weld strength vs. time duration is plotted in Figure 3.36. It is clear from Figure 3.36 that the weld strength decreases slightly with time duration. As the time duration for laser spot welding increases from 5 seconds to 15 seconds, the longer interaction time of the polymer with the laser beam results in increasing weld area with lower pull-off load values. This indicates weak welds being formed on the interface with large weld areas and consequently lower weld strengths. This makes the weld strength to decrease slightly with time duration.

**Table 3.17 Weld conditions and results for time duration**

Power (W)	Beam diameter (mm)	Time (sec)	Pressure (MPa)	Pull-Off Load (gf)	Weld diameter (mm)	Weld area (mm <sup>2</sup> )	Weld Strength (MPa)
70	1.5	5	26	3	0.525	0.216	0.136
70	1.5	10	26	5	0.700	0.384	0.127
70	1.5	15	26	7	0.850	0.567	0.120
70	1.5	20	26	7	0.880	0.608	0.111



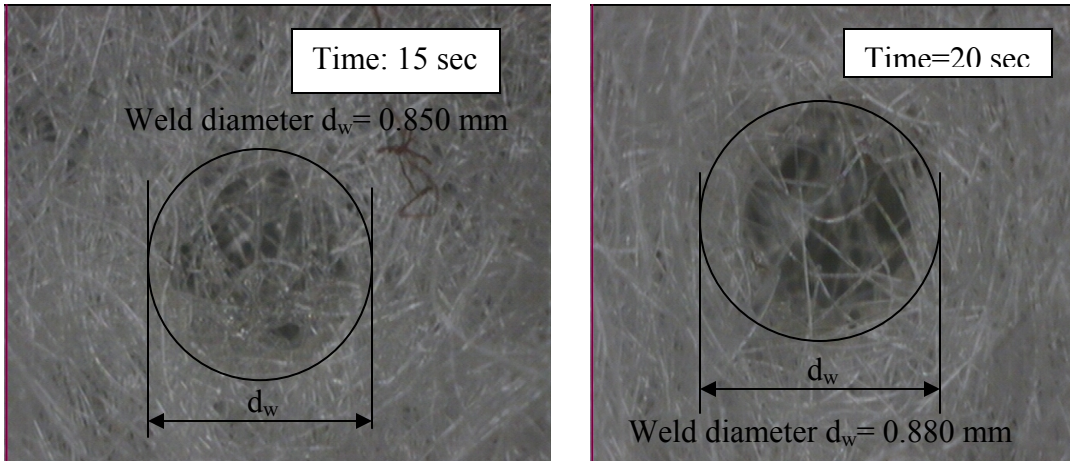


**Figure 3.35: Optical images of weld diameter with different time duration at beam diameter of 1.5 mm**

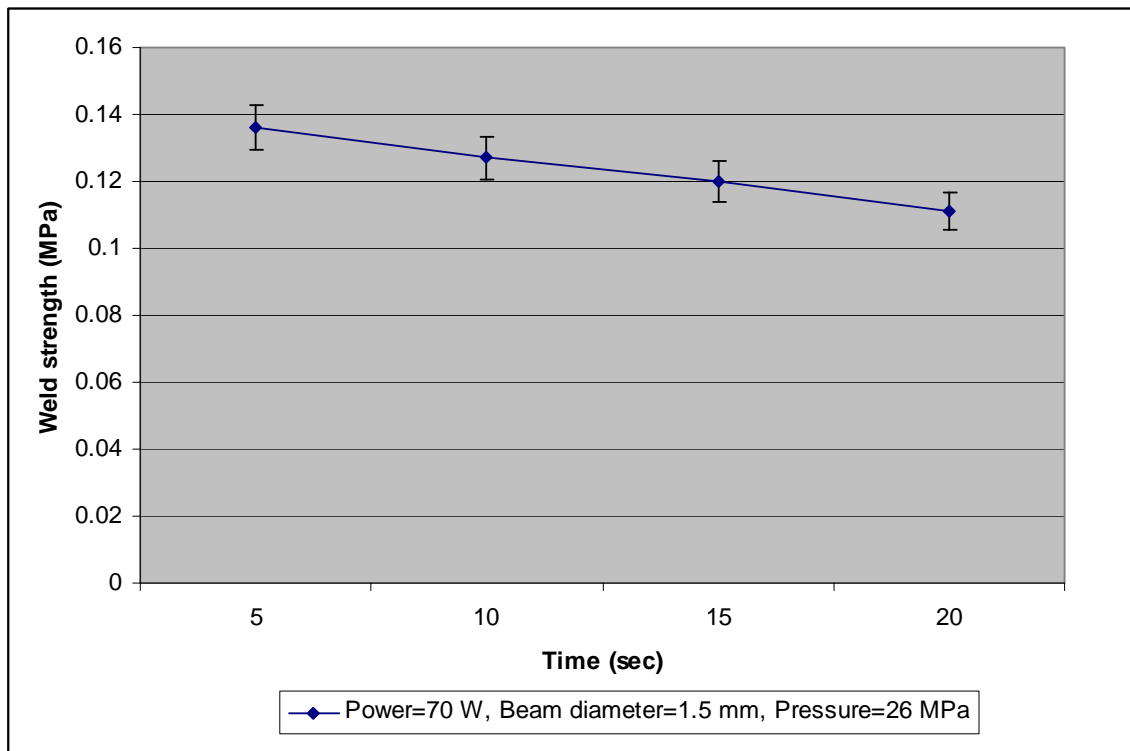


**Figure 3.36: Variation of weld strength with time duration**

### 3.3.4.4 Influence of Beam Diameter on Weld Strength

The weld conditions and results are shown in Table 3.18. To understand the effect of beam diameter, weld diameter and HAZ of the welded holes are directly measured from the optical images of weld strength vs. beam diameter as shown in Figures 3.37 at a magnification of 40 X. It can be clearly seen that the weld area increases with increase in beam diameter. As the distance of the laser source is moved farther to increase the beam diameter, the intensity of the laser beam on the PGA fiber sheets decreases gradually. This causes very weak welds to be formed on the interface as the beam diameter increases and therefore results in lower weld strength values. A graph is plotted with weld strength vs. beam diameter in Figure 3.38. It is clear from Figure 3.38 that weld strength decreases with beam diameter. It is obvious from our previous measurements that the increase in beam diameter directly increases the weld diameter but as the beam diameter increases the welds that are formed on the PGA fiber felts are not strong. The weld formed at beam diameter of 2 mm is not strong as the weld strength value obtained is very small. The graph as shown in Figure 3.38 shows that there is a negative relationship formed between beam diameter and weld strength. The weld strength value decreases as the beam diameter increases and the pull-off load needed to break the welded fibers apart also decreases.

**Table 3.18 Weld conditions and results for beam diameter**

<b>Power (W)</b>	<b>Beam diameter (mm)</b>	<b>Time (sec)</b>	<b>Pressure (MPa)</b>	<b>Pull-Off Load (gf)</b>	<b>Weld diameter (mm)</b>	<b>Weld area (mm<sup>2</sup>)</b>	<b>Weld Strength (MPa)</b>
70	1	15	26	15	0.790	0.490	0.300
70	1.5	15	26	7	0.850	0.567	0.120
70	2	15	26	2	0.900	0.636	0.030

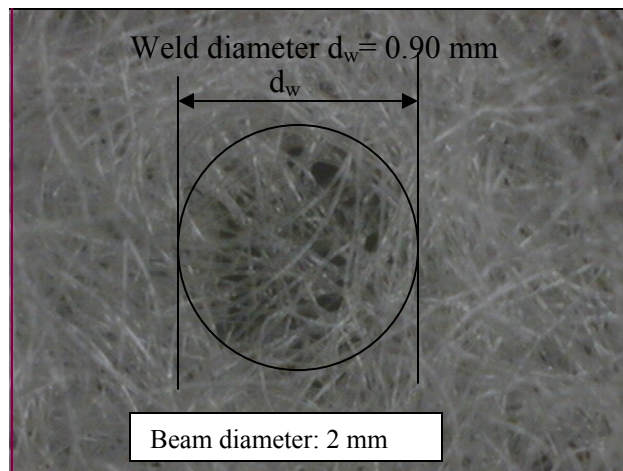
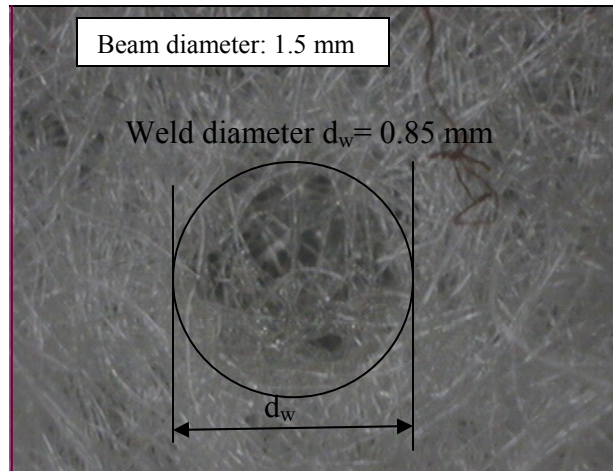
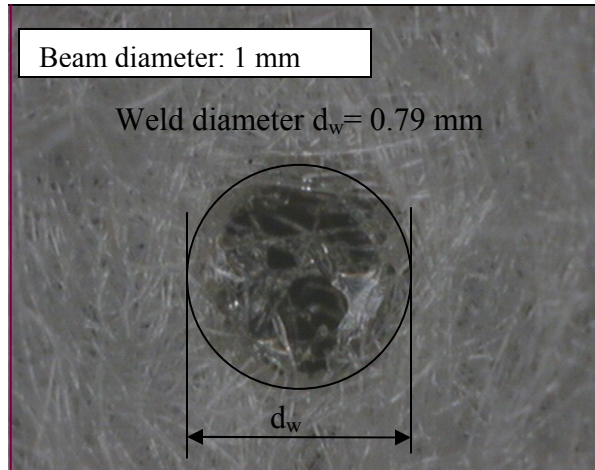


**Figure 3.37: Optical images of weld diameter for different beam diameter**

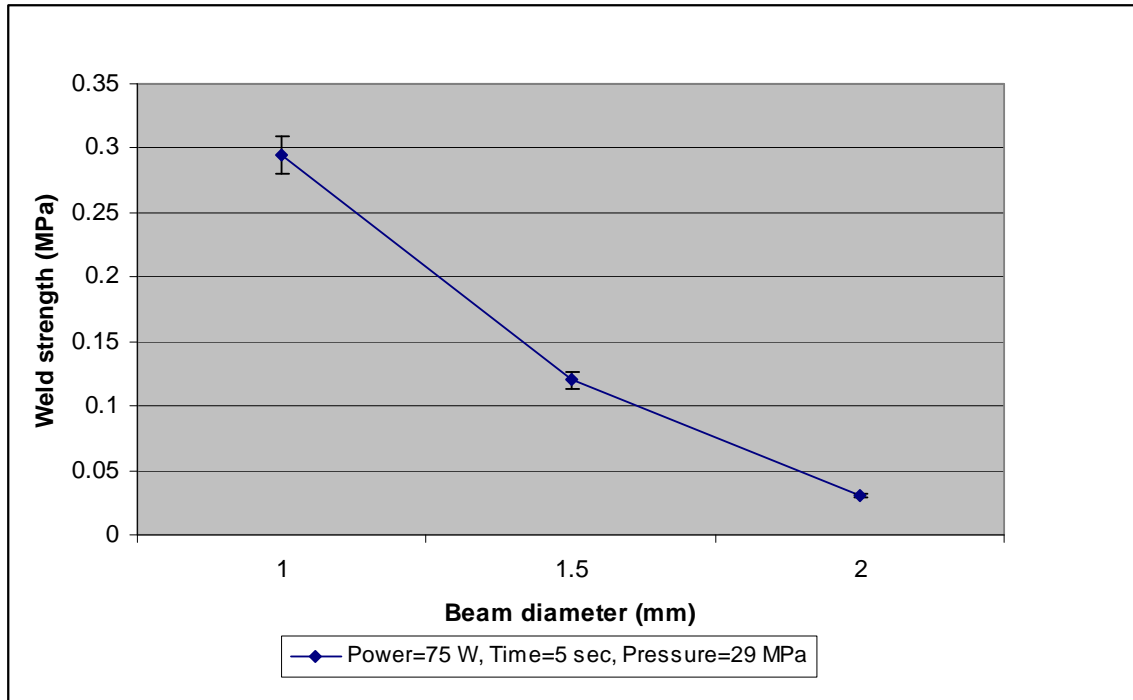


**Figure 3.38: Variation of weld strength with beam diameter**

### 3.3.4.5 Influence of Laser Intensity on Weld Diameter and Weld Strength

Laser intensity is an important parameter that results from the combination of two factors namely laser power and beam diameter. It is defined as the ratio of laser power at a surface per unit area. The effect of laser intensity on weld diameter and weld strength is investigated and the graphs are plotted as shown in Figures 3.39, 3.40, 3.41 and 3.42.

Figure 3.39 shows that weld strength increases with increase in laser intensity (at constant beam diameter of 1.5 mm) and Figure 3.40 shows that the weld strength decreases with decrease in laser intensity (at constant power of 70 W). This indicates that the laser intensity has a positive linear relationship with weld strength. Figure 3.41 shows that weld diameter increases with increase in laser intensity (at constant beam diameter of 1.5 mm) and from Figure 3.42 it can be seen that (at constant power of 70 W) the decrease in laser intensity leads to an increase in weld diameter.

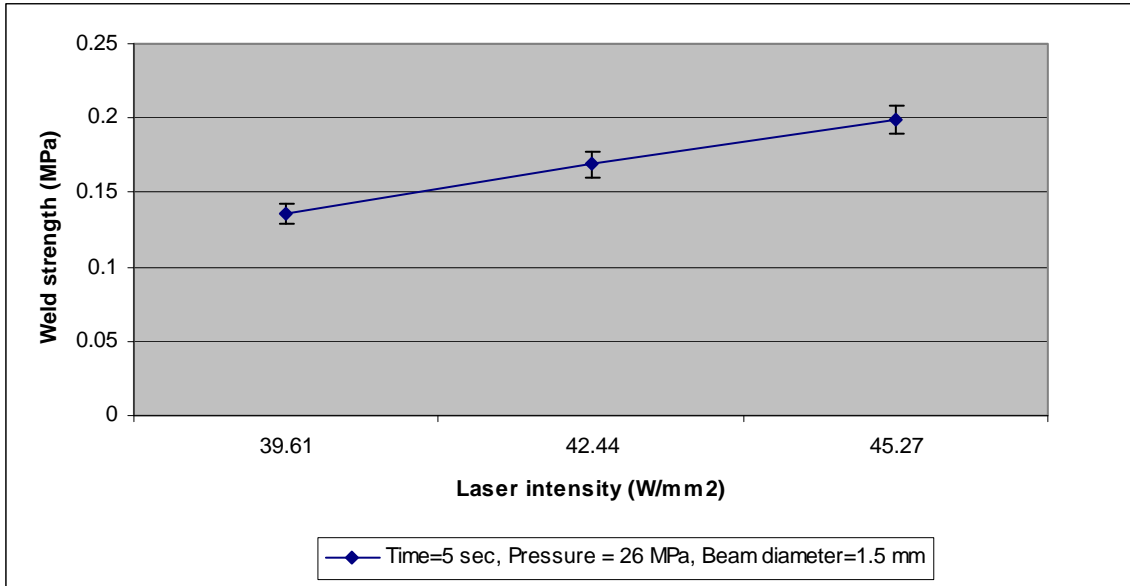


**Figure 3.39: Variation of weld strength with laser intensity**

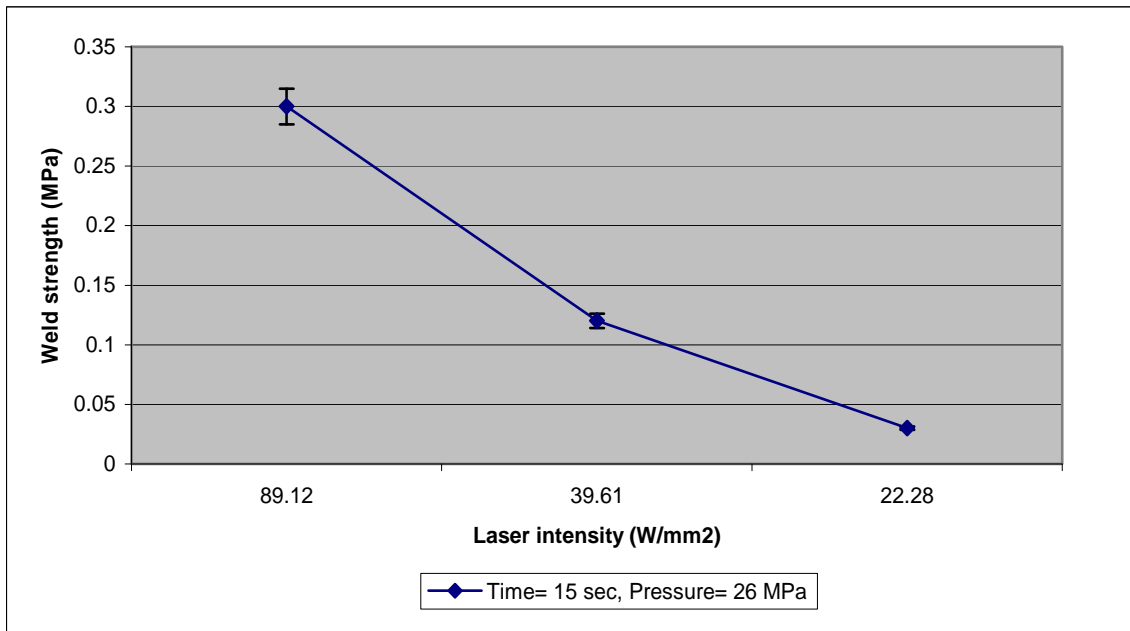


**Figure 3.40: Variation of weld strength with laser intensity**

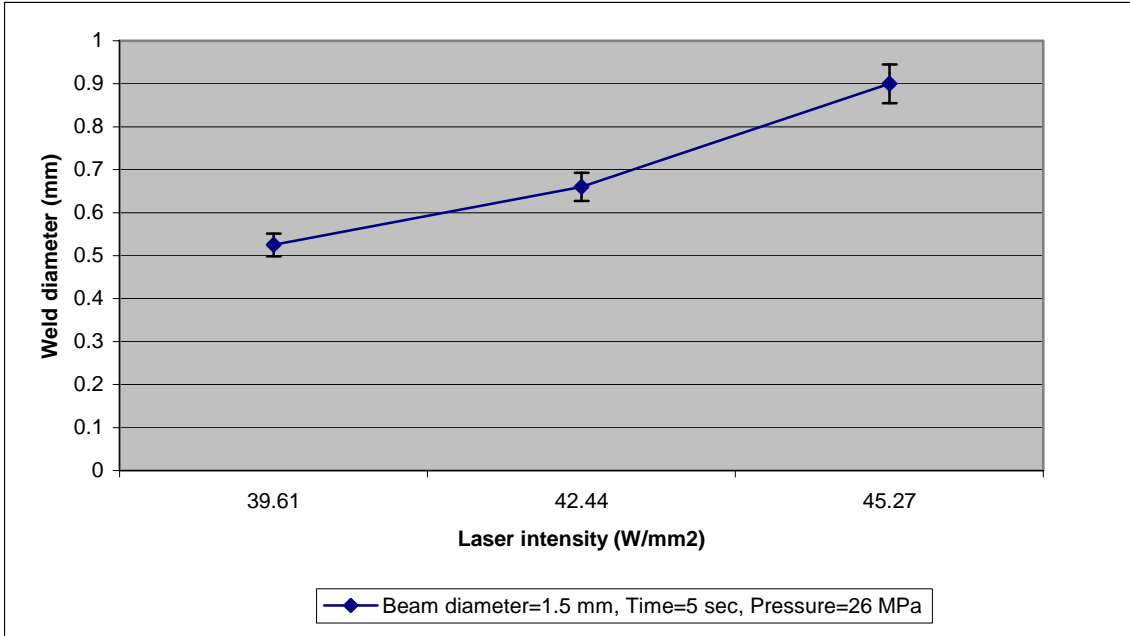


**Figure 3.41: Variation of weld diameter with laser intensity**

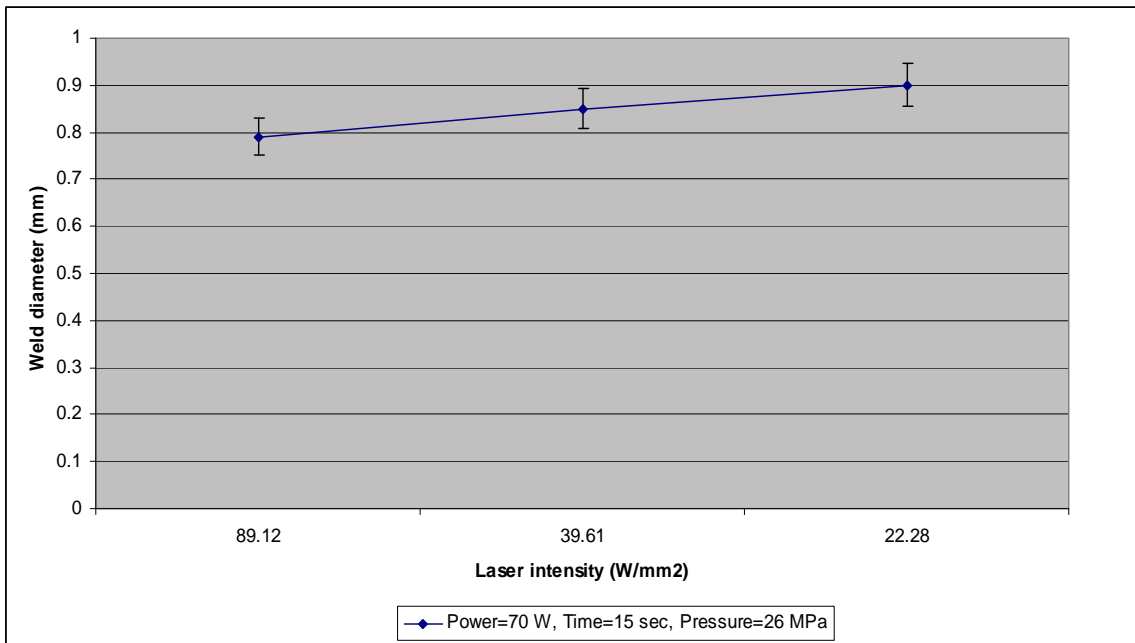


**Figure 3.42: Variation of weld diameter with beam laser intensity**

### 3.4 Comparison of weld strength

The weld strength of the PGA non woven felts is compared with the actual tensile strength of the specimen. This process determines whether the weld formed during the spot welding process is strong or not. The tensile strength of the PGA non woven mesh is found using ASTM standard test method. The weld strength values obtained should be equal to or more than the ultimate tensile strength of the specimen in order to be classified as a successful weld.

#### 3.4.1 Experimental setup for Tensile strength test of PGA non woven mesh

The tensile strength test of biodegradable PGA Biofelt is carried out using the experimental setup as shown in Figure 3.43. In this setup an Instron model 4466 universal testing machine with a load cell capacity of 2.5 N is used. The machine has pneumatic fiber grips with a maximum allowable specimen thickness of 3.968 mm and a maximum capacity of 500 g. The machine is interfaced with a computer and the type of test method to be conducted can be chosen.

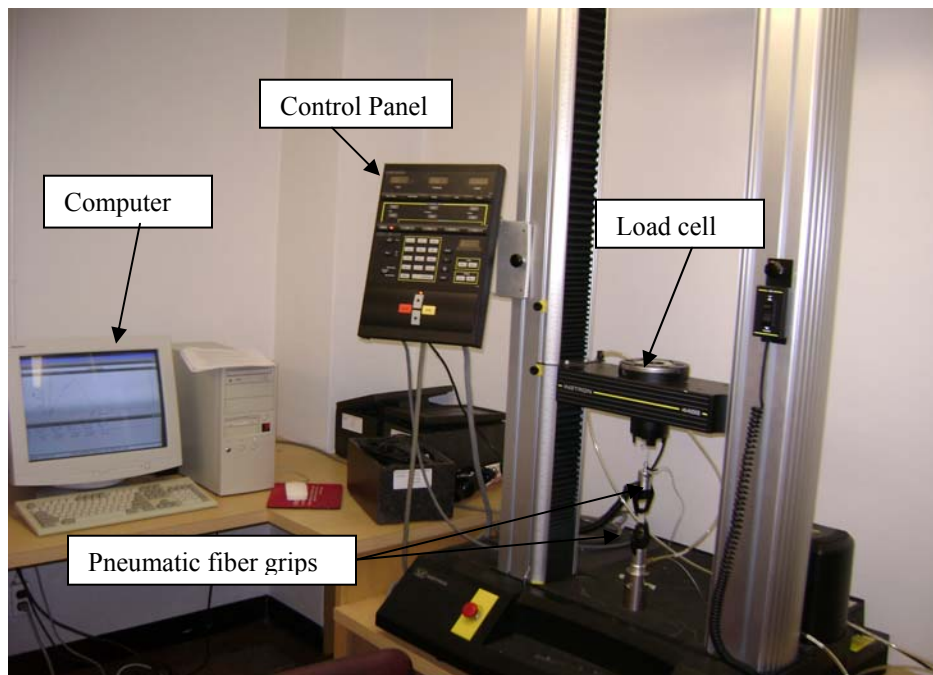


**Figure 3.43: Experimental setup for tensile test of PGA**

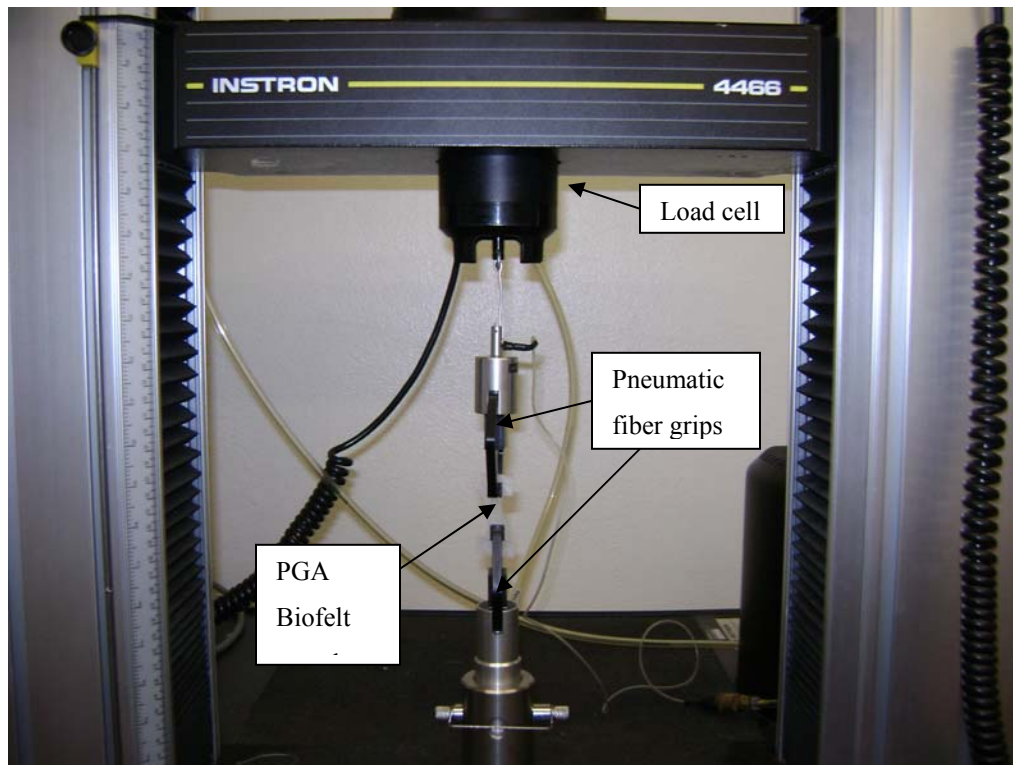


**Figure 3.44: PGA Biofelt sample placed between the pneumatic fiber grips**

The PGA test sample having dimensions of 12.60 mm in width in the center and 20 mm in width at the ends is clamped onto the pneumatic flat grips as shown in Figure 3.44. The gauge length used for the sample is 25 mm and the thickness is 1 mm. The crosshead speed used in the tensile test is 5 mm/min.

### **3.4.2 Experimental Run**

The specimen is fixed between the pneumatic grips and the test data is entered into the computer through the method editor button via the Instron Series IX software. By clicking on the Test button, the tensile test is started and the crosshead begins to move at the rate of 5 mm/min. The load cell calibrates and indicates the value of the tensile load simultaneously. The PGA specimen begins to elongate as the load increases and finally the fibers break at the maximum load. The computer generates the values of the maximum load, stress at maximum load and strain. The ultimate tensile strength of the

specimen is obtained once the specimen breaks at maximum load. Figure 3.45 shows the PGA sample specimen fibers breaking at the maximum load.

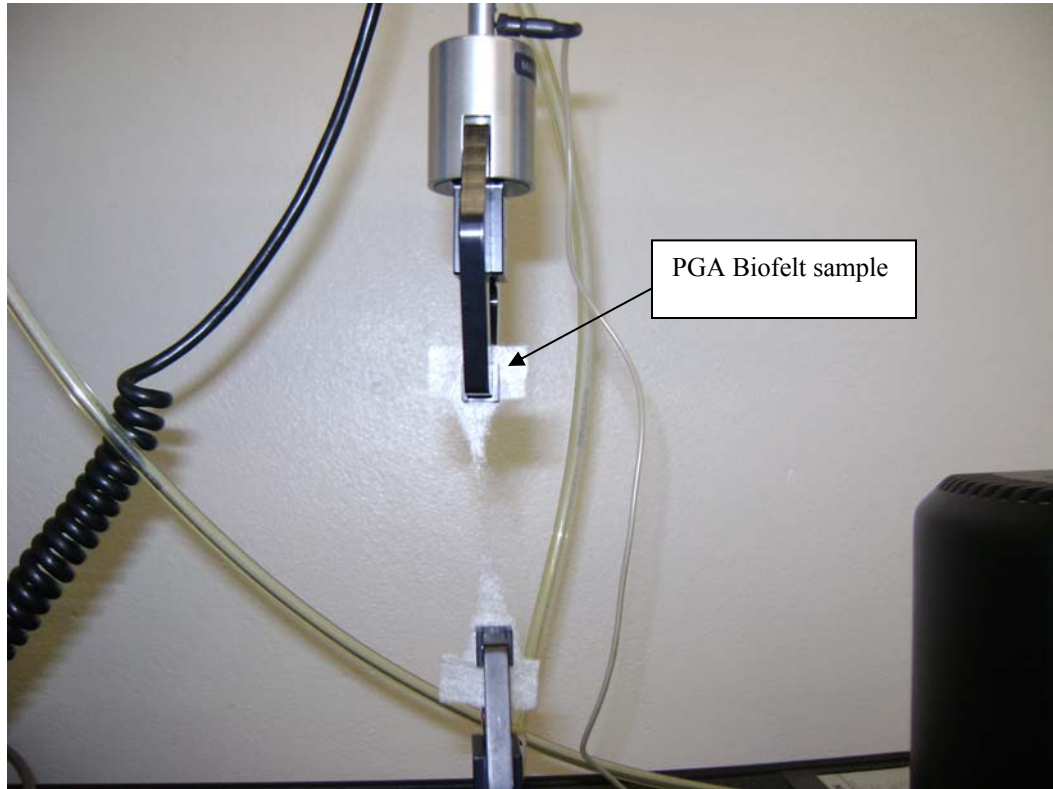


**Figure 3.45: PGA Biofelt fibers breaking at maximum load during tensile test**

**Table 3.19 Tensile stress values**

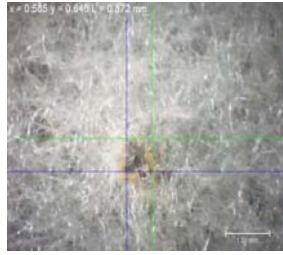
PGA Sample	Displacement at Max. Load (mm)	Maximum Load (kgf)	Stress at Max. Load (kgf/ mm <sup>2</sup> )	Strain at Max. Load (mm/mm)
Sample 1	7.650	0.200	0.02	0.306
Sample 2	9.430	0.200	0.02	0.377
Sample 3	5.550	0.135	0.014	0.222
Sample 4	13.660	0.083	0.008	0.546

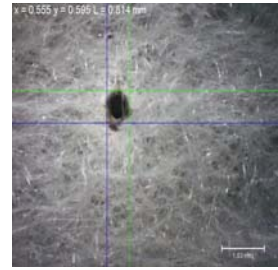
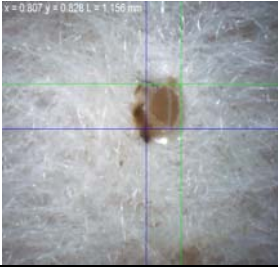
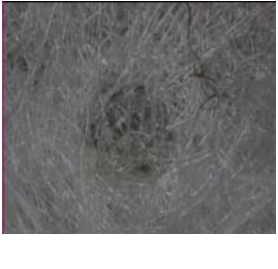
Four samples of PGA Biofelt are tested and the values of maximum load and tensile stress at maximum load are tabulated in Table 3.19. The average of the four samples is taken into account and the ultimate tensile strength of the non woven PGA fiber mesh is 0.015 kgf/mm<sup>2</sup> or 0.152 MPa.

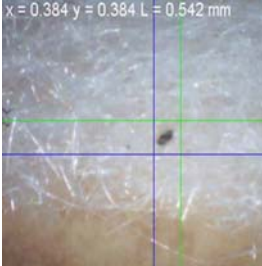
### 3.4.3 Summary and Observations

The values of the weld strength are calculated and tabulated for different laser operating conditions. The welds can be categorized into two types: Strong welds with hole/no hole condition and weak welds based on the ultimate tensile strength (0.152 MPa) of the PGA specimen. If the weld strength values are greater than or equal to the tensile strength of the specimen (0.152 MPa), then the weld obtained is treated as a strong weld or else it is considered to be a weak weld. Table 3.20 shows the types of weld obtained in comparison with the tensile strength of the PGA non woven Biofelt sample.

**Table 3.20 Types of Welds Obtained**

Power (watt)	Beam diameter (mm)	Time (sec)	Pressure(MPa)	Weld Strength (MPa)	Type of weld	Weld Images
70	1	10	26	0.321	Strong weld with a small hole and no discoloration	
75	1	10	26	0.349	Strong weld with a small hole and slight discoloration	
80	1	10	26	0.384	Strong weld with a big hole and no discoloration	

75	1	5	26	0.361	Strong weld with a hole and no discoloration at the boundary	
75	1	5	29	0.343	Strong weld with discoloration at the boundary	
75	1	5	31	0.325	Strong weld with hole formed and no discoloration	
70	1.5	15	26	0.120	Weak Weld With no discoloration	
70	2	15	26	0.030	Weak weld with no discoloration	

75	1.5	5	26	0.169	Strong weld with no discoloration	
75	1.5	5	29	0.155	Weak weld with no discoloration	
70	1	5	26	0.341	Strong weld with a slight hole and no discoloration	
70	1	15	26	0.300	Strong weld with a hole and discoloration	
75	1.5	15	26	0.144	Weak weld with a slight hole and discoloration	

### 3.4.3.1 Regression Analysis

Regression analysis is carried out to form correlations between weld quality and the operating parameters. We use a linear regression model since the results obtained from the previous sections indicate that the operating parameters have approximately a linear relation with the weld diameter and the weld strength. To verify this assumption we carry out the regression analysis. The linear regression equation usually takes the form of

$$Y = a + b_1X_1 + b_2X_2 + b_3X_3 + b_4X_4 + \dots + b_nX_n \quad (3.9)$$

where **Y** is the dependent variable that the equation tries to predict, **X** is the independent variable that is being used to predict **Y**, **a** is the Y-intercept of the line, and **b<sub>1</sub>, b<sub>2</sub>,..., b<sub>n</sub>** are the regression coefficients. In our case Y= weld diameter (mm) and weld strength (MPa); X<sub>1</sub>, X<sub>2</sub>, X<sub>3</sub>, and X<sub>4</sub> = Independent parameters such as laser power (W), time duration (sec), beam diameter (mm), and pressure (MPa), respectively.

#### Regression Analysis: weld diameter versus power, time, beam diameter, and pressure

A regression equation for weld diameter is calculated using Minitab. Out of the 36 experimental conditions, a sample of 21 is taken to formulate the regression equation. A sample of 10 operating conditions is used to verify the output of the regression equation. The regression equation obtained is

$$D_w = - 3.16 + 0.0323*L_p + 0.0230*T + 0.0854*B + 0.0464*P \quad (3.10)$$

where  $D_w$  = weld diameter (mm),  $L_p$  = laser power (W),  $T$  = time duration (sec),  $B$  = beam diameter (mm), and  $P$  = pressure (MPa).

Predictor	Coef	SE Coef	T	P
Constant	-3.1587	0.1991	-15.87	0.000
Power (W)	0.032282	0.001750	18.45	0.000
Time (sec)	0.022974	0.001736	13.23	0.000
Beam diameter (mm)	0.08536	0.02979	2.87	0.011
Pressure (MPa)	0.046362	0.005250	8.83	0.000

$$S = 0.0335661 \quad R-Sq = 96.9\% \quad R-Sq(adj) = 96.1\%$$

Analysis of Variance

Source	DF	SS	MS	F	P
Regression	4	0.56108	0.14027	124.50	0.000
Residual Error	16	0.01803	0.00113		
Total	20	0.57911			

Source	DF	Seq SS
Power (W)	1	0.32299
Time (sec)	1	0.14581
Beam diameter (mm)	1	0.00443
Pressure (MPa)	1	0.08785

The operating conditions for the verification of weld diameter results are listed in Table 3.21. The weld diameter values  $D_E$  from the experimental runs and the weld diameter values  $D_w$  calculated from the regression equation are given in the table. A graph as shown in Figure 3.46 shows the plots of the weld diameter values and by comparing the results it can be seen that these values do not differ significantly from each other. The R-sq value of 96.9 % is also high indicating that the linear regression model is a good fit. This verifies our assumption that the operating conditions have a linear relationship with the weld diameter.

**Table 3.21 Verification of regression model for weld diameter**

Power (W)	Time (sec)	Beam diameter (mm)	Pressure (MPa)	Weld diameter $D_E$ (mm) from experiments	Weld diameter $D_w$ (mm) from equation
80	15	1.5	26	1.10	1.10
70	10	1.5	29	0.83	0.80
70	15	1.5	29	0.98	0.92
80	15	1.5	29	1.23	1.24
75	15	1.5	29	1.09	1.08
70	15	1.5	26	0.85	0.78
75	15	1.0	29	1.04	1.04
75	10	1.0	26	0.73	0.78
70	5	1.0	29	0.60	0.65
75	10	1.5	29	0.94	0.97

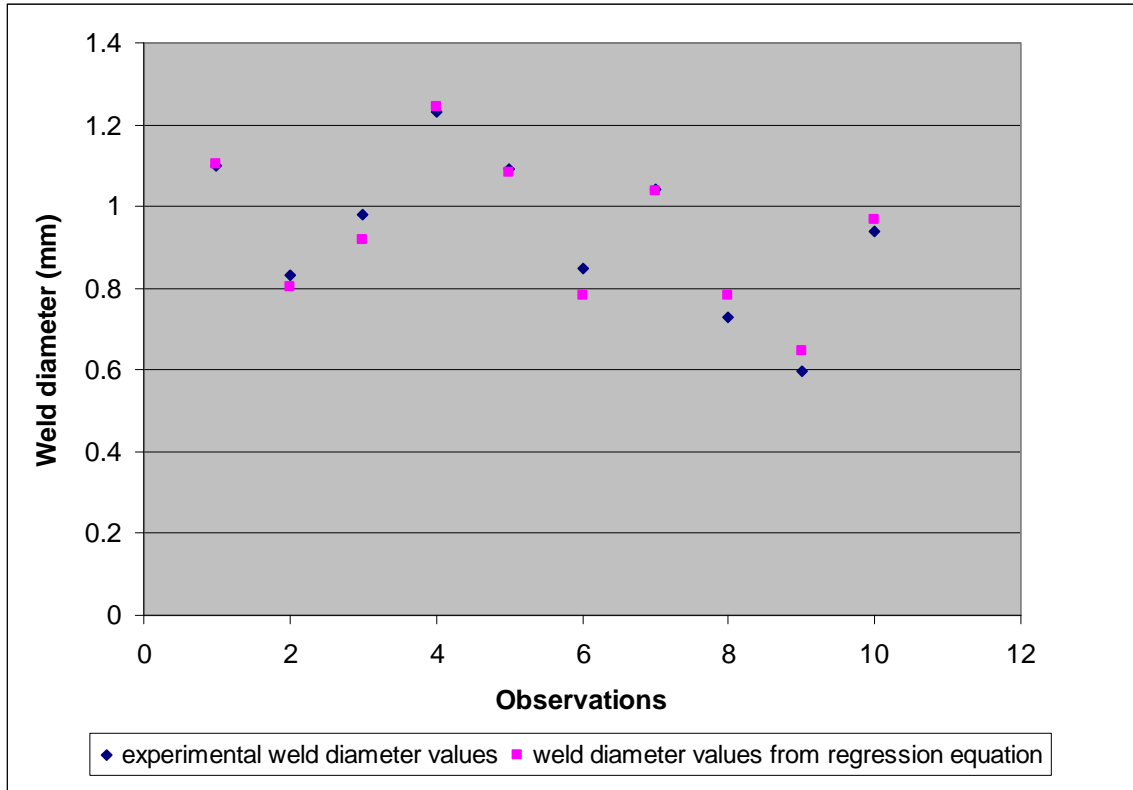


**Figure 3.46: Verification plot for weld diameter**

**Regression Analysis: weld strength versus power, time, beam diameter and pressure**

A regression equation for weld strength is calculated using Minitab. Out of the 36 experimental conditions, a sample of 21 is taken to formulate the regression equation. A sample of 10 operating conditions is used to verify the output of the regression equation. The regression equation obtained is

$$S_w = 0.561 + 0.0051 \cdot L_p - 0.00289 \cdot T - 0.380 \cdot B - 0.000716 \cdot P \quad (3.11)$$

where  $S_w$  = weld strength (MPa),  $L_p$  = laser power (W),  $T$  = time duration (sec),  $B$  = beam diameter (mm), and  $P$  = pressure (MPa).

Predictor	Coef	SE Coef	T	P
Constant	0.56093	0.01630	34.40	0.000
Power (W)	0.0051114	0.0001433	35.68	0.000
Time (sec)	-0.0028925	0.0001422	-20.34	0.000
Beam diameter (mm)	-0.380023	0.002439	-155.79	0.000
Pressure (MPa)	-0.0071625	0.0004300	-16.66	0.000

S = 0.00274879 R-Sq = 99.9% R-Sq(adj) = 99.9%  
 Analysis of Variance

Source	DF	SS	MS	F	P
Regression	4	0.194783	0.048696	6444.80	0.000
Residual Error	16	0.000121	0.000008		
Total	20	0.194904			

Source	DF	Seq SS
Power (W)	1	0.010608
Time (sec)	1	0.000778
Beam diameter (mm)	1	0.181300
Pressure (MPa)	1	0.002097

The operating conditions for the verification of weld strength results are listed in Table 3.22. The weld strength values  $S_E$  from the experimental runs and the weld strength values  $S_w$  calculated from the regression equation are given in the table. Figure 3.47 shows the plots of the weld strength values and by comparing the results it can be seen that these values do not differ significantly from each other. The R-sq value of 99.9 % is also high indicating that the linear regression model is a good fit. This verifies our assumption that the operating conditions have a linear relationship with the weld strength.

**Table 3.22 Verification of regression model for weld strength**

Power (W)	Time (sec)	Beam diameter (mm)	Pressure (MPa)	Weld strength $S_E$ (mm) from experiments	Weld strength $S_w$ (mm) from equation
80	15	1.5	26	0.165	0.170
70	10	1.5	29	0.114	0.112
70	15	1.5	29	0.100	0.098
80	15	1.5	29	0.148	0.149
75	15	1.5	29	0.121	0.123
70	15	1.5	26	0.120	0.119
75	15	1.0	29	0.310	0.313
75	10	1.0	26	0.349	0.349
70	5	1.0	29	0.320	0.317
75	10	1.5	29	0.138	0.138

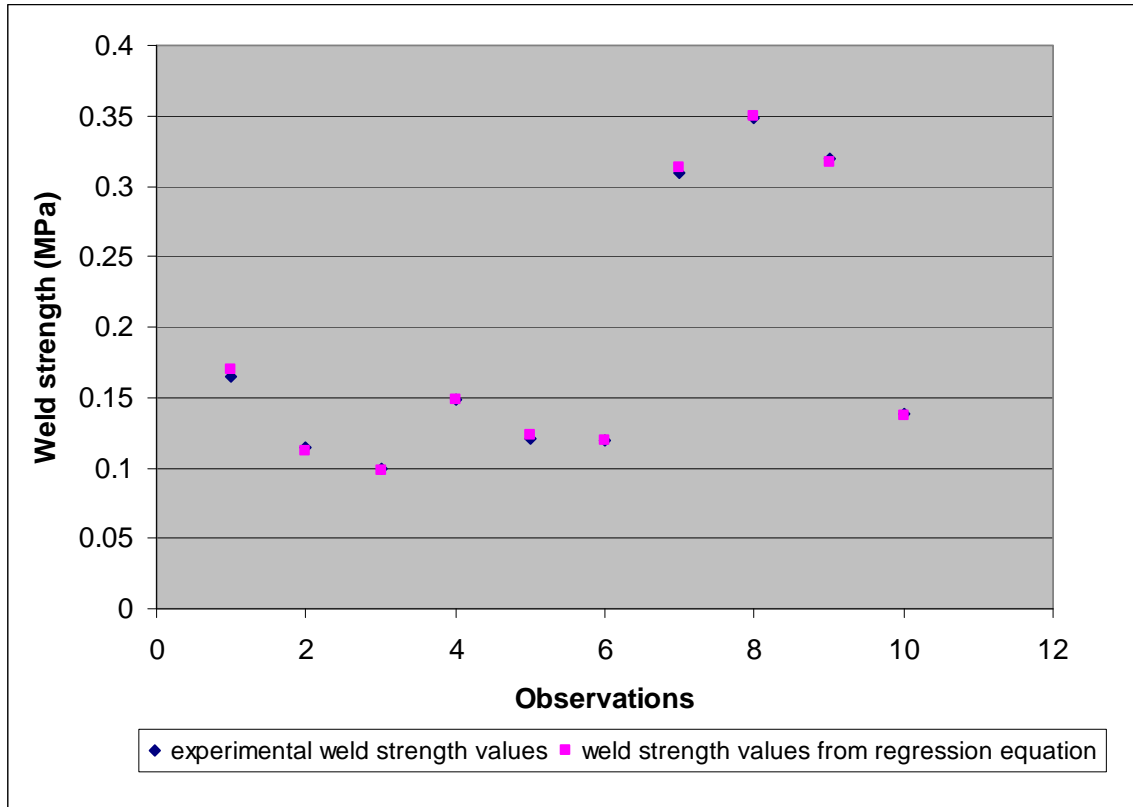


**Figure 3.47: Verification plot for weld strength**

The operating parameter such as laser power has a positive linear relationship with weld strength whereas time duration, beam diameter and pressure have a negative linear relationship with weld strength. This means that as we increase the laser power at certain conditions the weld strength value will increase and at certain conditions the weld strength value will decrease with increase in parameters like time duration, beam diameter and pressure. The residual plots as shown in Figure 3.48 indicate that the data points are independently and identically distributed (i.i.d) as the residuals are normally distributed and do not follow symmetrical pattern about the x-axis.

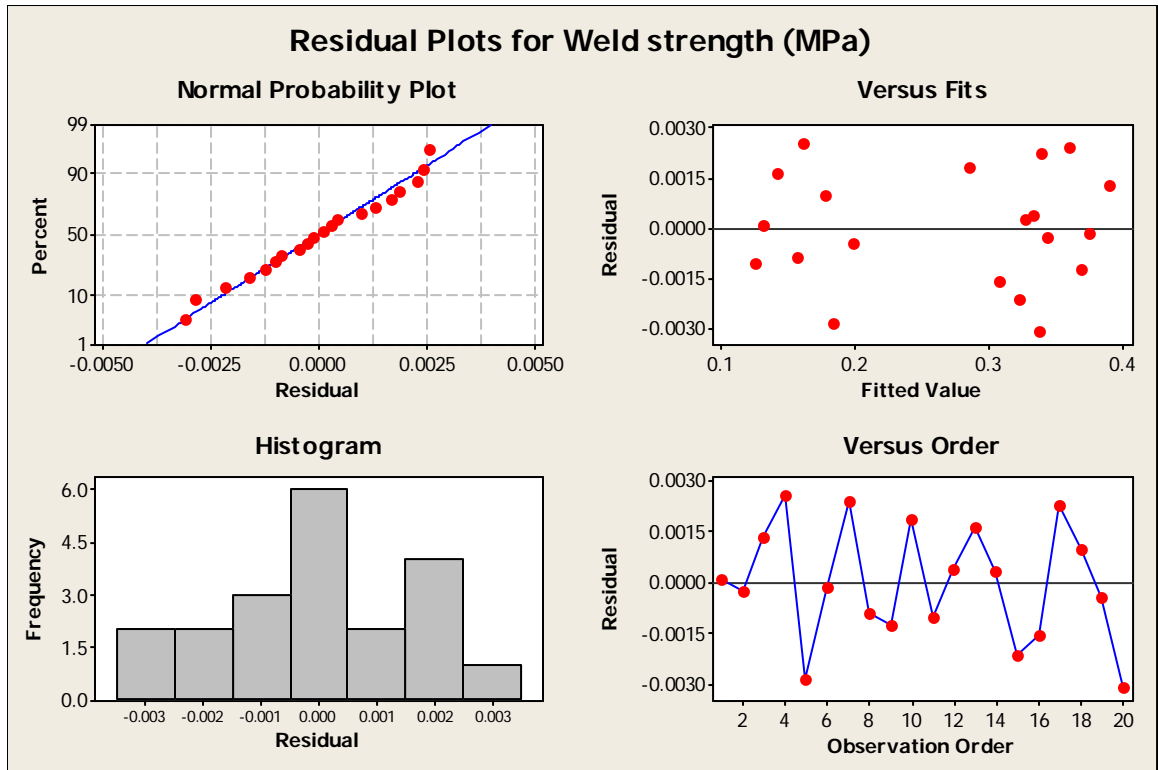
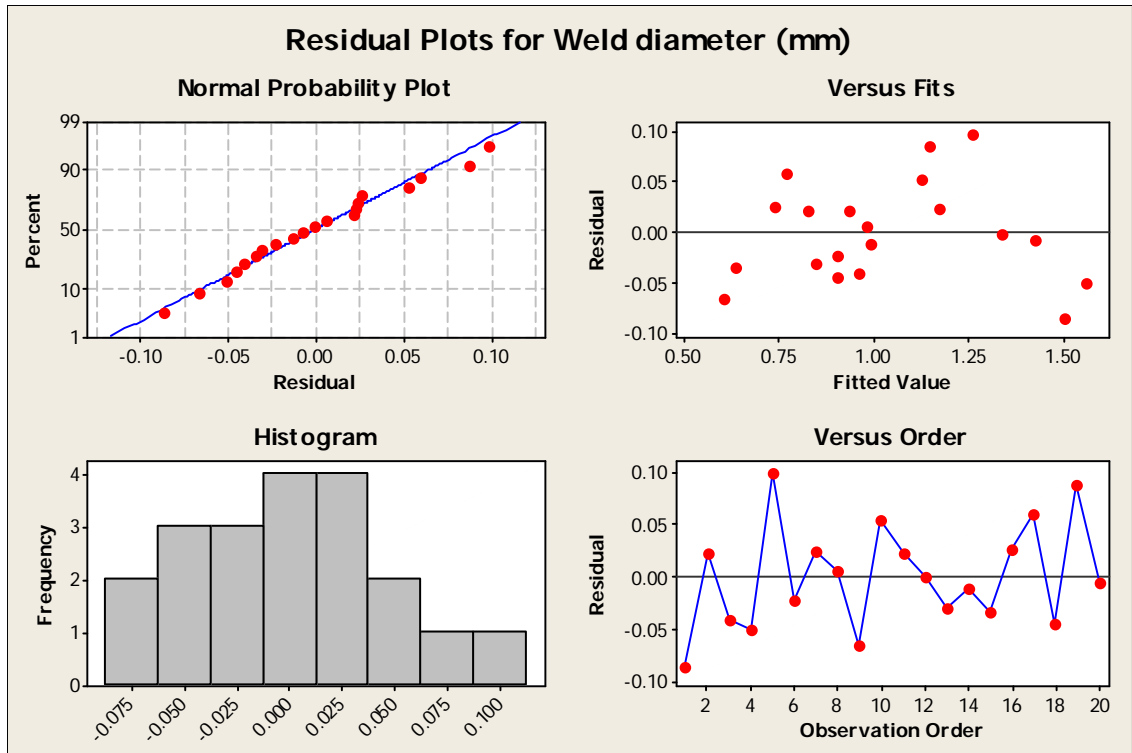


**Figure 3.48: Residual Plots for weld diameter and weld strength**

## **CHAPTER 4- Conclusions and Future Research**

### **4.1 Conclusions**

Laser spot welding of PGA biofelt scaffold polymers is a novel application in the area of Biomedical engineering. The welding setup necessary to facilitate the creation of spot welds is presented. The experiments are carried out based on a factorial design and the experimental results obtained played a vital role in understanding the effects of the various operating parameters necessary to carry out the welding process. Some conclusions from this study are summarized in the following:

1. Laser welding using CW diode lasers could be a promising technique in the area of biomedical engineering that offers benefits such as low costs, high efficiency, faster processing times and efficient weld seams.
2. Joining the PGA biofelts is achieved through laser welding with the use of BK 7 ball lens. The effects of various laser parameters such as laser power, beam diameter, time duration and pressure on the weld quality such as weld diameter and weld strength are studied. The operating parameters such as laser power, beam diameter, time duration and contact pressure exhibit a linear relationship with the weld diameter. The weld strength exhibits a positive linear relationship with laser power and a negative linear relationship with the beam diameter, time duration and contact pressure as observed in this study.
3. Regression analysis is done and a regression model is obtained for the effect of the operating conditions on the weld diameter and weld strength.
4. Efficient welding conditions are obtained that create a successful weld with no discoloration and proper weld strength. Based on these values, the welding is carried out to create a series of spot welds and tubular PGA scaffolds are obtained that can be used in the vascular tissue engineering.

## 4.2 Future research

1. This research can be further continued by analyzing other parameters such as temperature that affects the weld quality.
2. The whole welding process should be automated and the setup should be such that it facilitates continuous welding in order to produce seams. In this way the PGA fiber felts can be welded with continuous seams and different patterns can be obtained.
3. This work can be continued on other biodegradable scaffold materials such as PCL, PLLA, PLGA, etc.
4. Further research can be done to investigate the possibilities of carrying out the laser welding of scaffold materials in an *in situ* environment without affecting the internal tissues and organs.

## References

1. Rabkin, E., Schoen, F.J., 2002, "Cardiovascular tissue engineering," Cardiovascular Pathology., Vol.11, pp.305-317.
2. Hoerstrup, S.P., Zund, G., Sodian, R., Schnell, AM., Grunenfelder, J., Turina, MI., 2001, "Tissue engineering of small caliber vascular grafts," European Journal of Cardiothoracic Surgery., Vol.20, pp.164-169.
3. Langer, R., Vacanti, J., 1999, "Tissue Engineering: the challenges ahead," Scientific American., Vol.280, pp.62-65.
4. Tateishi, T., Chen, G., Ushida, T., 2002, "Biodegradable porous scaffolds for tissue engineering," The Japanese Society for Artificial Organs., Vol.5, pp.77-83.
5. Nikalson, Laura, E., Seruya, M., 2002, "Small diameter vascular grafts," Methods of Tissue Engineering, Chapter 80, pp.905-913.
6. Vacanti, J., Vacanti, C.A., 2000, "Principles of Tissue Engineering," Academic Press.
7. Langer, R., Vacanti, J., 1993, "Tissue Engineering," Science., Vol.260, pp.920-928.
8. Vacanti, J., Langer, R., 1999, "Tissue Engineering: the design and fabrication of living replacement devices for surgical reconstruction and transplantation," Vol.354, (Suppl 1):SI32-4.
9. Ma, P, X., Kroschwitz, J, I., 2004, "Tissue Engineering," Encyclopedia of Polymer Science and Technology (3rd Edition ed.), John Wiley & Sons, NJ.
10. Friedrich, G., Bachmann., Ulrich, A., Russek., 2002, "Laser Welding of Polymers Using High Power Diode Lasers," Proc. SPIE, Vol. 4637B.
11. Kneser, U., Schaefer, D.J., Munder, B., Klemt, C., Andree, C., Stark, G.B., 2002, "Tissue engineering of bone," Min Invas Ther & Allied Tech., Vol.11, pp.107-116.
12. Vats, A., Tolley, N.S., Polak, JM., Gough, JE., 2003, "Scaffolds and biomaterials for tissue engineering: a review of clinical applications," Clinical-Otolaryngol, Vol.28, pp.165-172 .

13. Peter, X., Ma., 2004, "Scaffolds for tissue fabrication," *Materials Today*, Vol.7, pp.30-40.
14. Fuchs, JR., Nasser, BA., Vacanti, JP., 2001, "Tissue Engineering: A 21st Century Solution to Surgical Reconstruction," *Annals of Thoracic Surgery*, Vol.72, pp.577-591.
15. Tateishi, T., Chen, G., Ushida, T., 2002, "Biodegradable porous scaffolds for tissue engineering," *The Japanese Society for Artificial Organs*, Vol.5, pp.77-83.
16. Freed, LE., Vunjak-Novakovic, G., Biron, RJ., Eagles, DB., Lesnoy, DC., Barlow, SK., Langer, R., 1994, "Biodegradable Polymer Scaffolds for Tissue Engineering," *Nature Biotechnology*, Vol.12, pp.689-693.
17. Edwards, S.L., Mitchell, W., Matthews, J.B., Ingham, E., Russell, S.J., 2004, "Design of nonwoven scaffold structures for tissue engineering of the anterior cruciate ligament," *AUTEX Research Journal*, Vol.4, pp.86-94.
18. Griffith, LG., Naughton, G., 2002, "Tissue engineering-current challenges and expanding opportunities," *Science*, Vol.295, pp.1009-1014.
19. Shoufeng, Yang., Kah-fai, Leong., Zhaohui, Du., Chee-Kai, Chua., 2001, "The Design of Scaffolds for Use in Tissue Engineering. Part I. Traditional Factors," *Tissue Engineering*, Vol.7, pp.679-689.
20. Peter, Ma, X., Elisseff, Jennifer., 2006, "Scaffolding in Tissue Engineering," CRC Press, Taylor and Francis Group, USA, xvi.
21. <http://web.utk.edu/~mse/Textiles/Needle%20Punched%20Nonwovens.htm>
22. Mooney, D, J., Mazzoni, C, L., Breuer, C., McNamara, K., Hern, D., Vacanti, J, P., Langer, R., 1996, "Stabilized polyglycolic acid fibre-based tubes for tissue engineering," *Biomaterials*, Vol.17, pp.115-124.
23. Thomson, R.C., Wake, M.C., Yaszemski, M.J., and Mikos, A. G., 1995, "Biodegradable polymer scaffolds to regenerate organs," *Advances in Polymer Science*, Vol.122, pp.245-274.
24. Mikos, AG., Bao, Y., Cima, LG., Ingeber DE., Vacanti, JP., Langer, RB., 1993, "Preparation of poly(glycolic acid) bonded fiber structures for cell attachment and transplantation," *Journal of Biomedical Material Research*, Vol.27, pp.183-189.

25. Lunenschloss, L., and Albrecht, W., 1985, "Non-woven Bonded Fabrics," John Wiley & Sons Inc., New York.
26. Self-cohering, continuous filament non-woven webs, United States Patent 6309423
27. Dahl, S.L.M., Caroline, Rhim., Ying, C. Song., and Laura, E. Niklason., 2007, "Mechanical Properties and Compositions of Tissue Engineered and Native Arteries," Annals of Biomedical Engineering, Vol.35, pp.348-355.
28. Stekelenburg, M., 2006, "Strain-based optimization of human tissue-engineered small diameter blood vessels," PhD. Thesis, Eindhoven University of Technology.
29. [http://machinedesign.com/BDE/FASTENING/bdefj1/bdefj1\\_5.html](http://machinedesign.com/BDE/FASTENING/bdefj1/bdefj1_5.html)
30. Yousefpour, Ali., 2004, "Fusion Bonding/Welding of Thermoplastic Composites," Journal of Thermoplastic Composite Materials, Vol.17, pp.303-341.
31. Marcus, Warwick., and Marcus, Gordon., 2006, "Application studies using through-transmission laser welding of polymers," Joining Plastics, London, National Physical Laboratory (NPL).
32. Leister Systems laser welding concept, <http://www.leisterlaser.com/overview.asp>
33. Friedrich, G, Bachmann., Ulrich, A, Russek., 2002, "Laser Welding of Polymers Using High Power Diode Lasers," Photonics West Conference, Proc. SPIE Vol. 4637B.
34. Leister Systems Globo welding concept, <http://www.leisterlaser.com/globo.asp>
35. Concordia Medical's New BIOFELT™ Tissue Engineering Scaffolds, <http://www.concordiafibers.com/productcapabilities/biofelt.html>.
36. Concordia Regenerative Solution, <http://concordiafibers.com/pressrelease08.pdf>
37. [http://www.mellesgriot.com/products/optics/mp\\_3\\_1.htm](http://www.mellesgriot.com/products/optics/mp_3_1.htm)
38. <http://www accuratus.com/silinit.html>

## Appendix 'A': Tensile test specimen

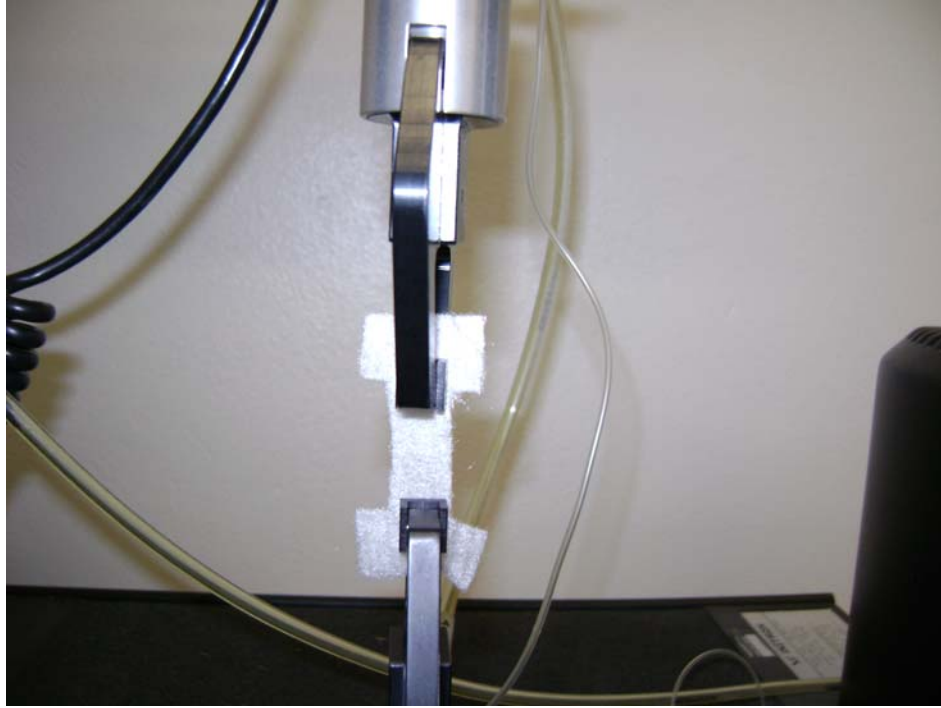


**Figure 3.49: Tensile test specimen before loading**



**Figure 3.50: Tensile test specimen after loading**

## Appendix 'B': Factorial Analysis

**General Linear Model: Weld diameter, Weld Strength versus Power, Beam diameter, Time duration, Pressure**

Factor	Type	Levels	Values
Power	fixed	3	1, 2, 3
Beam diameter	fixed	2	1, 2
Time duration	fixed	3	1, 2, 3
Pressure	fixed	2	1, 2

Analysis of Variance for Weld diameter, using Adjusted SS for Tests

Source	DF	Seq SS	Adj SS	Adj MS	F
Power	2	1.011048	1.011048	0.505524	114.51
Beam diameter	1	0.071913	0.071913	0.071913	16.29
Time duration	2	0.857778	0.857778	0.428889	97.15
Pressure	1	0.398792	0.398792	0.398792	90.33
Power*Beam diameter	2	0.003515	0.003515	0.001758	0.40
Power*Time duration	4	0.008738	0.008738	0.002184	0.49
Power*Pressure	2	0.031242	0.031242	0.015621	3.54
Beam diameter*Time duration	2	0.013993	0.013993	0.006997	1.58
Beam diameter*Pressure	1	0.001260	0.001260	0.001260	0.29
Time duration*Pressure	2	0.020066	0.020066	0.010033	2.27
Power*Beam diameter*Time duration	4	0.050108	0.050108	0.012527	2.84
Power*Beam diameter*Pressure	2	0.028848	0.028848	0.014424	3.27
Power*Time duration*Pressure	4	0.013613	0.013613	0.003403	0.77
Beam diameter*Time duration*Pressure	2	0.001863	0.001863	0.000932	0.21
Error	4	0.017659	0.017659	0.004415	
Total	35	2.530437			

Source	P
Power	0.000
Beam diameter	0.016
Time duration	0.000
Pressure	0.001
Power*Beam diameter	0.696
Power*Time duration	0.744
Power*Pressure	0.130
Beam diameter*Time duration	0.311
Beam diameter*Pressure	0.621
Time duration*Pressure	0.219
Power*Beam diameter*Time duration	0.168
Power*Beam diameter*Pressure	0.144
Power*Time duration*Pressure	0.596
Beam diameter*Time duration*Pressure	0.818
Error	
Total	

S = 0.0664430    R-Sq = 99.30%    R-Sq(adj) = 93.89%

Analysis of Variance for Weld Strength, using Adjusted SS for Tests

Source	DF	Seq SS	Adj SS	Adj MS	F
Power	2	0.025061	0.025061	0.012530	45.01
Beam diameter	1	0.304152	0.304152	0.304152	1092.44
Time duration	2	0.005618	0.005618	0.002809	10.09
Pressure	1	0.006373	0.006373	0.006373	22.89
Power*Beam diameter	2	0.000201	0.000201	0.000100	0.36
Power*Time duration	4	0.000054	0.000054	0.000013	0.05
Power*Pressure	2	0.001308	0.001308	0.000654	2.35

Beam diameter*Time duration	2	0.000739	0.000739	0.000369	1.33
Beam diameter*Pressure	1	0.001056	0.001056	0.001056	3.79
Time duration*Pressure	2	0.000014	0.000014	0.000007	0.03
Power*Beam diameter*Time duration	4	0.001281	0.001281	0.000320	1.15
Power*Beam diameter*Pressure	2	0.000067	0.000067	0.000033	0.12
Power*Time duration*Pressure	4	0.000130	0.000130	0.000033	0.12
Beam diameter*Time duration*Pressure	2	0.000817	0.000817	0.000409	1.47
Error	4	0.001114	0.001114	0.000278	
Total	35	0.347985			

Source	P
Power	0.002
Beam diameter	0.000
Time duration	0.027
Pressure	0.009
Power*Beam diameter	0.718
Power*Time duration	0.994
Power*Pressure	0.212
Beam diameter*Time duration	0.362
Beam diameter*Pressure	0.123
Time duration*Pressure	0.975
Power*Beam diameter*Time duration	0.448
Power*Beam diameter*Pressure	0.890
Power*Time duration*Pressure	0.969
Beam diameter*Time duration*Pressure	0.333
Error	
Total	

S = 0.0166858    R-Sq = 99.68%    R-Sq(adj) = 97.20%

Least Squares Means

		--Weld diameter--		--Weld Strength--	
		Mean	SE Mean	Mean	SE Mean
Power					
1		0.72008	0.019180	0.20342	0.004817
2		0.90117	0.019180	0.24408	0.004817
3		1.12967	0.019180	0.26725	0.004817
Beam diameter					
1		0.87228	0.015661	0.33017	0.003933
2		0.96167	0.015661	0.14633	0.003933
Time duration					
1		0.72908	0.019180	0.25325	0.004817
2		0.91467	0.019180	0.23883	0.004817
3		1.10717	0.019180	0.22267	0.004817
Pressure					
1		0.81172	0.015661	0.25156	0.003933
2		1.02222	0.015661	0.22494	0.003933
Power*Beam diameter					
1	1	0.67617	0.027125	0.29383	0.006812
1	2	0.76400	0.027125	0.11300	0.006812
2	1	0.84400	0.027125	0.33417	0.006812
2	2	0.95833	0.027125	0.15400	0.006812
3	1	1.09667	0.027125	0.36250	0.006812
3	2	1.16267	0.027125	0.17200	0.006812
Power*Time duration					
1	1	0.52625	0.033221	0.21750	0.008343
1	2	0.74150	0.033221	0.20450	0.008343
1	3	0.89250	0.033221	0.18825	0.008343
2	1	0.71850	0.033221	0.25775	0.008343
2	2	0.90000	0.033221	0.24600	0.008343
2	3	1.08500	0.033221	0.22850	0.008343

3	1			0.94250	0.033221	0.28450	0.008343
3	2			1.10250	0.033221	0.26600	0.008343
3	3			1.34400	0.033221	0.25125	0.008343
Power*Pressure							
1	1			0.65250	0.027125	0.22517	0.006812
1	2			0.78767	0.027125	0.18167	0.006812
2	1			0.76167	0.027125	0.25217	0.006812
2	2			1.04067	0.027125	0.23600	0.006812
3	1			1.02100	0.027125	0.27733	0.006812
3	2			1.23833	0.027125	0.25717	0.006812
Beam diameter*Time duration							
1		1		0.69400	0.027125	0.34600	0.006812
1		2		0.88783	0.027125	0.33583	0.006812
1		3		1.03500	0.027125	0.30867	0.006812
2		1		0.76417	0.027125	0.16050	0.006812
2		2		0.94150	0.027125	0.14183	0.006812
2		3		1.17933	0.027125	0.13667	0.006812
Beam diameter*Pressure							
1		1		0.76111	0.022148	0.34889	0.005562
1		2		0.98344	0.022148	0.31144	0.005562
2		1		0.86233	0.022148	0.15422	0.005562
2		2		1.06100	0.022148	0.13844	0.005562
Time duration*Pressure							
1		1		0.65583	0.027125	0.26633	0.006812
1		2		0.80233	0.027125	0.24017	0.006812
2		1		0.80167	0.027125	0.25150	0.006812
2		2		1.02767	0.027125	0.22617	0.006812
3		1		0.97767	0.027125	0.23683	0.006812
3		2		1.23667	0.027125	0.20850	0.006812
Power*Beam diameter*Time duration							
1	1	1		0.46500	0.046982	0.30450	0.011799
1	1	2		0.70850	0.046982	0.31050	0.011799
1	1	3		0.85500	0.046982	0.26650	0.011799
1	2	1		0.58750	0.046982	0.13050	0.011799
1	2	2		0.77450	0.046982	0.09850	0.011799
1	2	3		0.93000	0.046982	0.11000	0.011799
2	1	1		0.69700	0.046982	0.35350	0.011799
2	1	2		0.81000	0.046982	0.33800	0.011799
2	1	3		1.02500	0.046982	0.31100	0.011799
2	2	1		0.74000	0.046982	0.16200	0.011799
2	2	2		0.99000	0.046982	0.15400	0.011799
2	2	3		1.14500	0.046982	0.14600	0.011799
3	1	1		0.92000	0.046982	0.38000	0.011799
3	1	2		1.14500	0.046982	0.35900	0.011799
3	1	3		1.22500	0.046982	0.34850	0.011799
3	2	1		0.96500	0.046982	0.18900	0.011799
3	2	2		1.06000	0.046982	0.17300	0.011799
3	2	3		1.46300	0.046982	0.15400	0.011799
Power*Beam diameter*Pressure							
1	1	1		0.61333	0.038361	0.32267	0.009634
1	1	2		0.73900	0.038361	0.26500	0.009634
1	2	1		0.69167	0.038361	0.12767	0.009634
1	2	2		0.83633	0.038361	0.09833	0.009634
2	1	1		0.72667	0.038361	0.34767	0.009634
2	1	2		0.96133	0.038361	0.32067	0.009634
2	2	1		0.79667	0.038361	0.15667	0.009634
2	2	2		1.12000	0.038361	0.15133	0.009634
3	1	1		0.94333	0.038361	0.37633	0.009634
3	1	2		1.25000	0.038361	0.34867	0.009634
3	2	1		1.09867	0.038361	0.17833	0.009634
3	2	2		1.22667	0.038361	0.16567	0.009634

Power*Time duration*Pressure						
1	1	1	0.46250	0.046982	0.23850	0.011799
1	1	2	0.59000	0.046982	0.19650	0.011799
1	2	1	0.67500	0.046982	0.22400	0.011799
1	2	2	0.80800	0.046982	0.18500	0.011799
1	3	1	0.82000	0.046982	0.21300	0.011799
1	3	2	0.96500	0.046982	0.16350	0.011799
2	1	1	0.63000	0.046982	0.26500	0.011799
2	1	2	0.80700	0.046982	0.25050	0.011799
2	2	1	0.76500	0.046982	0.25250	0.011799
2	2	2	1.03500	0.046982	0.23950	0.011799
2	3	1	0.89000	0.046982	0.23900	0.011799
2	3	2	1.28000	0.046982	0.21800	0.011799
3	1	1	0.87500	0.046982	0.29550	0.011799
3	1	2	1.01000	0.046982	0.27350	0.011799
3	2	1	0.96500	0.046982	0.27800	0.011799
3	2	2	1.24000	0.046982	0.25400	0.011799
3	3	1	1.22300	0.046982	0.25850	0.011799
3	3	2	1.46500	0.046982	0.24400	0.011799
Beam diameter*Time duration*Pressure						
1	1	1	0.61667	0.038361	0.36467	0.009634
1	1	2	0.77133	0.038361	0.32733	0.009634
1	2	1	0.77667	0.038361	0.34800	0.009634
1	2	2	0.99900	0.038361	0.32367	0.009634
1	3	1	0.89000	0.038361	0.33400	0.009634
1	3	2	1.18000	0.038361	0.28333	0.009634
2	1	1	0.69500	0.038361	0.16800	0.009634
2	1	2	0.83333	0.038361	0.15300	0.009634
2	2	1	0.82667	0.038361	0.15500	0.009634
2	2	2	1.05633	0.038361	0.12867	0.009634
2	3	1	1.06533	0.038361	0.13967	0.009634
2	3	2	1.29333	0.038361	0.13367	0.009634

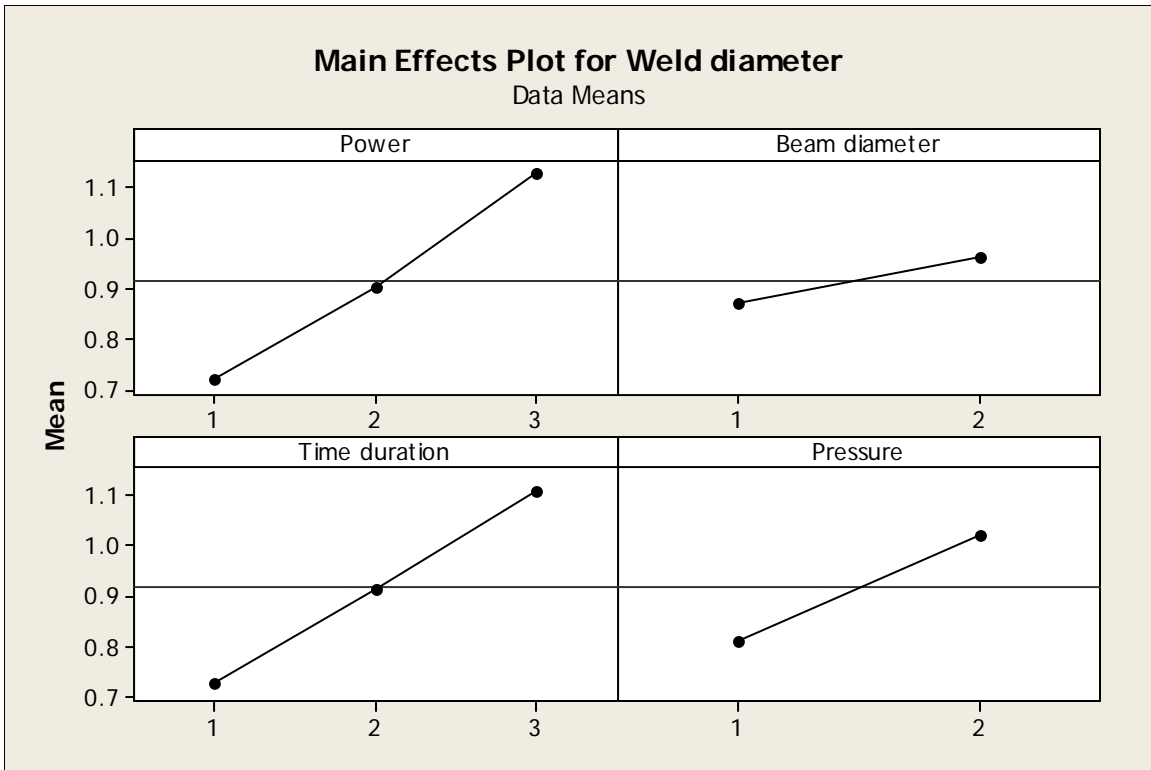


**Figure 3.51: Main Effects plot for Weld diameter**

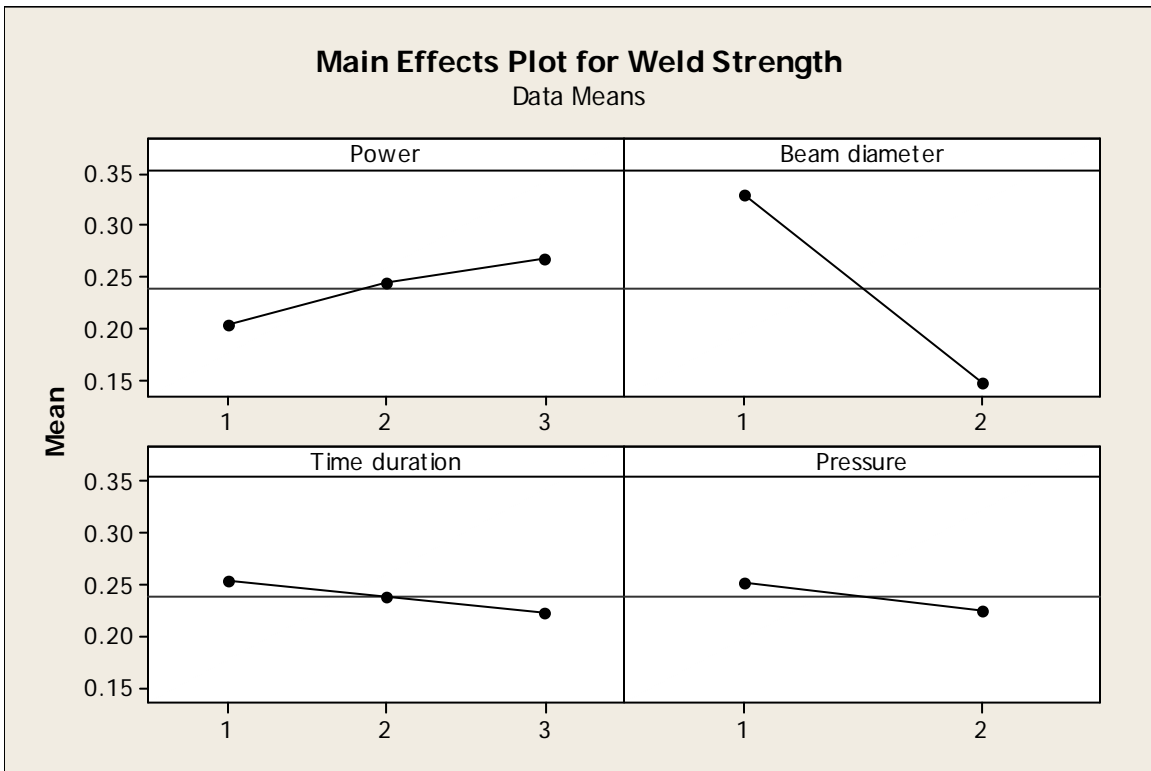


**Figure 3.52: Main Effects plot for Weld Strength**

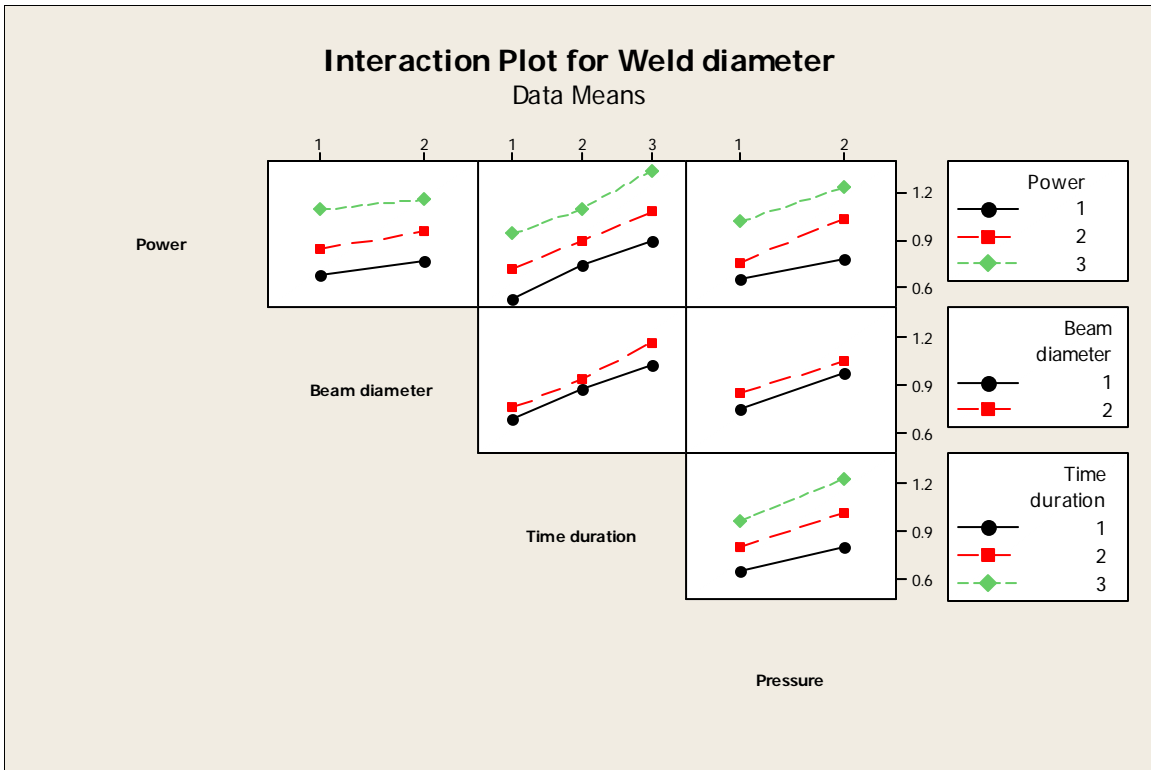


Figure 3.53: Interaction plot for Weld diameter

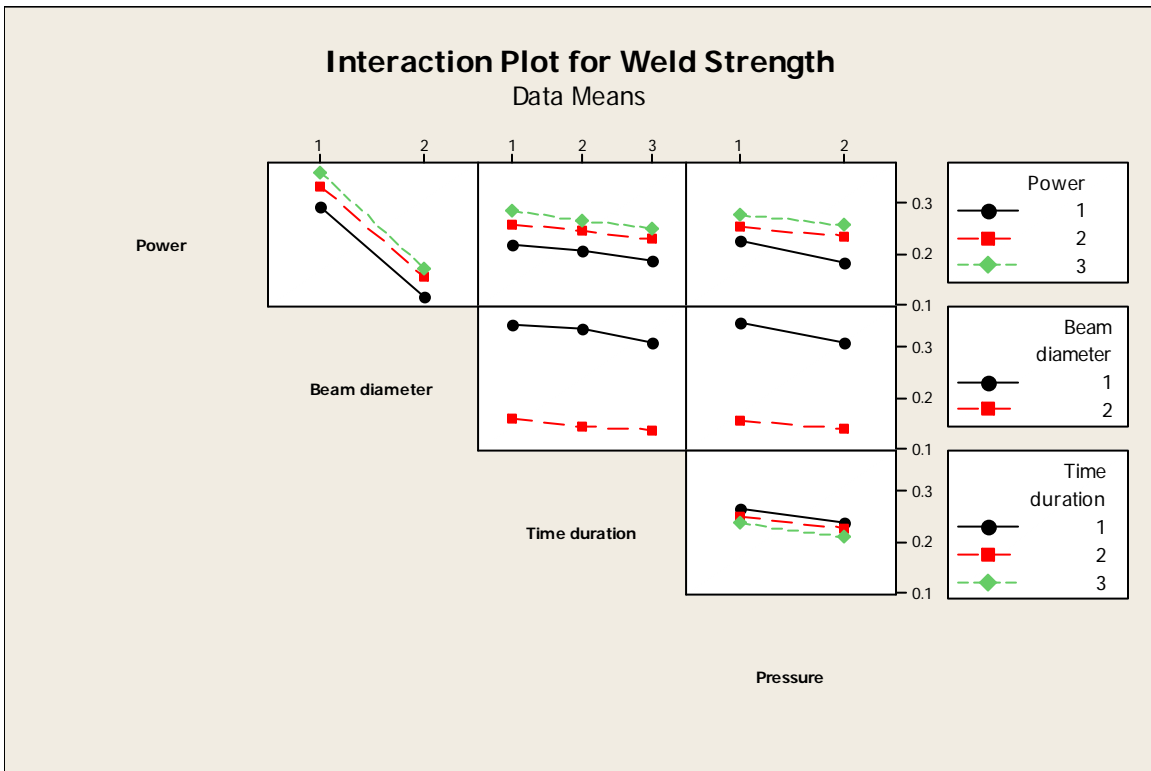


Figure 3.54: Interaction plot for Weld Strength